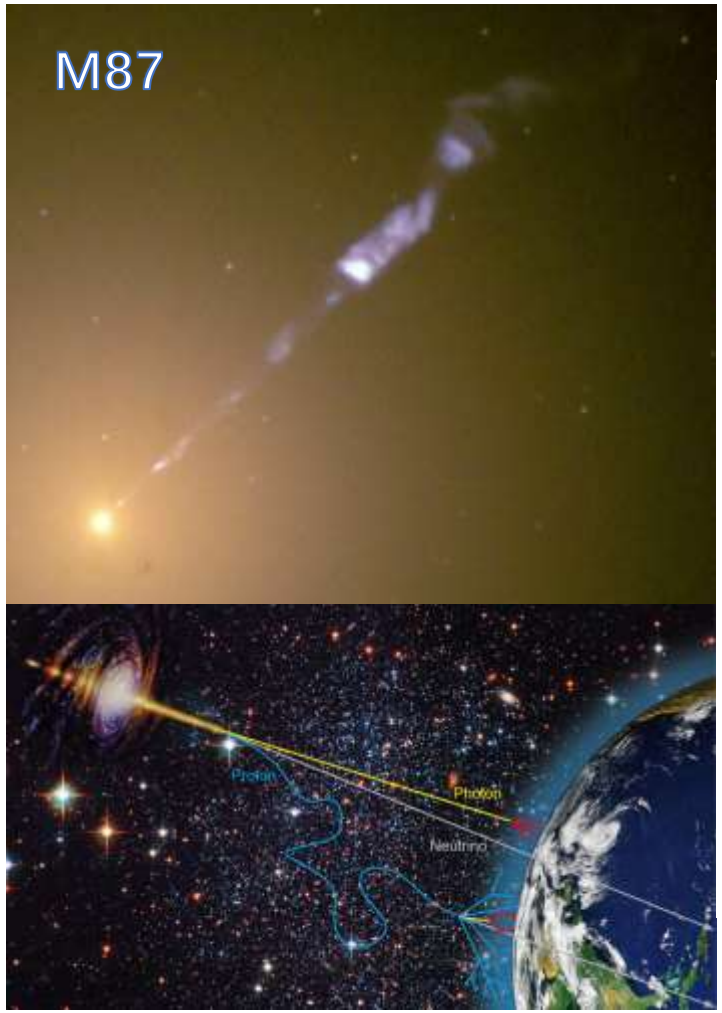

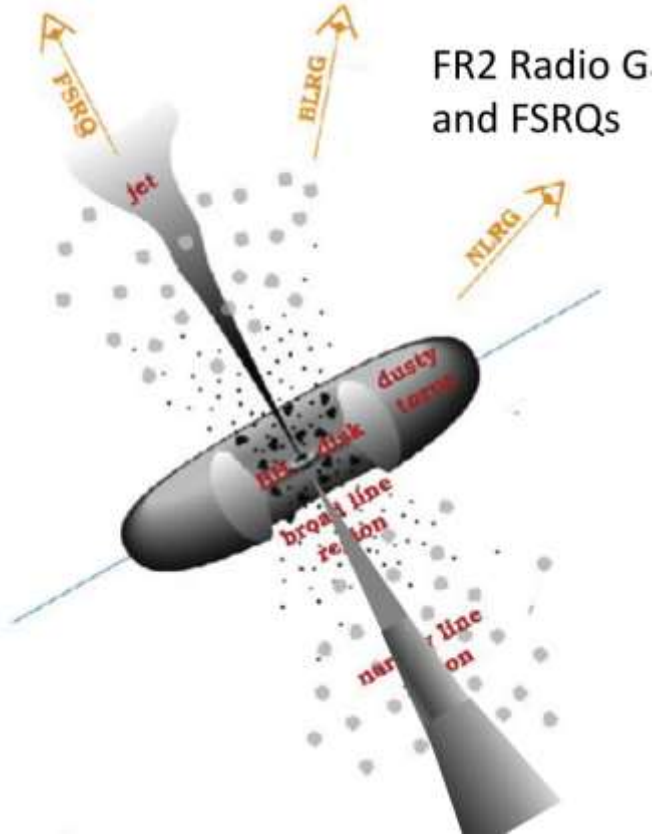

AGN物理

陈亮
中科院上海天文台

20240807@2024LHAASO暑期学校

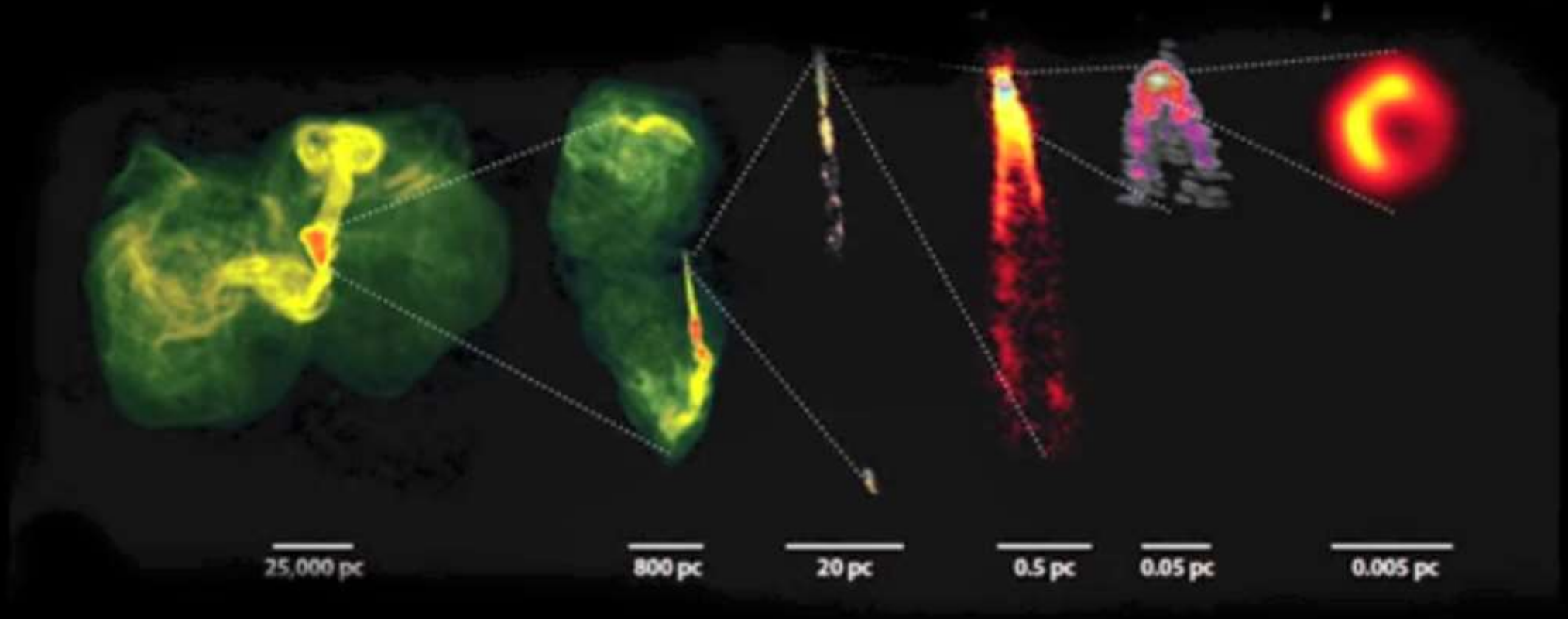
25,000 pc
800 pc
20 pc
0.5 pc
0.05 pc
0.005 pc

类星体发现

- 3C 273 （Schmidt 1963）

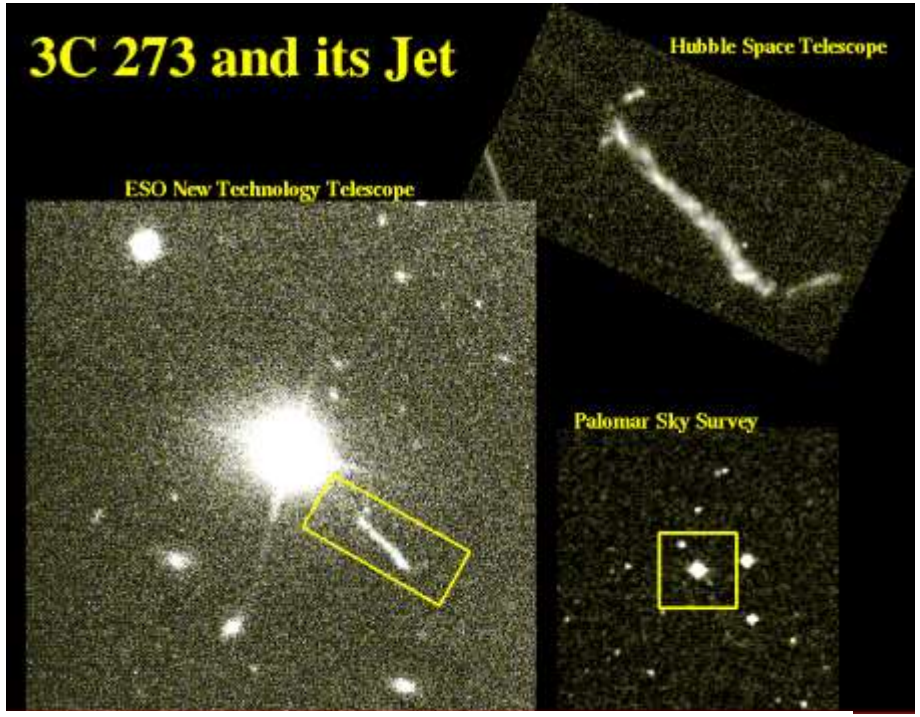

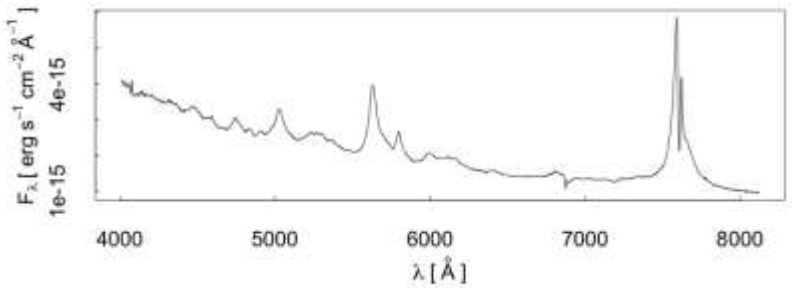

3C 273 : A STAR-LIKE OBJECT WITH LARGE RED-SHIFT

By Dr. M. SCHMIDT

Mount Wilson and Palomar Observatories, Carnegie Institution of Washington, California Institute of Technology, Pasadena

THE only objects seen on a 200-in. plate near the positions of the components of the radio source 3*C* 273 reported by Hazard, Mackey and Shimmins in the preceding article are a star of about thirteenth magnitude and a faint wisp or jet. The jet has a width of 1″–2″ and extends away from the star in position angle 43°. It is not visible within 11″ from the star and ends abruptly at 20″ from the star. The position of the star, kindly furnished by Dr. T. A. Matthews, is R.A. 12h 26m 33·35s ±0·04s, Decl. +2° 19′ 42·0″ ±0·5″ (1950), or 1″ east of component *B* of the radio source. The end of the jet is 1″ east of component *A*. The close correlation between the radio structure and the star with the jet is suggestive and intriguing.

Spectra of the star were taken with the prime-focus spectrograph at the 200-in. telescope with dispersions of 400 and 190 Å per mm. They show a number of broad emission features on a rather blue continuum. The most prominent features, which have widths around 50 Å, are, in order of strength, at 5632, 3239, 5792, 5032 Å. These and other weaker emission bands are listed in the first column of Table 1. For three faint bands with widths of 100–200 Å the total range of wave-length is indicated.

The only explanation found for the spectrum involves a considerable red-shift. A red-shift $\Delta\lambda/\lambda_0$ of 0·158 allows identification of four emission bands as Balmer lines, as indicated in Table 1. Their relative strengths are in agreement with this explanation. Other identifications based on the above red-shift involve the Mg II lines around 2798 Å, thus far only found in emission in the solar chromosphere, and a forbidden line of [O III] at 5007 Å. On this basis another [O III] line is expected at 4959 Å with a strength one-third of that of the line at 5007 Å. Its detectability in the spectrum would be marginal. A weak emission band suspected at 5705 Å, or 4927 Å reduced for red-shift, does not fit the wave-length. No explanation is offered for the three very wide emission bands.

It thus appears that six emission bands with widths around 50 Å can be explained with a red-shift of 0·158. The differences between the observed and the expected wave-lengths amount to 6 Å at the most and can be entirely understood in terms of the uncertainty of the measured wave-lengths. The present explanation is supported by observations of the infra-red spectrum communicated by Oke in a following article, and by the spectrum of another star-like object associated with the radio source 3*C* 48 discussed by Greenstein and Matthews in another communication.

Table 1. Wave-lengths and Identifications

λ	λ/1·158	λ_0	
3239	2797	2798	Mg II
4595	3968	3970	Hε
4753	4104	4102	Hδ
5032	4345	4340	Hγ
5200–5415	4490–4675		
5632	4864	4861	Hβ
5792	5002	5007	[O III]
6005–6190	5186–5345		
6400–6510	5527–5622		

The unprecedented identification of the spectrum of an apparently stellar object in terms of a large red-shift suggests either of the two following explanations.

(1) The stellar object is a star with a large gravitational red-shift. Its radius would then be of the order of 10 km. Preliminary considerations show that it would be extremely difficult, if not impossible, to account for the occurrence of permitted lines and a forbidden line with the same red-shift, and with widths of only 1 or 2 per cent of the wave-length.

(2) The stellar object is the nuclear region of a galaxy with a cosmological red-shift of 0·158, corresponding to an apparent velocity of 47,400 km/sec. The distance would be around 500 megaparsecs, and the diameter of the nuclear region would have to be less than 1 kiloparsec. This nuclear region would be about 100 times brighter optically than the luminous galaxies which have been identified with radio sources thus far. If the optical jet and component *A* of the radio source are associated with the galaxy, they would be at a distance of 50 kiloparsecs, implying a time-scale in excess of 10^5 years. The total energy radiated in the optical range at constant luminosity would be of the order of 10^{59} ergs.

Only the detection of an irrefutable proper motion or parallax would definitively establish 3*C* 273 as an object within our Galaxy. At the present time, however, the explanation in terms of an extragalactic origin seems most direct and least objectionable.

I thank Dr. T. A. Matthews, who directed my attention to the radio source, and Drs. Greenstein and Oke for valuable discussions.

Radio loud vs radio quite AGN

$$R \equiv \frac{f_{5GHz}}{f_{4400\,A}}$$

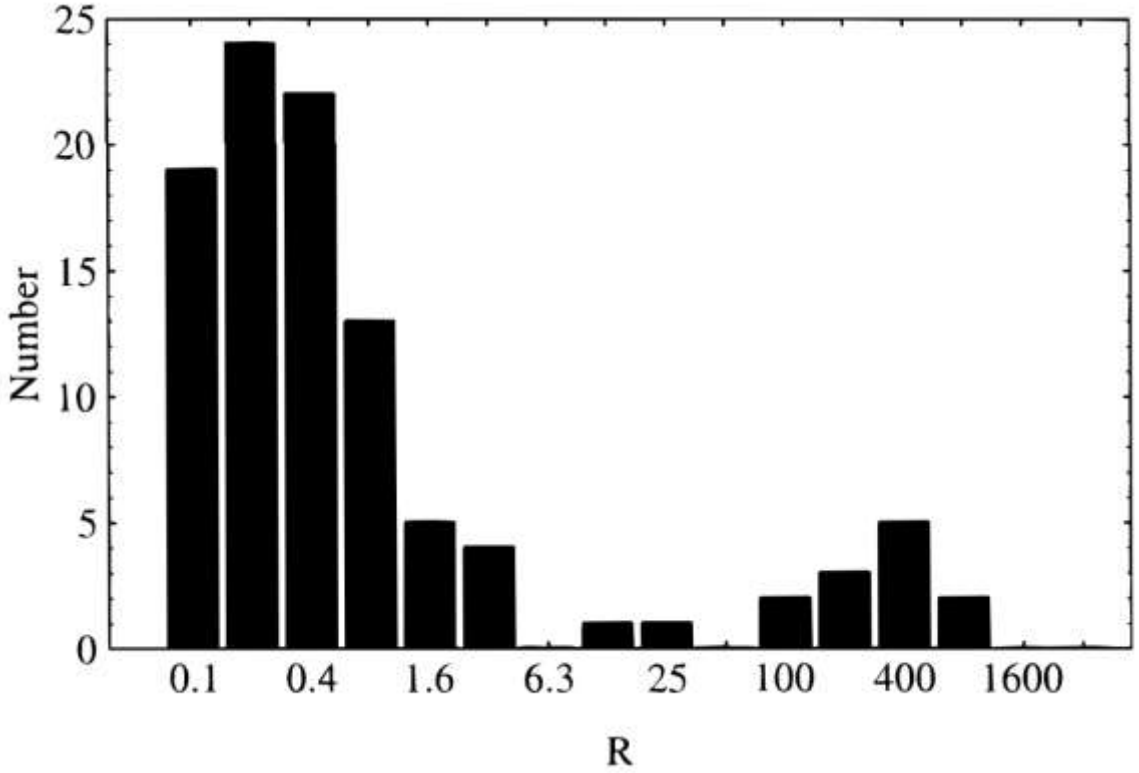

Palomar-Green (PG) quasars
Falcke et al. 1996

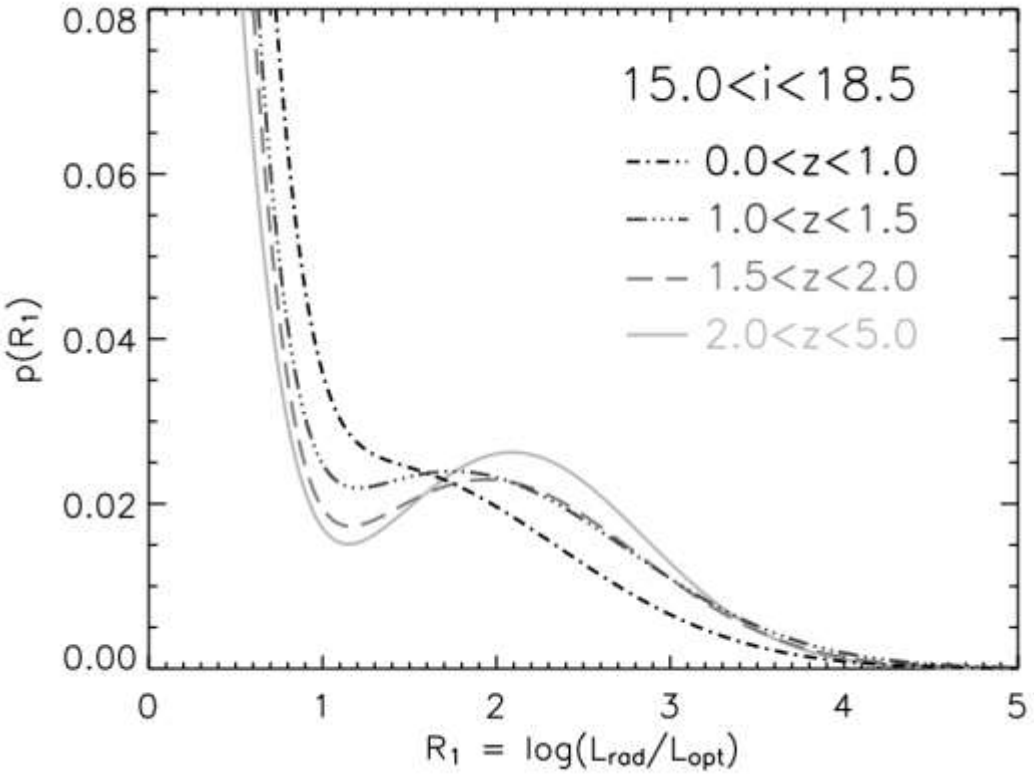

SDSS–FIRST sample
Baloković et al. 2012

活动星系核能谱分布

Radio loud
Radio quiet

Elvis et al. 1994
Shang et al. 2011

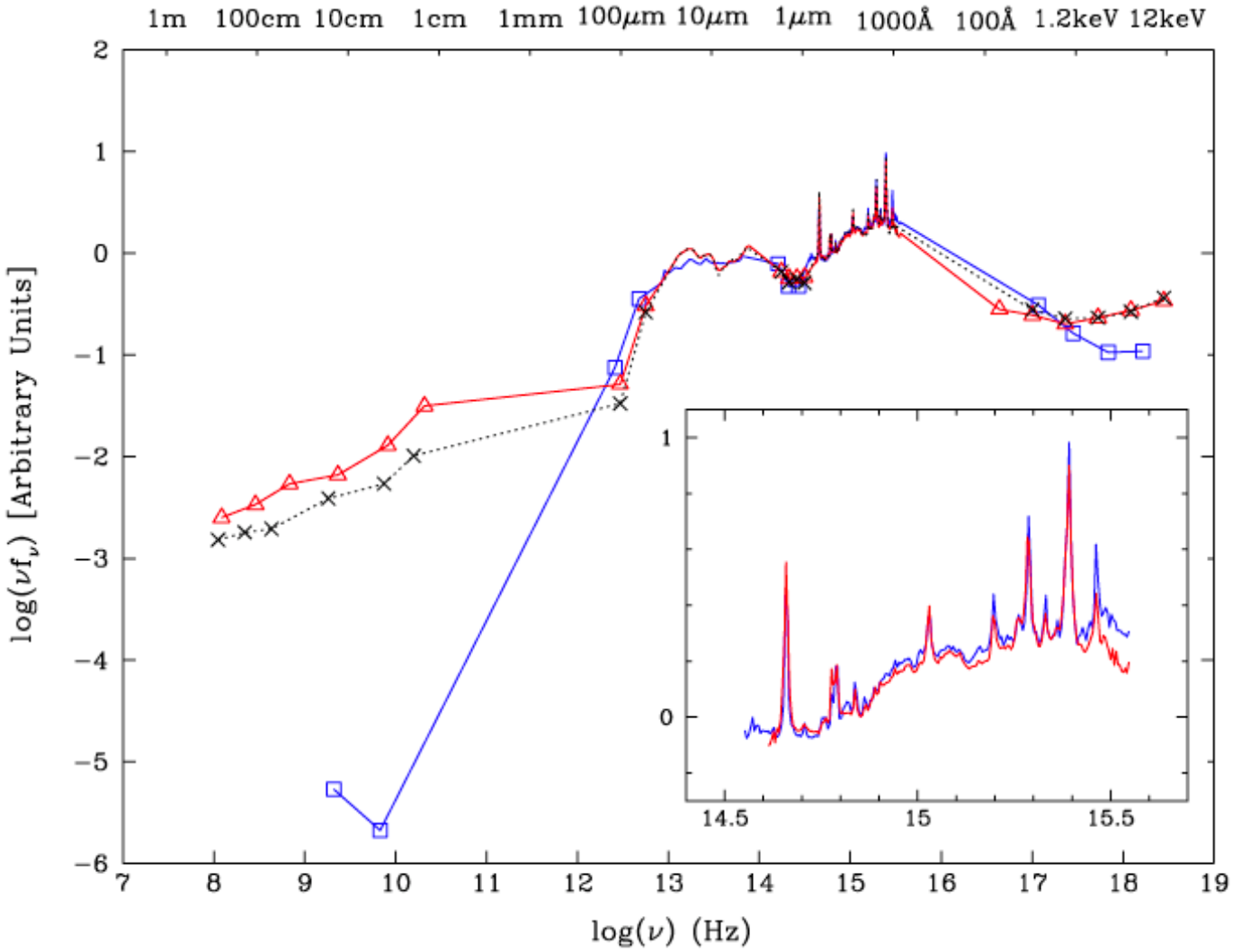

Active Galactic Nuclei

- Radio Quiet
- ~90%
- No jet

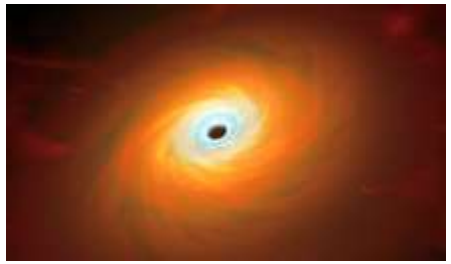

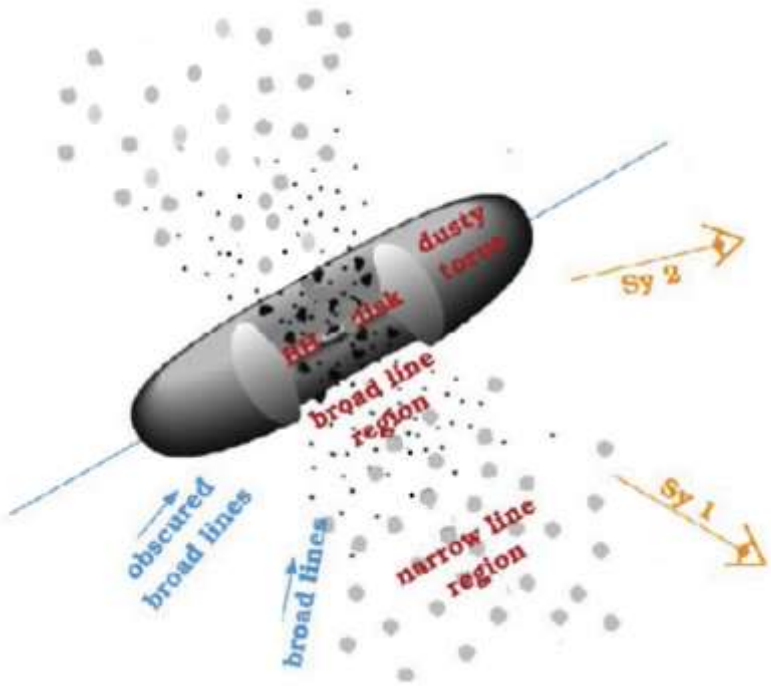

- Radio Loud
- ~10%
- Jet

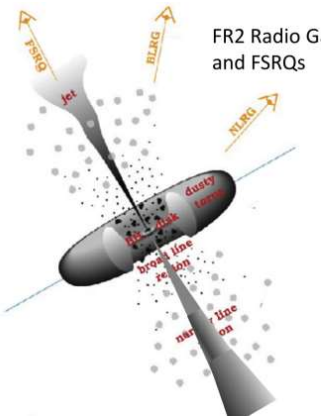

AGN辐射

- 吸积盘
- 宽窄线区
- 尘埃环

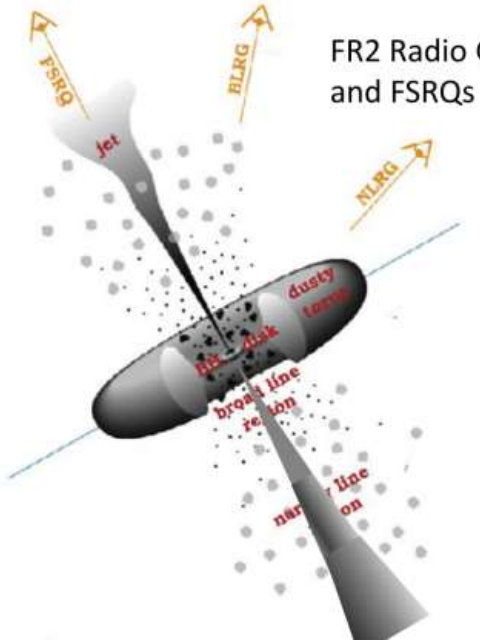

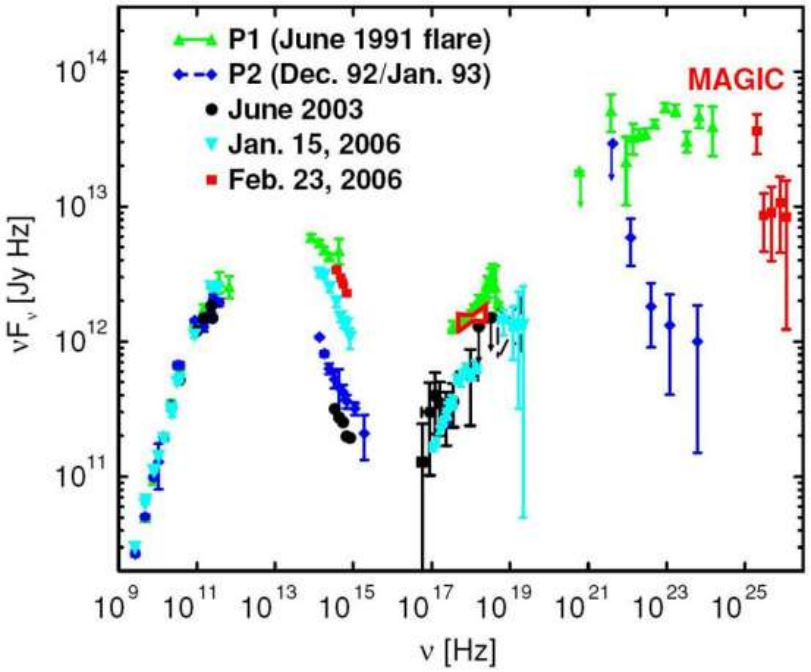

- 喷流：非热辐射

  射电、光学、X-ray、伽玛射线

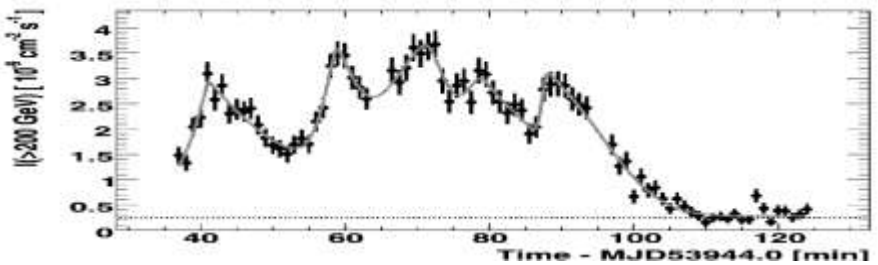

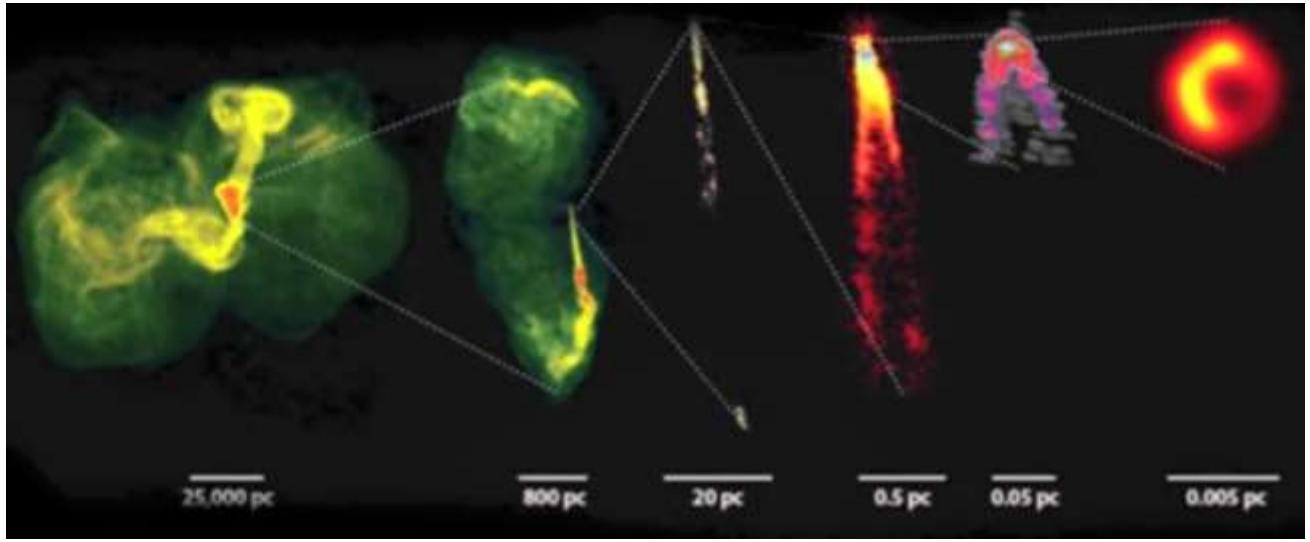

AGN jet Heber Curtis (1918)

Exceedingly bright; the sharp nucleus shows well in 5m exposure. The brighter central portion is about 0'.5 in diameter, and the total diameter about 2'; nearly round. No spiral structure is discernible. A curious straight ray lies in a gap in the nebulosity in p.a. 20°, apparently connected with the nucleus by a thin line of matter. The ray is brightest at its inner end, which is 11" from the nucleus. 20 s.n.

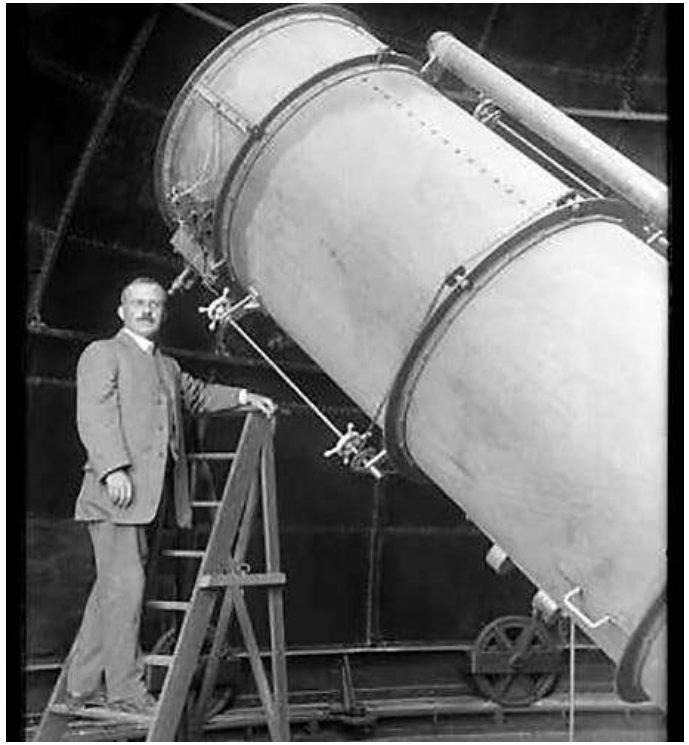

AGN jet Heber Curtis (1918)

Exceedingly bright; the sharp nucleus shows well in 5m exposure. The brighter central portion is about 0.5 in diameter, and the total diameter about 2′; nearly round. No spiral structure is discernible. A curious straight ray lies in a gap in the nebulosity in p.a. 20°, apparently connected with the nucleus by a thin line of matter. The ray is brightest at its inner end, which is 11″ from the nucleus. 20 s.n.

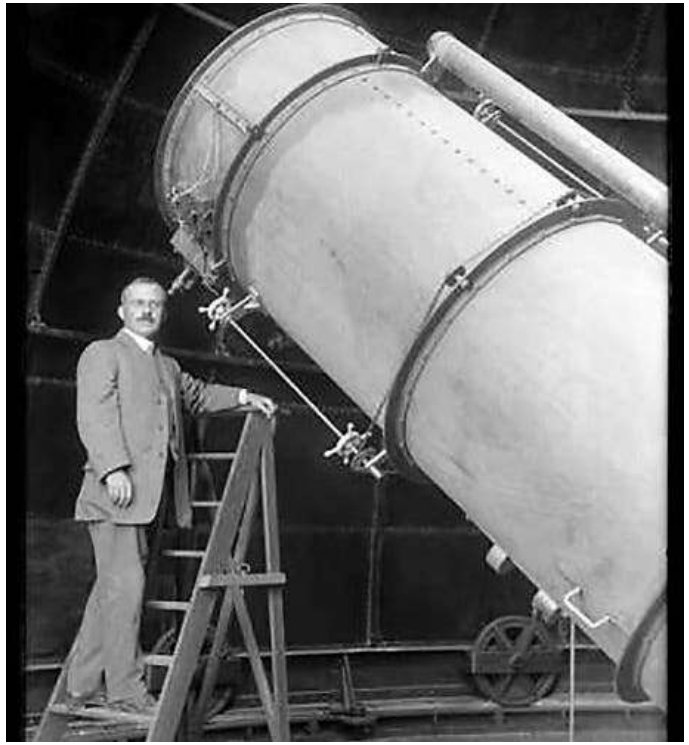

AGN jet Heber Curtis (1918)

Exceedingly bright; the sharp nucleus shows well in 5m exposure. The brighter central portion is about 0'.5 in diameter, and the total diameter about 2'; nearly round. No spiral structure is discernible. A curious straight ray lies in a gap in the nebulosity in p.a. 20°, apparently connected with the nucleus by a thin line of matter. The ray is brightest at its inner end, which is 11" from the nucleus. 20 s.n.

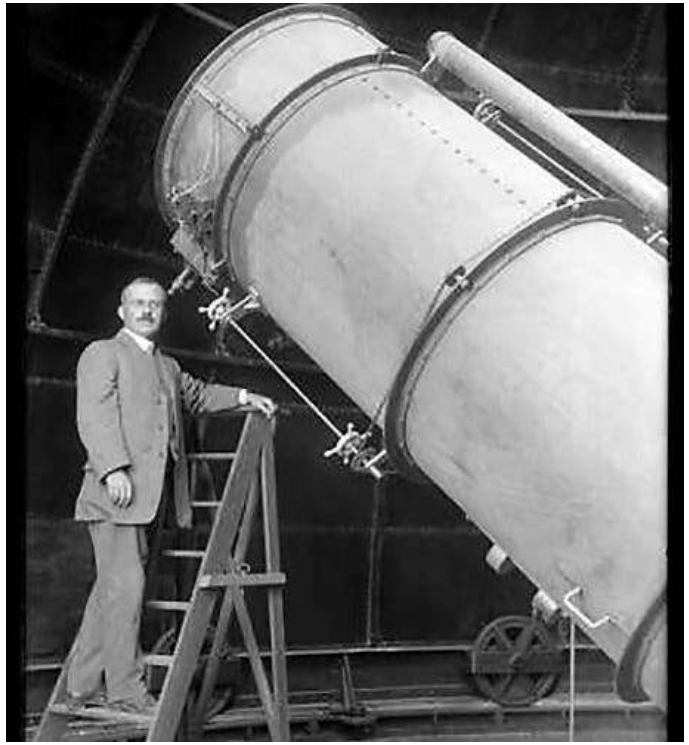

M87喷流与黑洞

Astrophysical jets

- Various astrophysical systems
- Jet process is universal

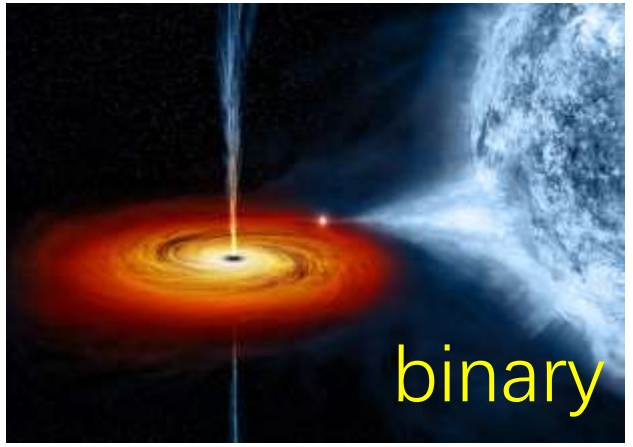

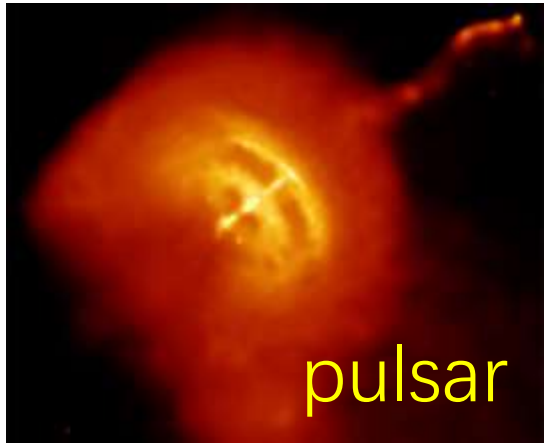

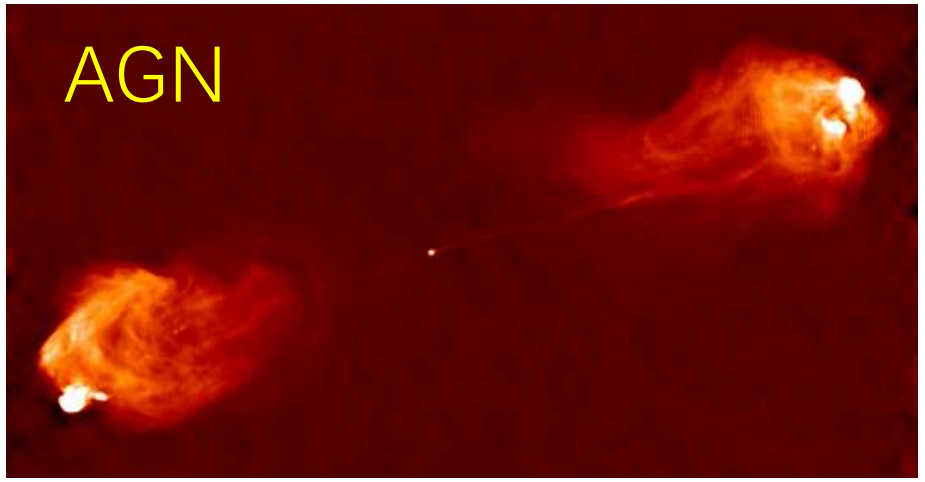

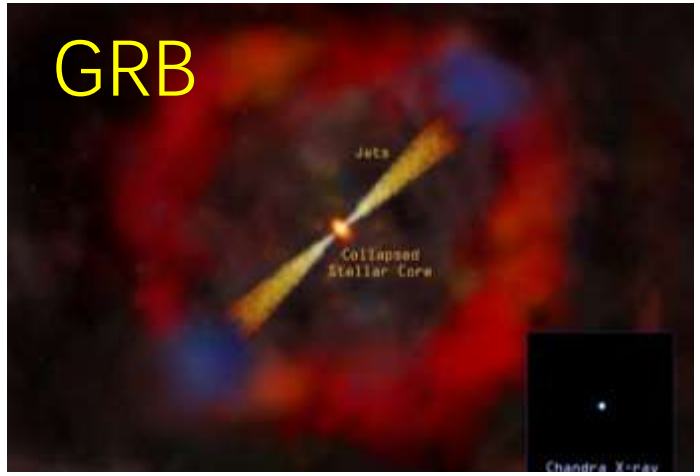

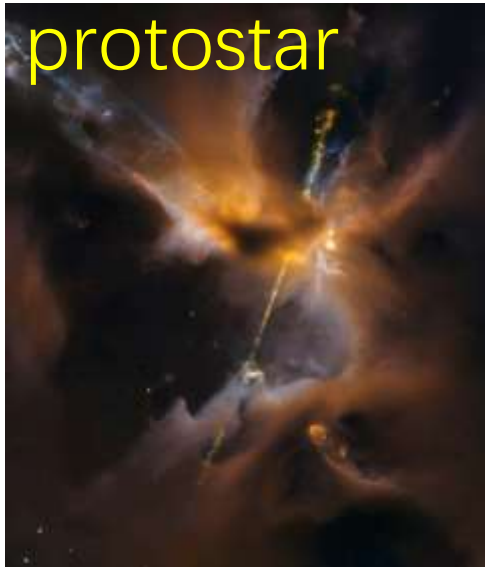

喷流：宇宙生态系统

- 黑洞反馈
- 喷流和风的作用

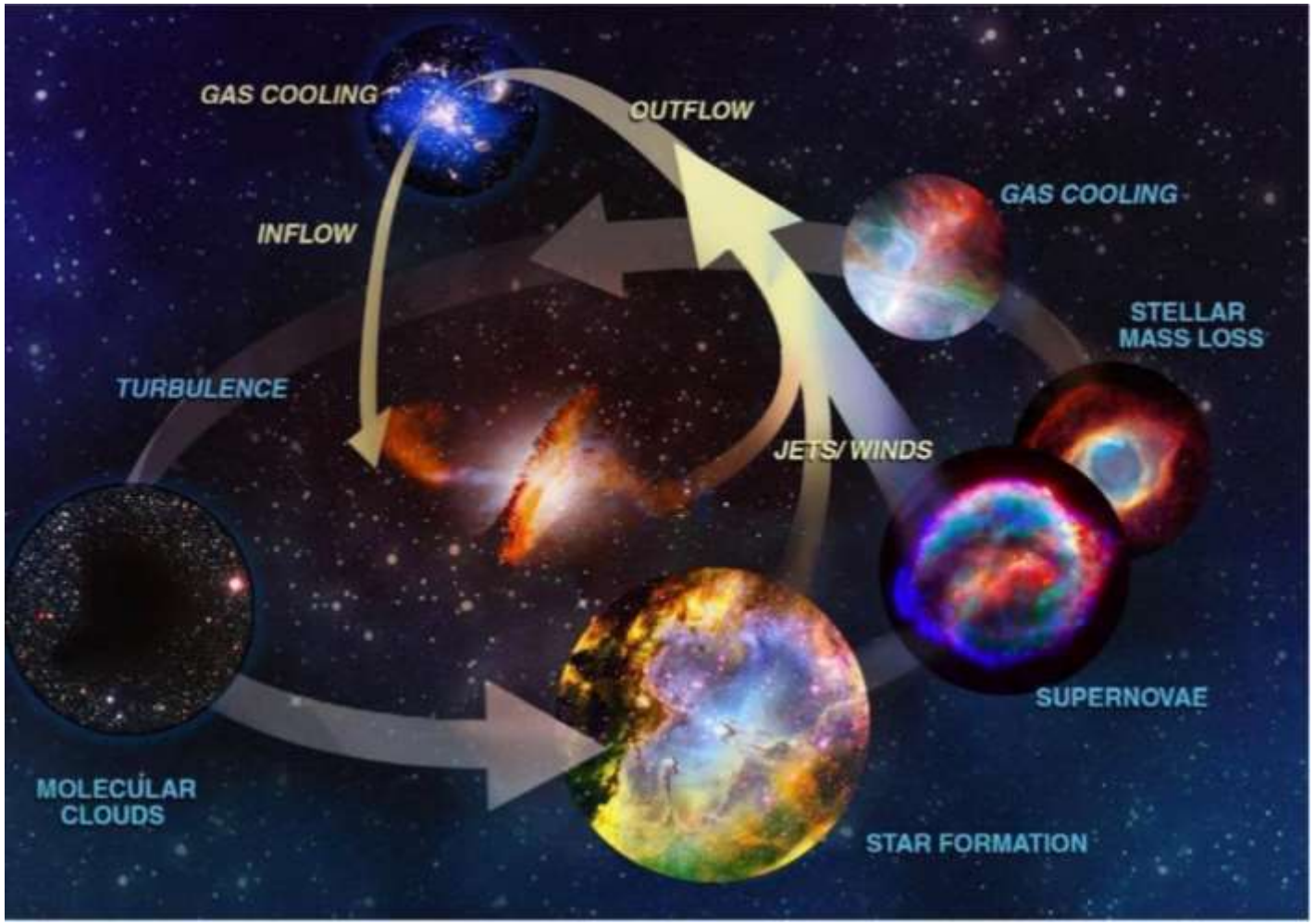

美国国家科学院，Astro2020

喷流：高能天体物理

- 黑洞

  喷流物理

- 高能宇宙线

- 高能中微子

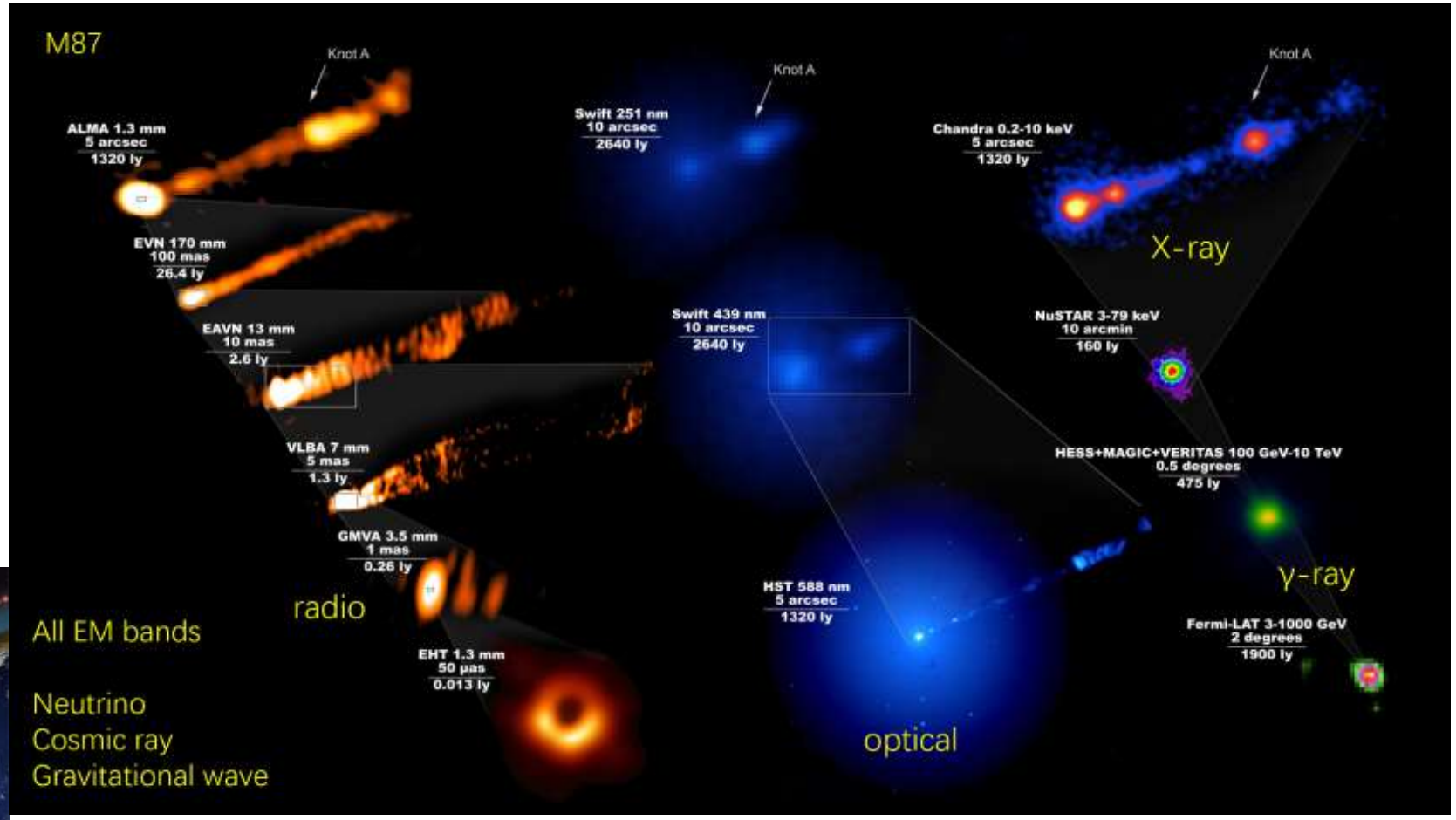

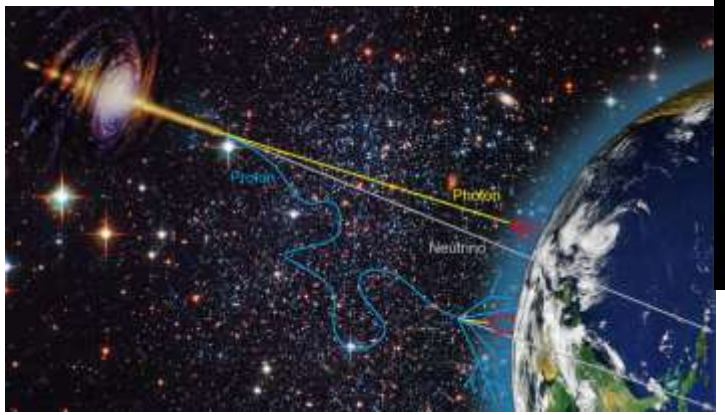

AGN jets

- Large size (3C 236)

  $z = 0.1$

  $M_\bullet \sim 3\times10^8 M_\odot$

  $D = 2.3\ \mathrm{Mpc} \approx 10^{11} R_S$

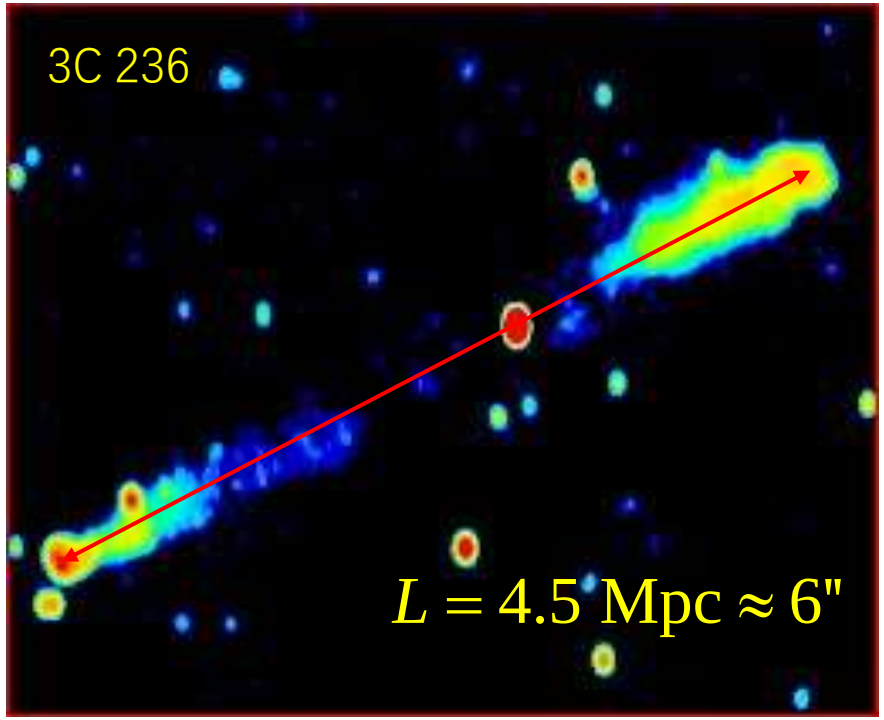

- Superluminal motion

  velocity reaches $v_{app} > 50c$

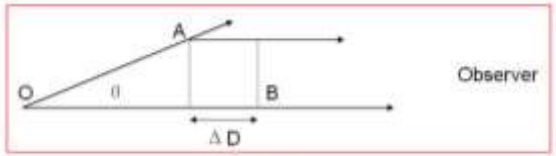

$$\Delta D/c = \Delta t - \beta \Delta t \cos\theta$$

$$\beta_{app} \equiv \frac{v_{app}}{c} = \frac{1}{c}\frac{OA\sin\theta}{\Delta t - \beta\Delta t\cos\theta} = \frac{\beta\sin\theta}{1-\beta\cos\theta}$$

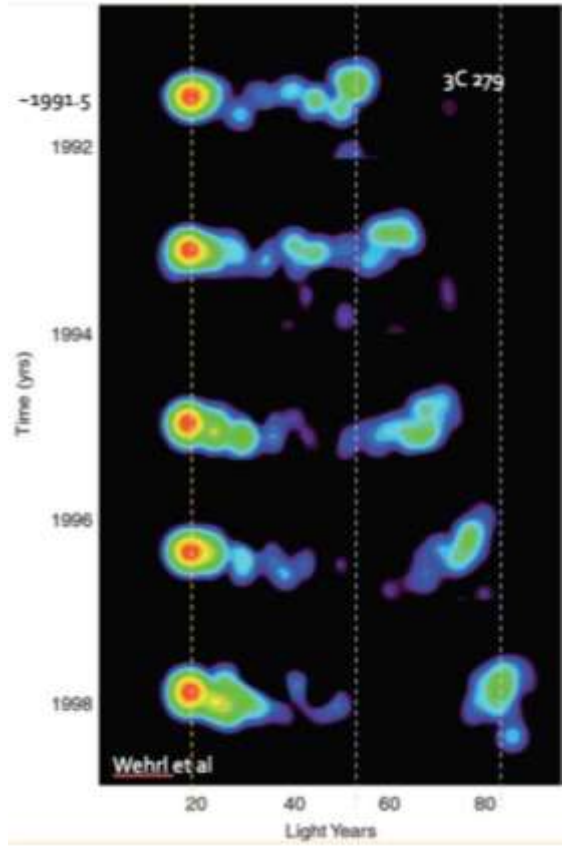

- Polarization
- Variability
- Broadband emission……

AGN jets: problems

- Jet launching, acceleration and collimation
- Jet propagation, energy dissipation and radiative processes
- …

The key role: B !

- From observations
- From theoretical arguments

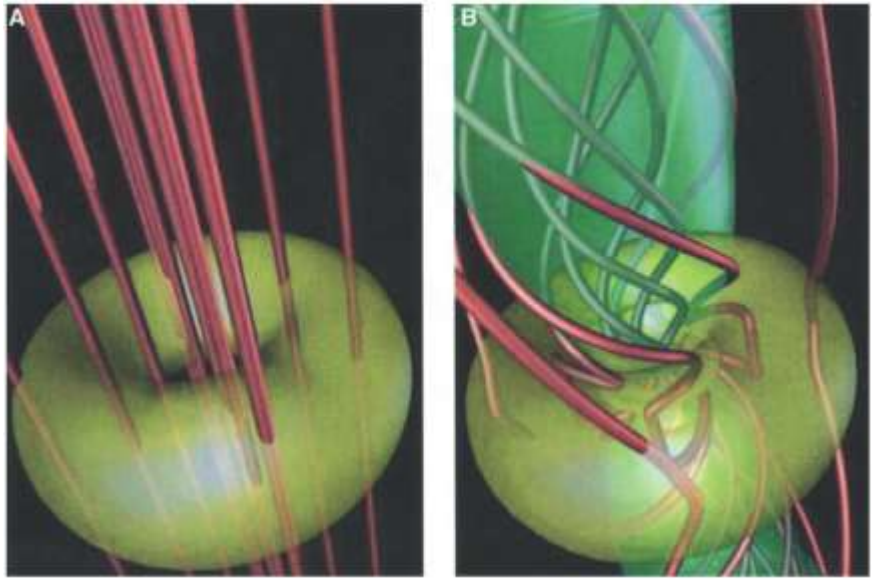

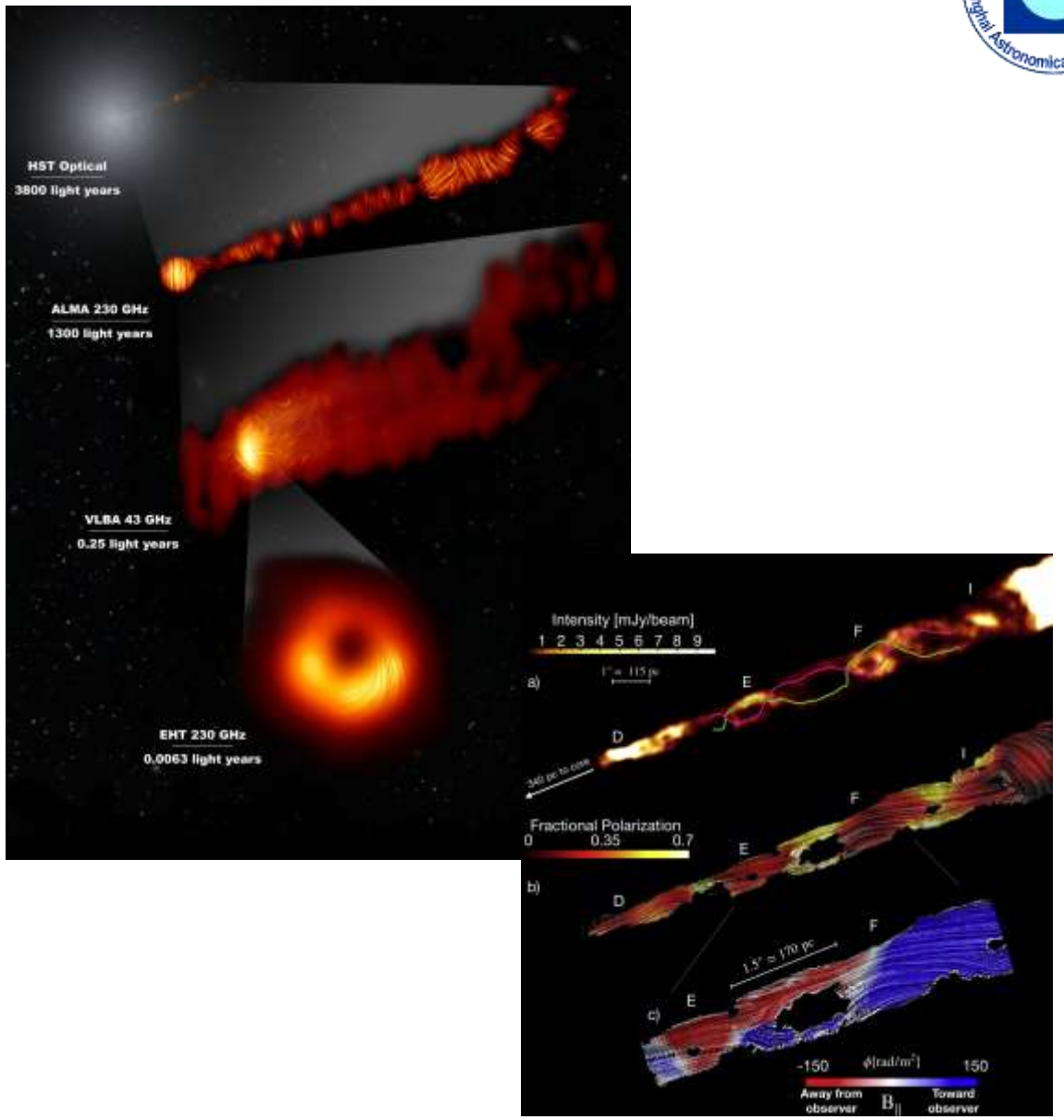

Jet launching

$$\sigma\left(\vec{E}+\vec{v}\times\vec{B}\right)=\vec{j}$$

Conductivity

$\sigma \to +\infty$

$$\begin{aligned}\frac{d}{dt}\int_S \mathbf{B}\cdot d\mathbf{S} &= \int_S \frac{\partial \mathbf{B}}{\partial t}\cdot d\mathbf{S}+\int_C \mathbf{B}\cdot(\mathbf{v}\times d\mathbf{l})\\ &= \int_S \frac{\partial \mathbf{B}}{\partial t}\cdot d\mathbf{S}+\int_C (\mathbf{B}\times\mathbf{v})\cdot d\mathbf{l}\\ &= -\int_S \nabla\times\mathbf{E}\cdot d\mathbf{S}+\int_S [\nabla\times(\mathbf{B}\times\mathbf{v})]\cdot d\mathbf{S}\\ &= -\int_S [\nabla\times(\mathbf{E}+\mathbf{v}\times\mathbf{B})]\cdot d\mathbf{S}\\ &= -\int_C (\mathbf{E}+\mathbf{v}\times\mathbf{B})\cdot d\mathbf{l}\\ &= 0.\end{aligned}$$

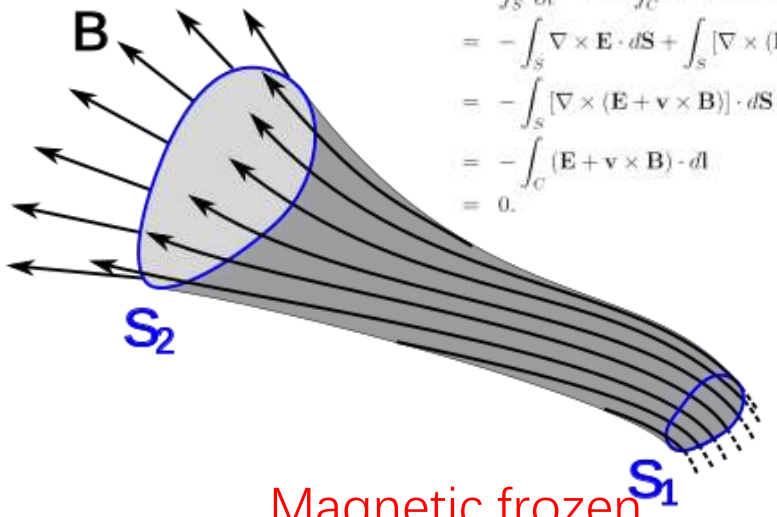

Magnetic frozen

Effective potential

$$\Phi_e = -\frac{GM}{r}-\frac{1}{2}\Omega^2 R^2$$

$$\Omega = \sqrt{\frac{GM}{R_0^3}}$$

$$\left.\frac{\partial^2\Phi_e}{\partial s^2}\right|_{s=0} = \Omega^2\left(\sin^2\theta-3\cos^2\theta\right)$$

$$\theta_c = \tan^{-1}\left(\sqrt{3}\right)=60°$$

Magnetic field line

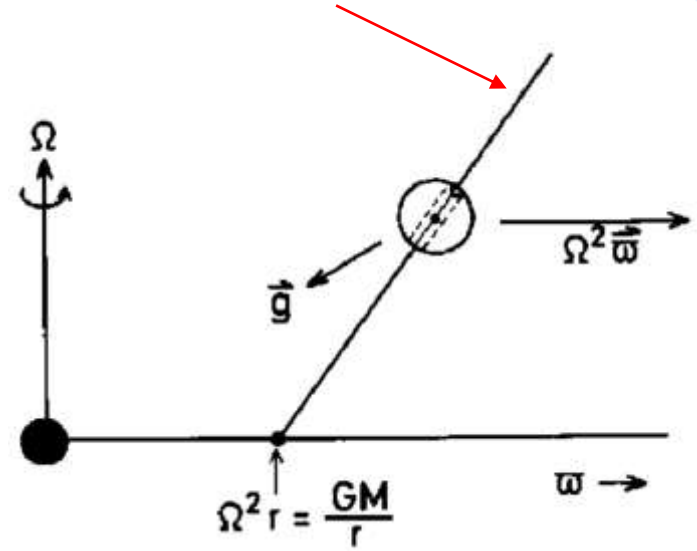

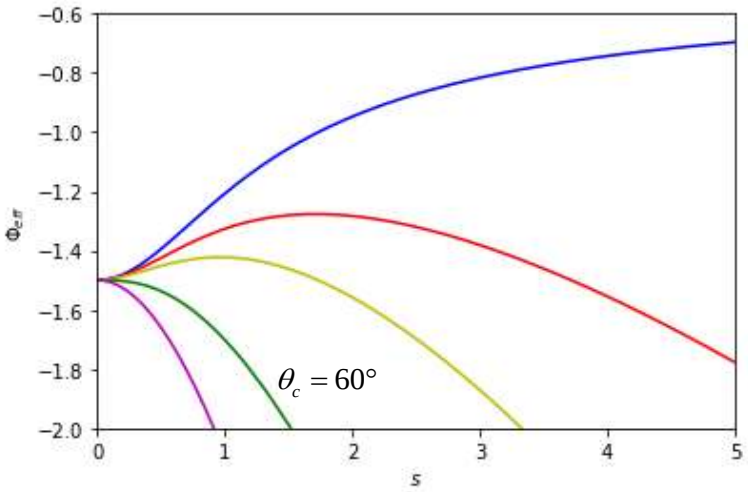

Jet acceleration and collimation

$$F_L = j \times B + \rho_e E$$

$$= -\frac{B^2}{4\pi}\frac{\hat{R}_B}{R_B} + \nabla_\perp\left(\frac{B^2}{8\pi}\right) + \frac{1}{4\pi}(\nabla \cdot \mathbf{E})\,\mathbf{E}$$

magnetic pressure gradient

$$= \underbrace{\mathbf{j}_p \times \mathbf{B}_p}_{1,\hat{\phi}} + \underbrace{(\mathbf{j}_p \times \mathbf{B}_\phi)_{B_p}\hat{B}_p}_{2,\hat{B}_p} + \underbrace{(\mathbf{j}_p \times \mathbf{B}_\phi)_E \hat{E}}_{3,\hat{E}} + \underbrace{\mathbf{j}_\phi \times \mathbf{B}_p}_{4,\hat{E}} + \underbrace{\rho_e \mathbf{E}}_{5,\hat{E}}$$

pinch

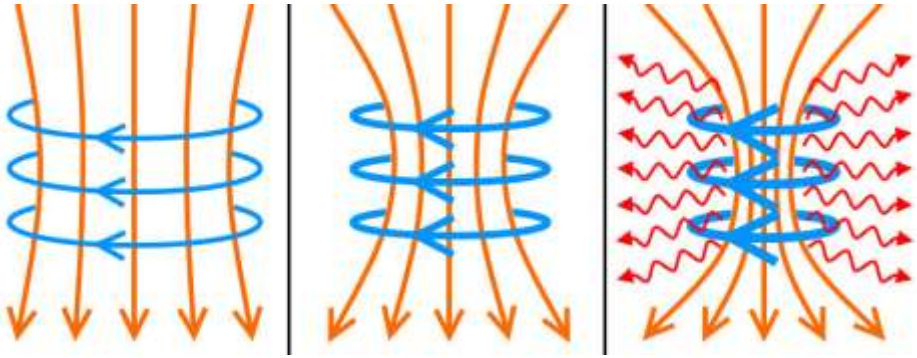

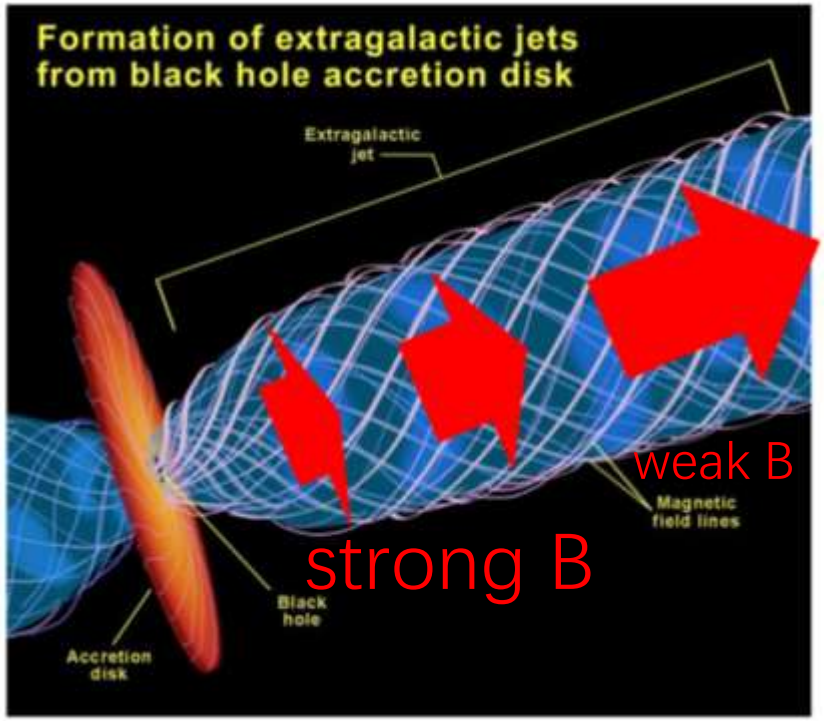

黑洞：弯曲的时空、无实体表面

如何驱动喷流？

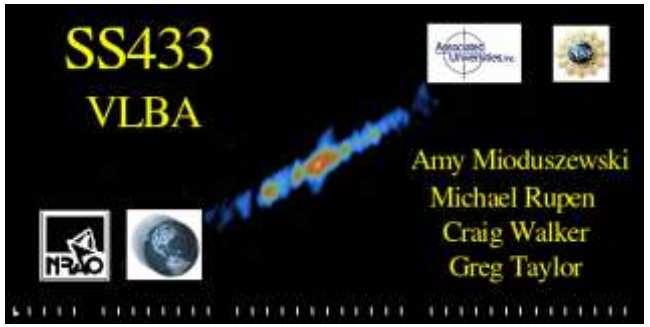

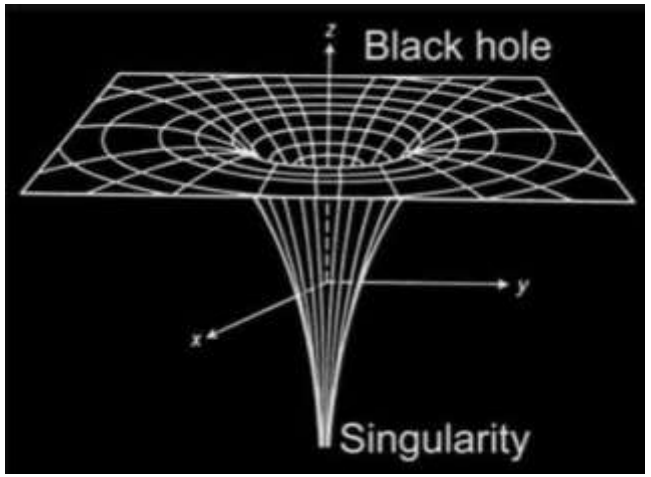

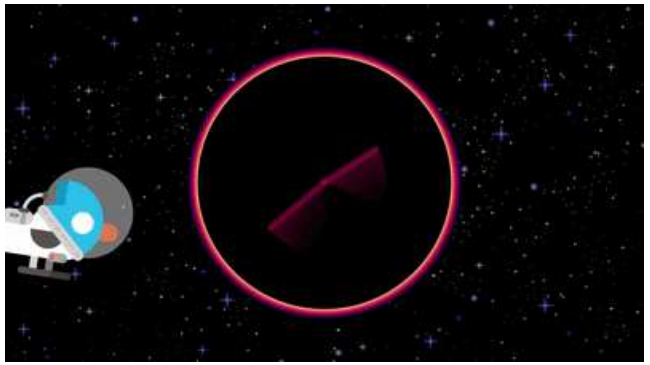

从法拉第转盘到黑洞“发电机”

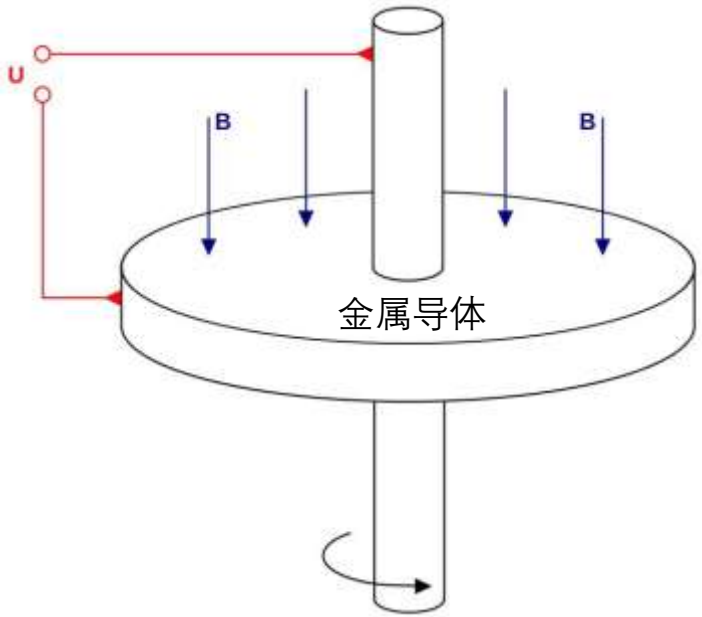

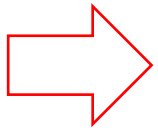

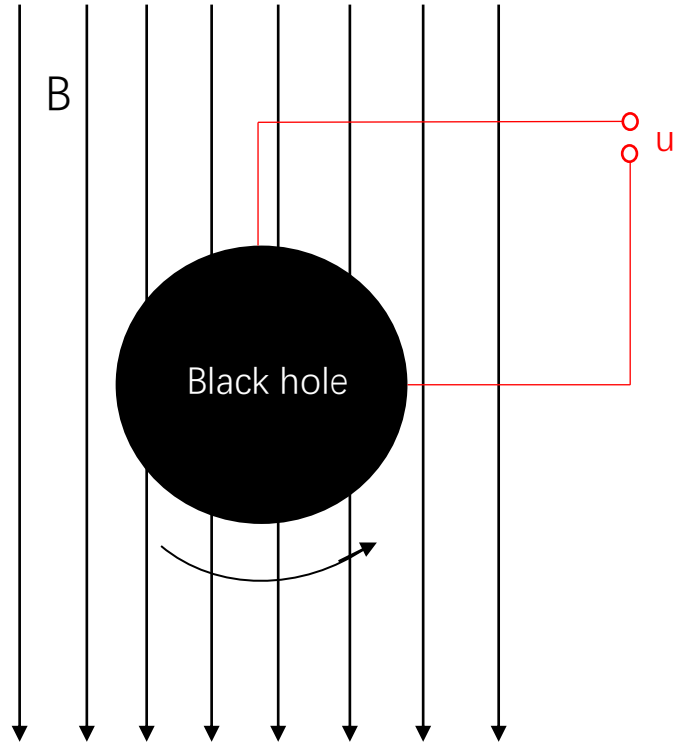

平直时空电磁学

弯曲时空电磁学

Magnetic driven

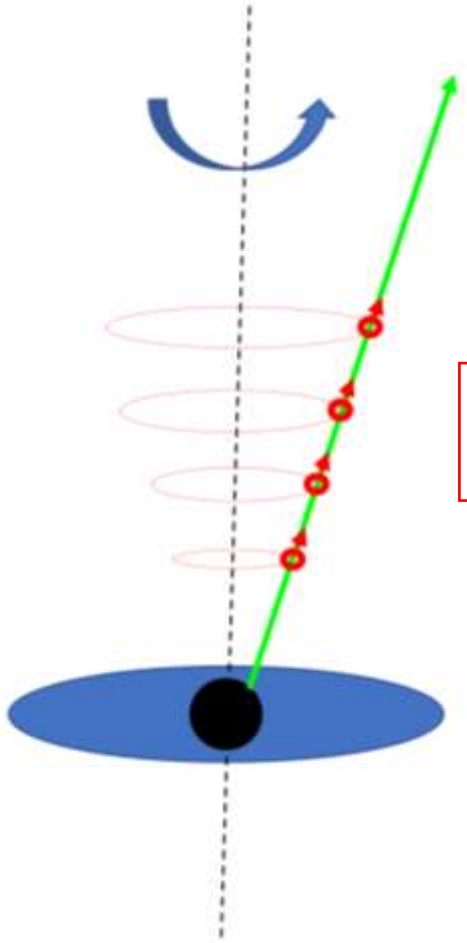

Black hole spin/accretion
Magnetic field rotating

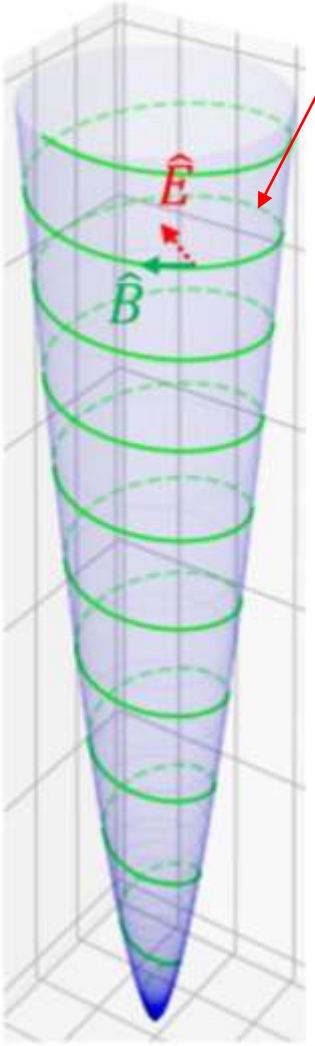

Magnetic
stream surface

$$\mathbf{B} = \frac{1}{r^2\sin\theta}\frac{\partial\Psi}{\partial\theta}\hat{\mathbf{r}} - \frac{1}{r\sin\theta}\frac{\partial\Psi}{\partial r}\hat{\boldsymbol{\theta}} + \frac{\Phi}{r\sin\theta}\hat{\boldsymbol{\phi}}$$

$$\Psi = r\sin\theta A_\phi \qquad \Phi = r\sin\theta B_\phi \qquad \mathbf{B} = \nabla\times\mathbf{A}$$

$$\frac{\mathbf{j}}{\sigma_\parallel} = \mathbf{E} + \mathbf{v}\times\mathbf{B} \xrightarrow{\text{ideal MHD}} 0$$

$$\mathbf{E} = -\Omega\nabla\Psi = -\Omega r\sin\theta\hat{\boldsymbol{\phi}}\times\mathbf{B}$$

$$\mathbf{v} = \Omega r\sin\theta\hat{\boldsymbol{\phi}} + \kappa\mathbf{B}$$

$$\rho(\mathbf{u}\cdot\nabla)\mathbf{u} = \rho_e\mathbf{E} + \mathbf{j}\times\mathbf{B}$$

$$\nabla\cdot(\rho\mathbf{u}) = 0$$

$$\mathbf{u} = \Gamma\mathbf{v}$$

conserved qualities

$$(\mathbf{B}\cdot\nabla\Psi = 0)$$

$$4\pi\rho\Gamma\kappa = \eta(\Psi)$$

mass

$$\Gamma - \frac{B_\phi\Omega R}{\eta} = \mathcal{E}(\Psi)$$

energy

$$R\Gamma v_\phi - \frac{RB_\phi}{\eta} = \mathcal{L}(\Psi)$$

angular momentum

$\hat{B}$

Moving eq.

Stream surface projection:
energy, angular momentum conservation

Radial projection: jet shape

$\hat{E}$

$$\frac{\partial^2\Psi}{\partial r^2} + \frac{1}{r^2}\frac{\partial^2\Psi}{\partial\theta^2} - \frac{\cot\theta}{r^2}\frac{\partial\Psi}{\partial\theta}$$

$$+\Phi'\Phi - \left\{\frac{\Omega'}{\Omega}\left[\left(\frac{\partial\Psi}{\partial r}\right)^2 + \left(\frac{1}{r}\frac{\partial\Psi}{\partial\theta}\right)^2\right] + \frac{\partial^2\Psi}{\partial r^2} + \frac{2}{r}\frac{\partial\Psi}{\partial r} + \frac{1}{r^2}\frac{\partial^2\Psi}{\partial\theta^2} + \frac{\cot\theta}{r^2}\frac{\partial\Psi}{\partial\theta}\right\}(\Omega r\sin\theta)^2 = 0$$

the pulsar equation

磁主导喷流解析模型-典型物理量

- 喷流轮廓 $R = C_2^{-1/2} \Psi^{1/2} z^{1-\nu/2}$
- 磁场结构 $B_p \simeq \frac{2\Psi}{R^2} \simeq B_0 \left(\frac{z}{R_0}\right)^{-2+\nu}$

$$B_\phi \simeq -\frac{2\Omega\Psi}{R} \simeq B_0 \frac{\Omega R_0}{c\sqrt{C_2}} \left(\frac{z}{R_0}\right)^{-1+\nu/2}$$

- 速度分布

$$v\Gamma \propto \frac{\Omega R_0}{\sqrt{C_2}} \left(\frac{z}{R_0}\right)^{1-\nu/2}$$

$$v_\phi = \Omega r \sin\theta \frac{B_p^2}{B^2} \approx \frac{\Omega R}{1+(\Omega R)^2},$$

$$v_p = -\Omega r \sin\theta \frac{B_\phi B_p}{B^2} \approx \frac{(\Omega R)^2}{1+(\Omega R)^2},$$

- 转折1 (阿尔文面)

$$z_{t1} \approx R_0 \left(\frac{c\sqrt{C_2}}{\Omega R_0}\right)^{2/(2-\nu)}$$

- 转折2 (磁能-动能主导)

$$z_{t2} \approx R_0 \left(\frac{c\sqrt{C_2}}{\Omega R_0}\sigma_0\right)^{2/(2-\nu)}$$

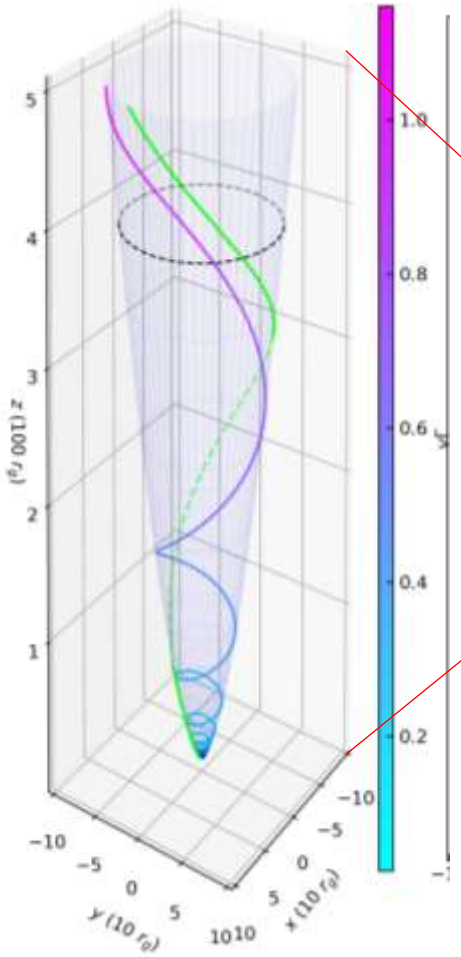

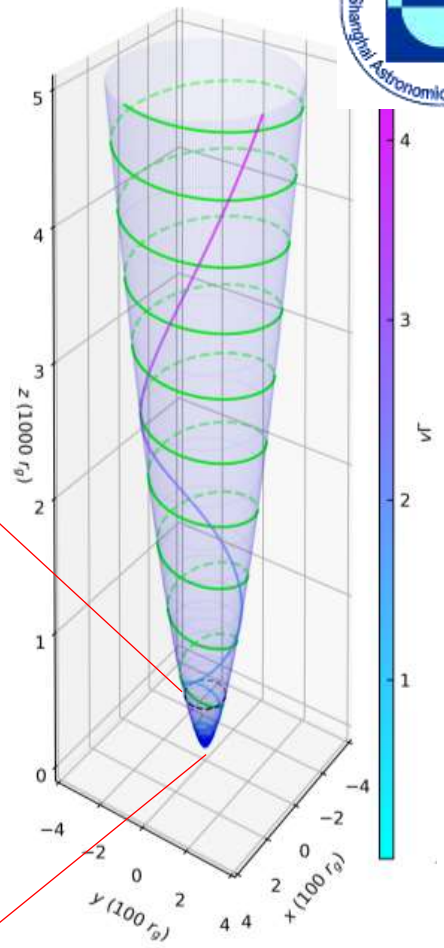

BH jet a=0.1

Chen & Zhang 2021

磁主导喷流解析模型

磁主导	磁主导	动能主导
抛物线轮廓	抛物线轮廓	锥形轮廓
逐渐加速	逐渐加速	均速或减速
非相对论性速度	相对论性速度	(非)相对论性速度
环向速度主导	极向速度主导	极向速度主导
极向磁场主导	环向磁场主导	环向磁场主导

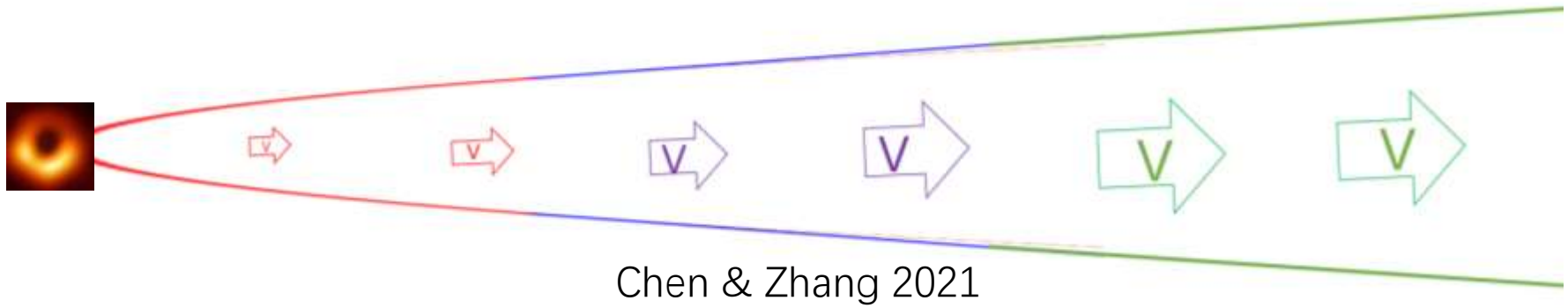

Chen & Zhang 2021

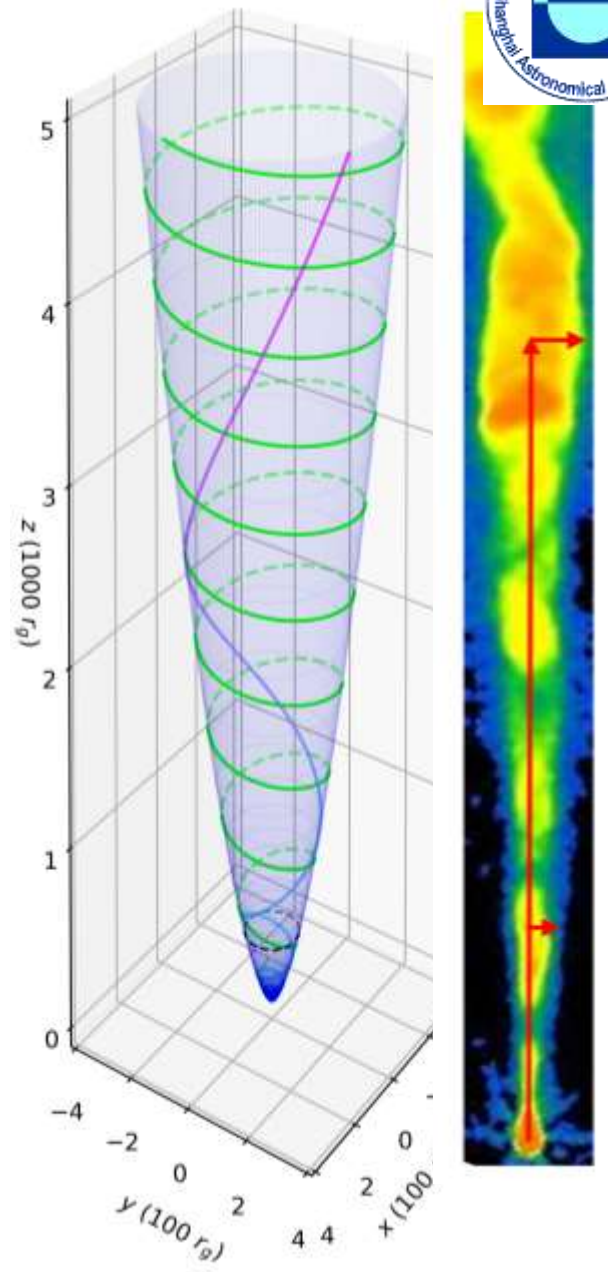

Is relativistic jet driven by black hole?

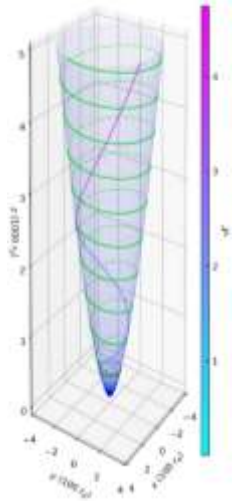

GRMHD

- BZ/BP

$$\eta = \frac{P_{jet}}{\dot{M}c^2}$$

$$\langle \eta \rangle \approx 150\%$$

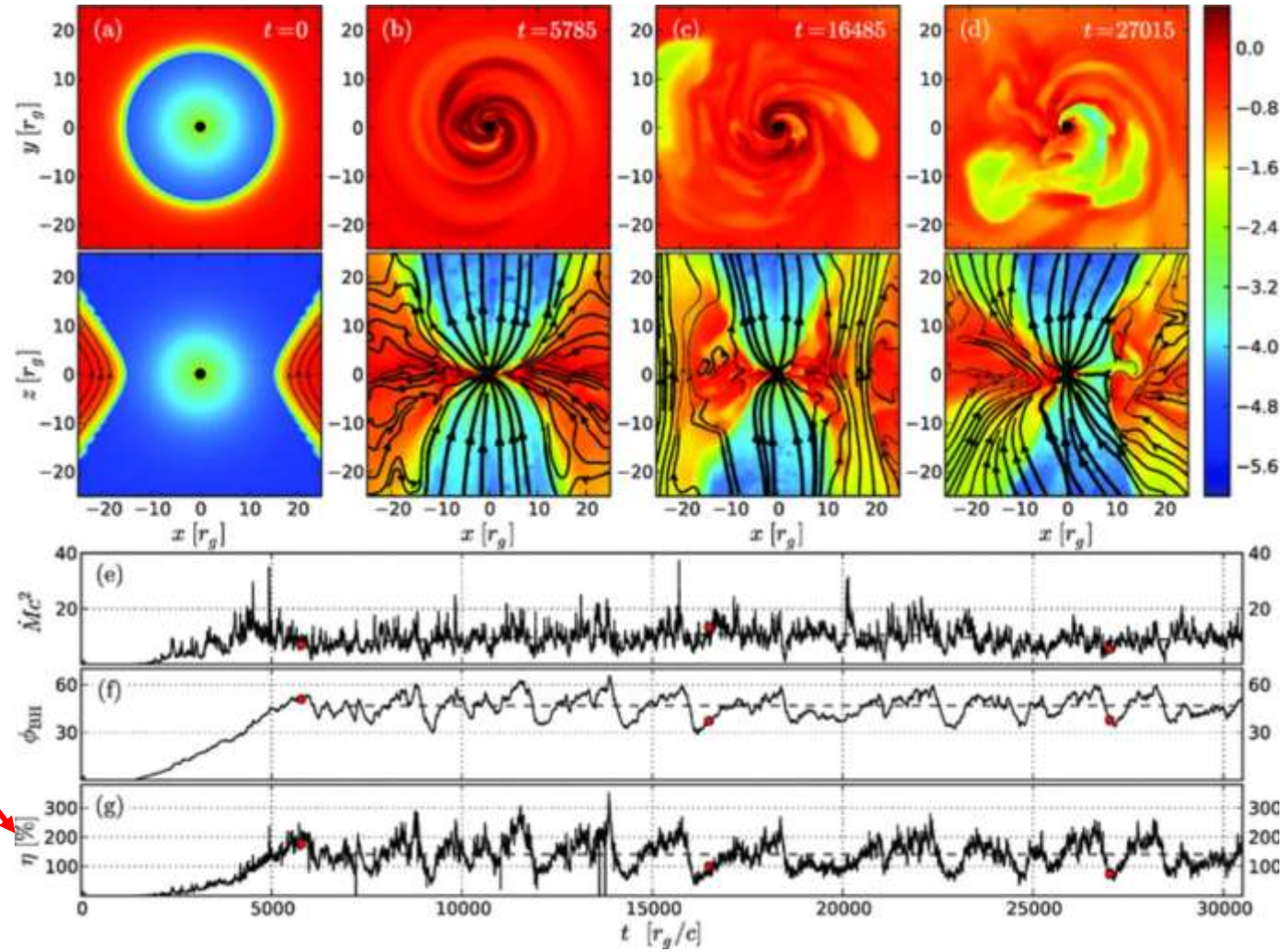

Tchekhovskoy et al. 2011

Jet power

- Jet power > accretion power

$$\eta > 1$$

- Accretion disk driven ☹
- Black spin driven ☺

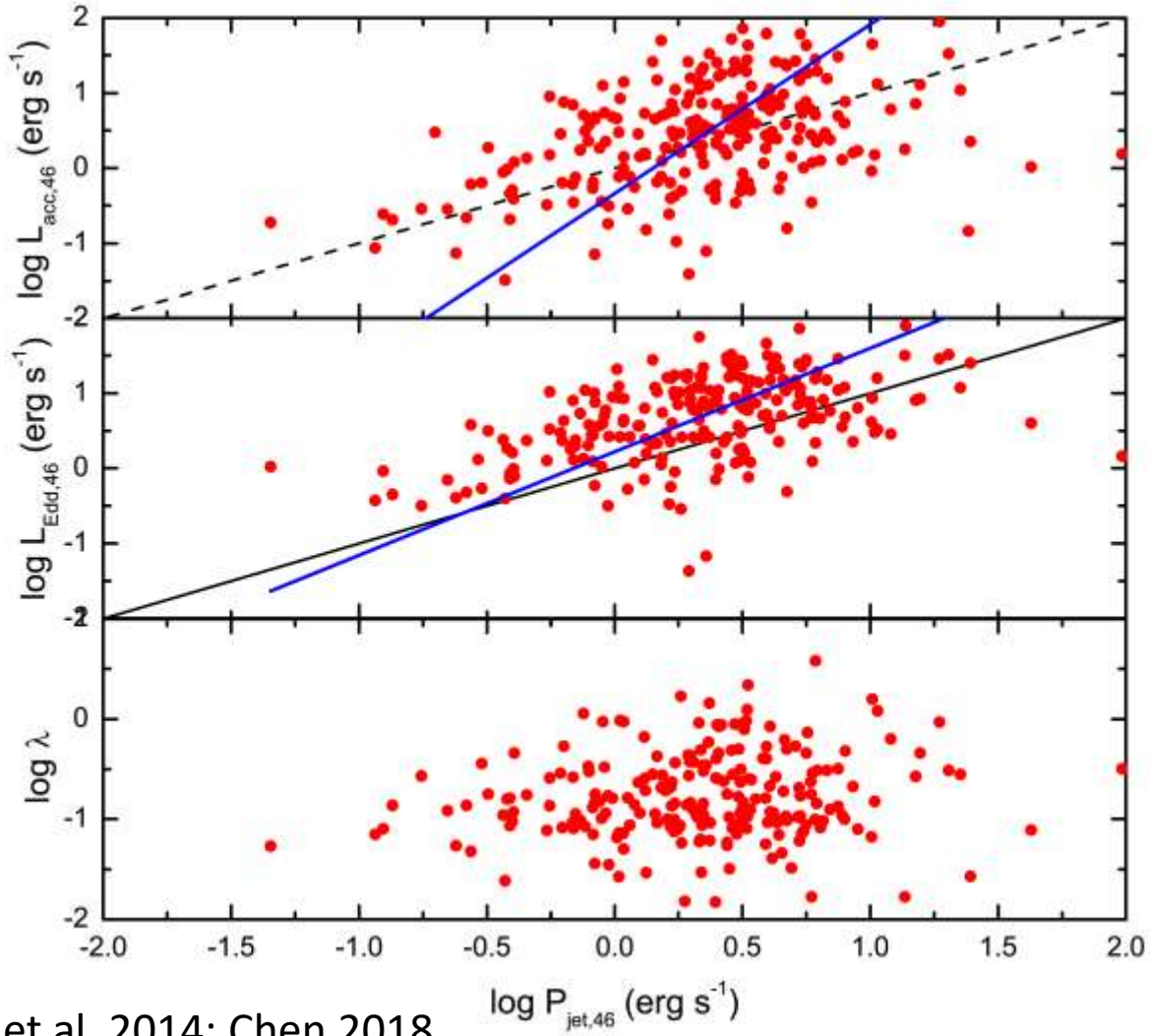

Ghisellini et al. 2014; Chen 2018

射电核-核移

- 核位置：频率依赖
- 同步辐射光深效应
- 磁场

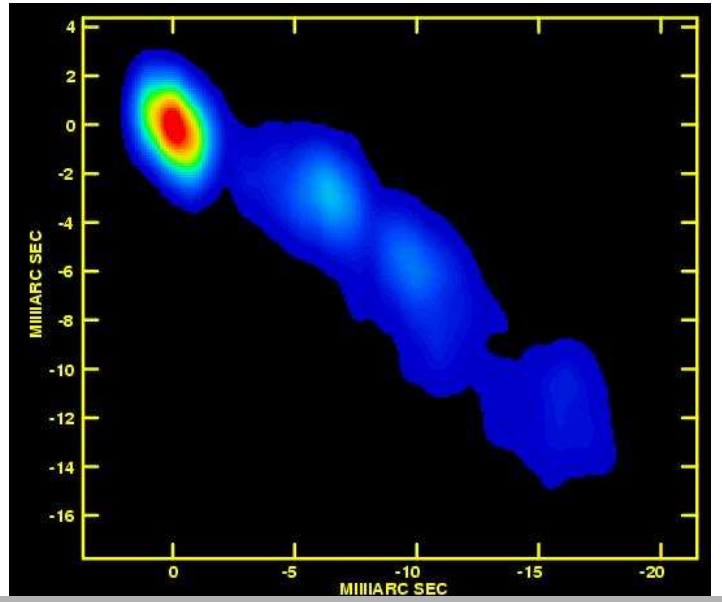

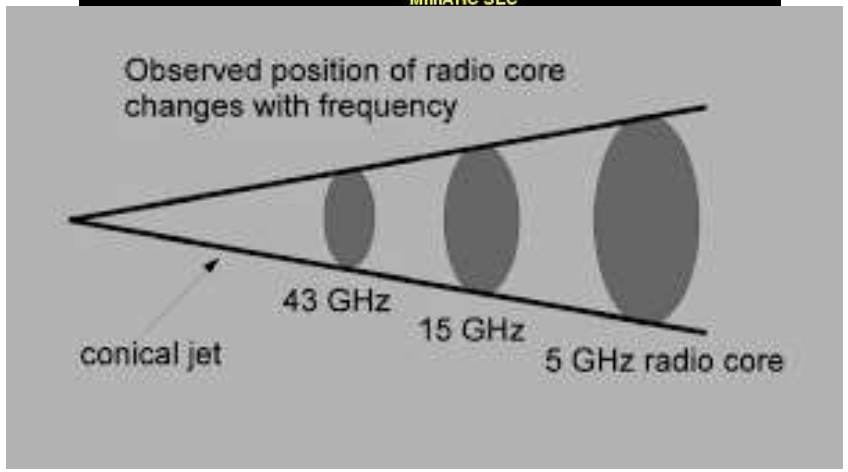

平谱

光学厚

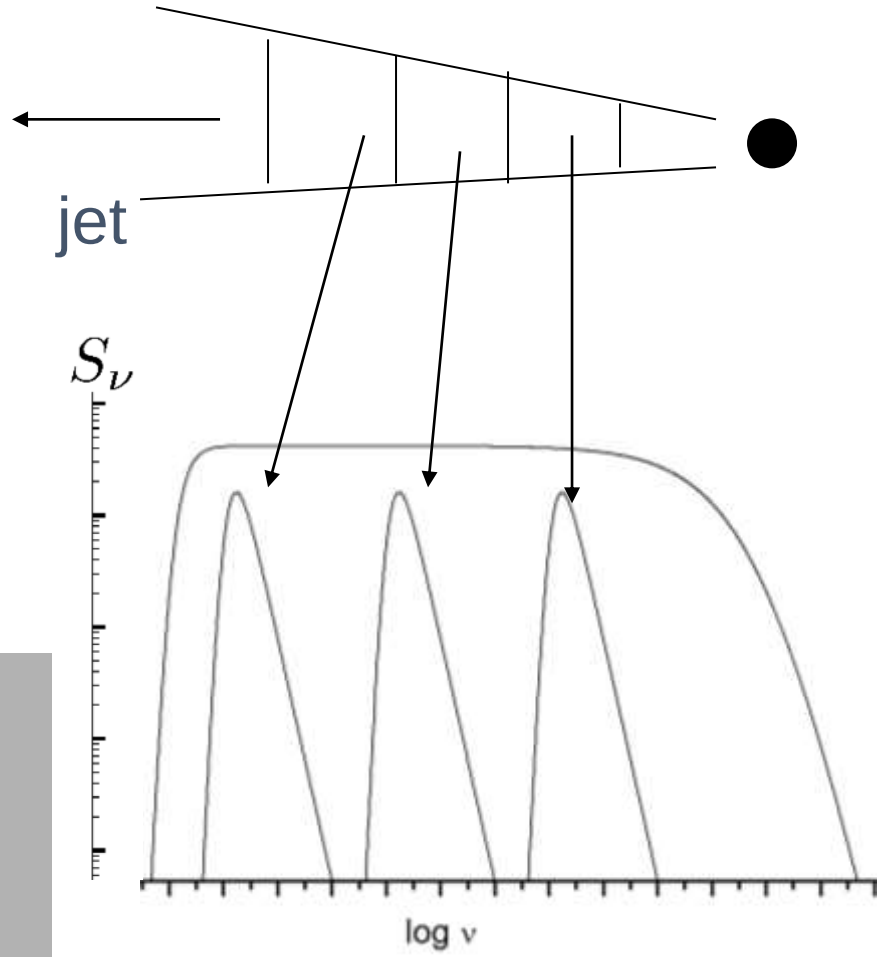

Black hole accretion

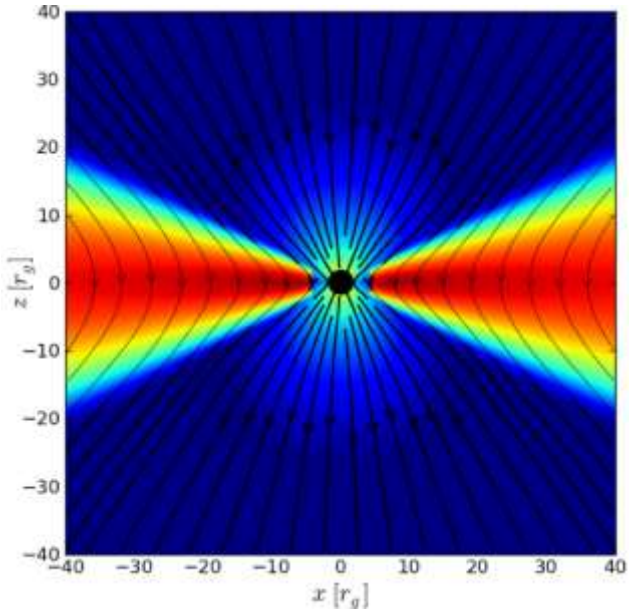

- Magnetically Arrested Disk (MAD)

Observational test:

- Radio → magnetic flux
- Optical → accretion

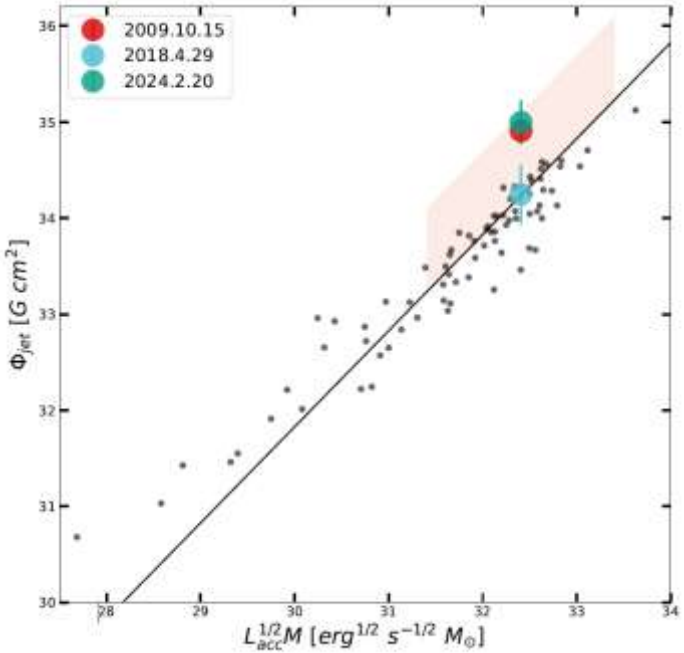

Zamaninasab et al. 2014
Guo et al. 2024

黑洞驱动喷流
Jet morphology near black hole

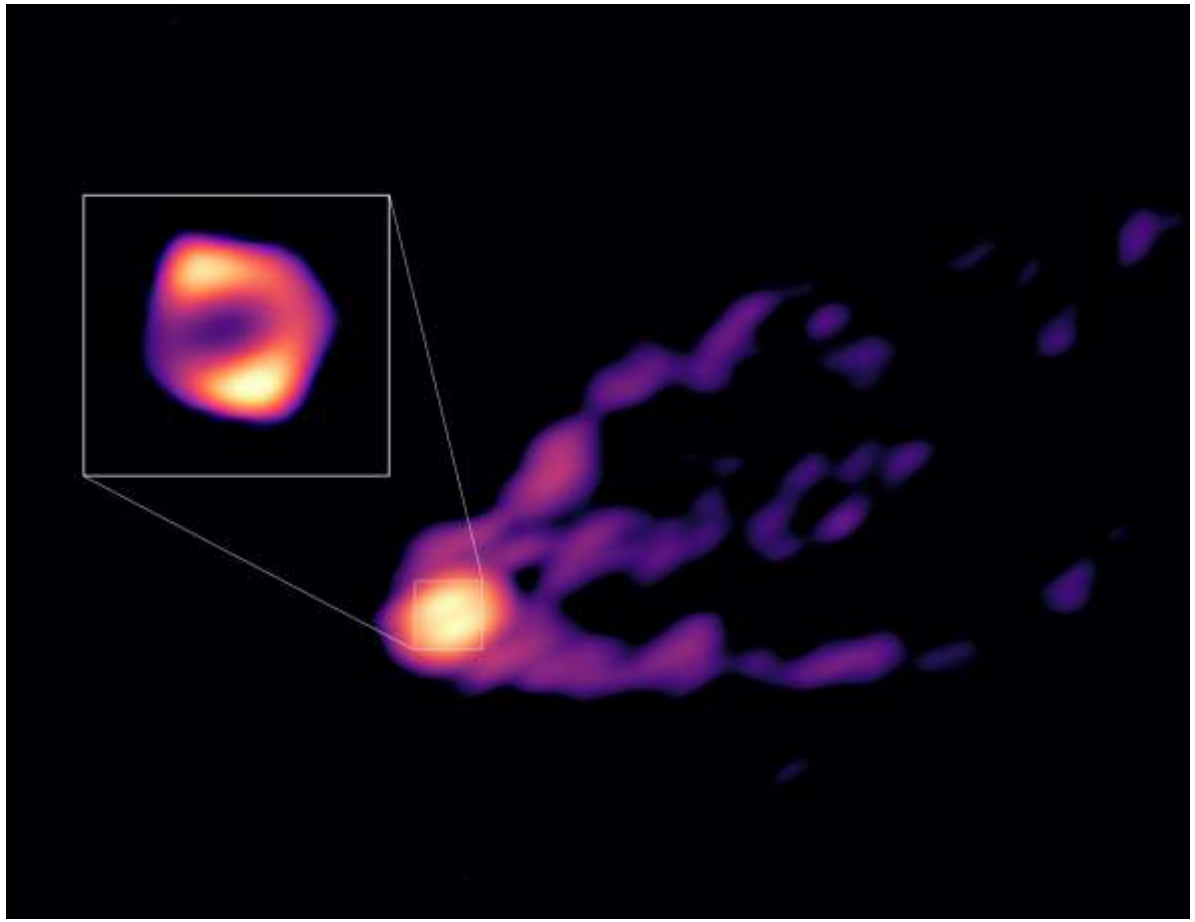

Lu et al. 2023

Black hole driven? direct measure?

$$S_r = -\frac{\Omega R}{4\pi} B_\phi B_r$$

@~5Rg, Poynting flux flow out!

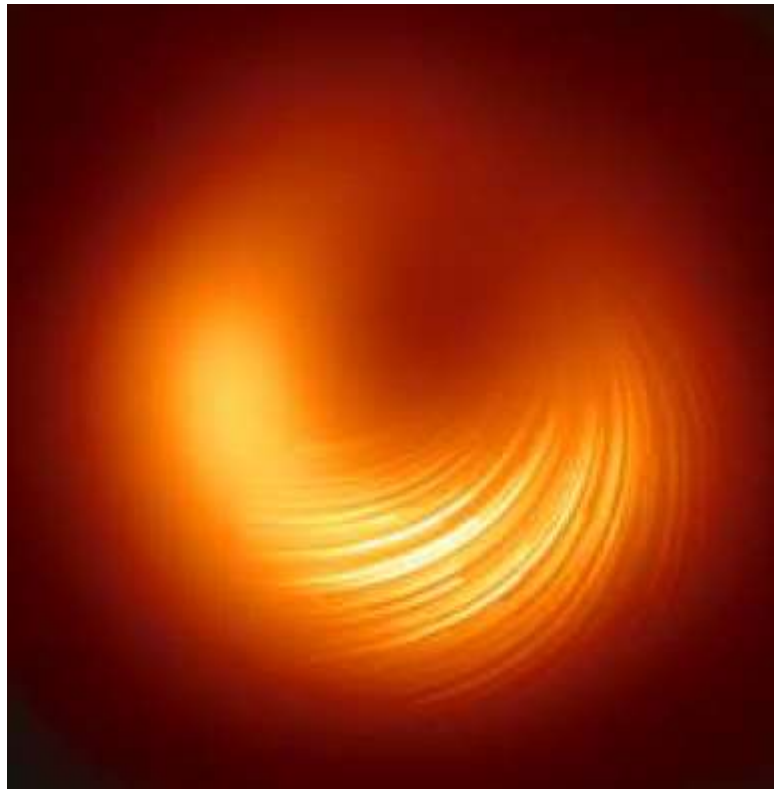

The EHT collaboration 2021

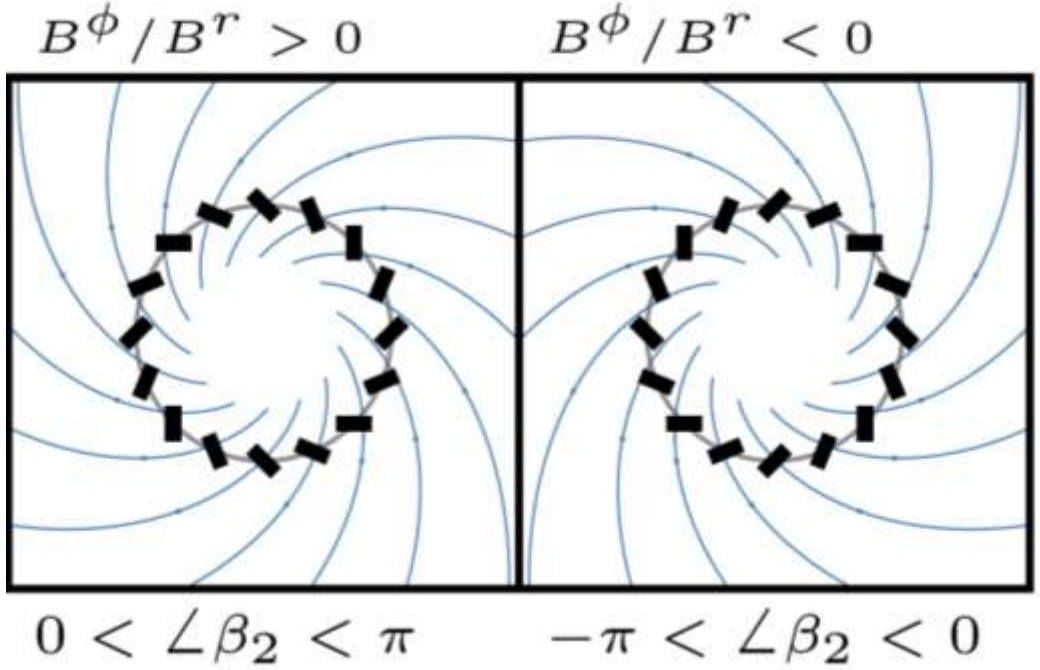

Chael et al. 2023

Jet production

- X-ray dip relate to knot production
- Jet base – corona?
- Similar to microquasar: GRS1915+105

Mirabel & Rodríguez 1998

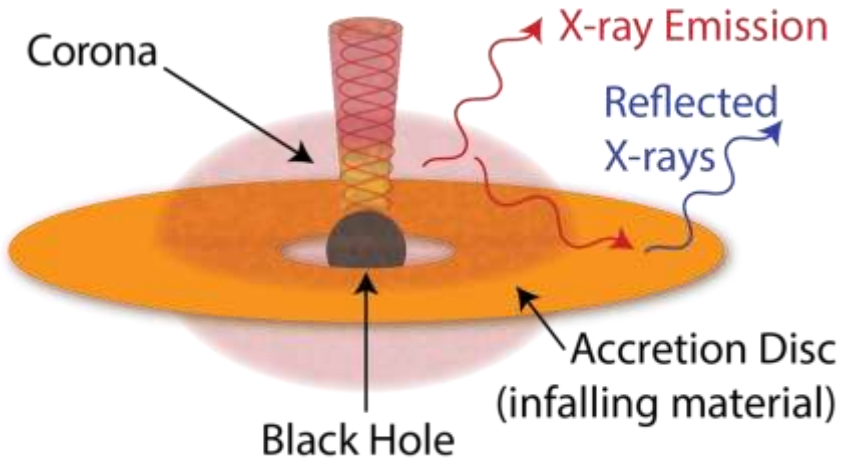

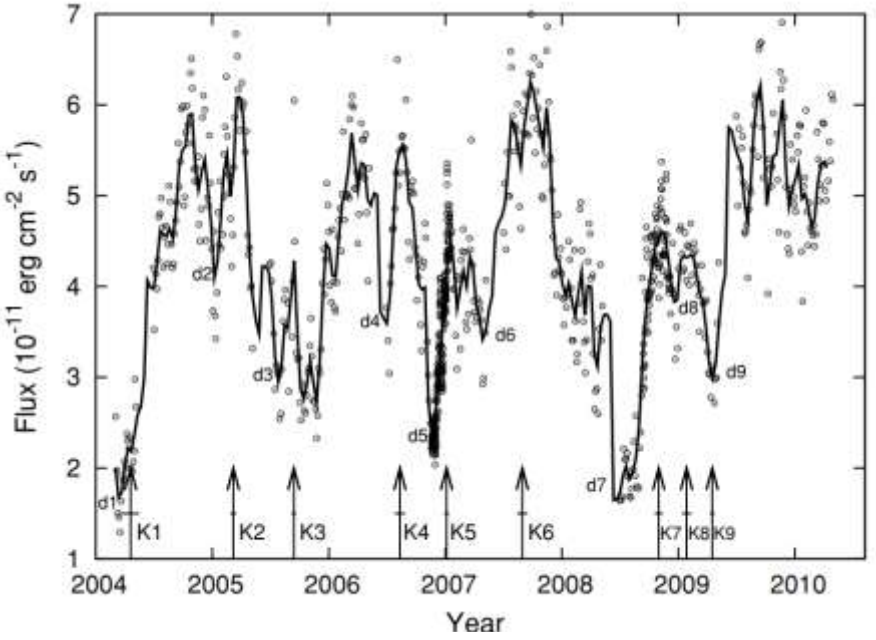

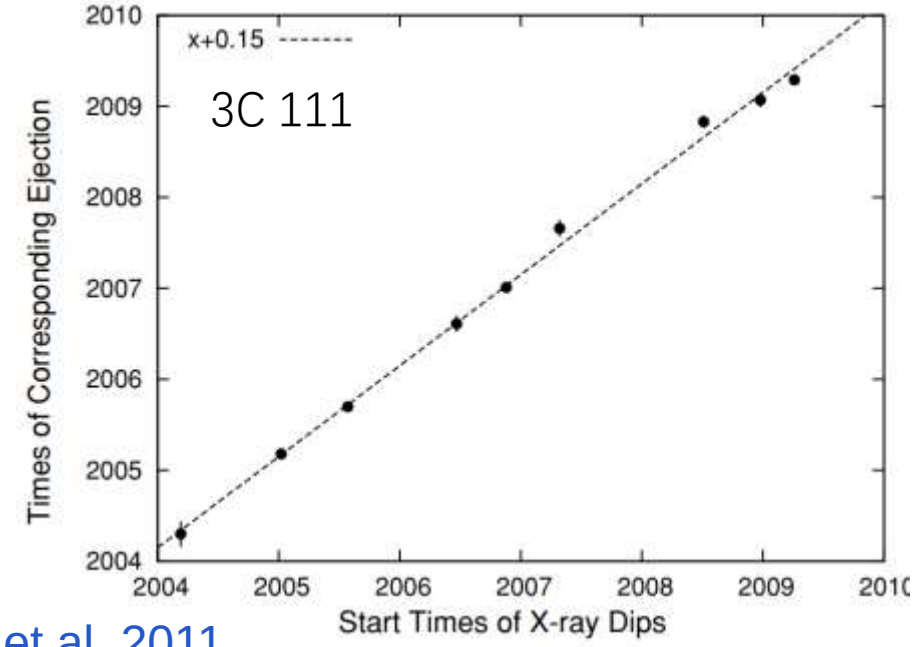

Chatterjee et al. 2011

Is relativistic jet magnetic driven?

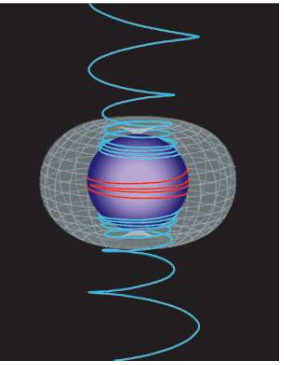

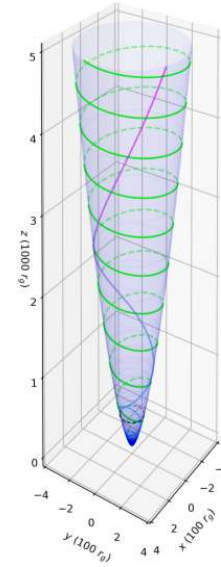

Magnetic driven for relativistic jet

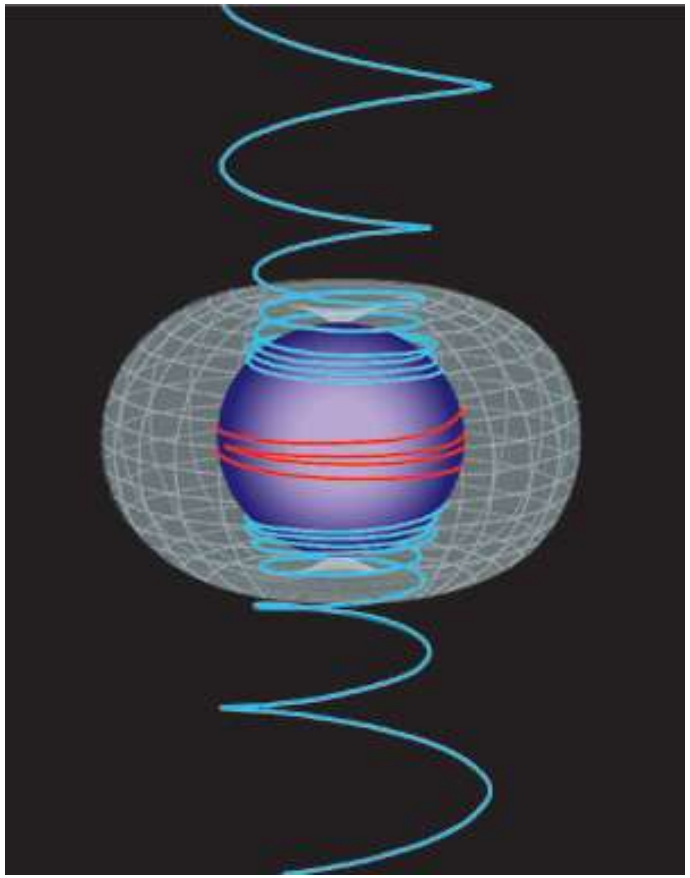

- Magnetic driven
- Accepted model

⇕

- Almost no competition models
- Validity?

need observational check

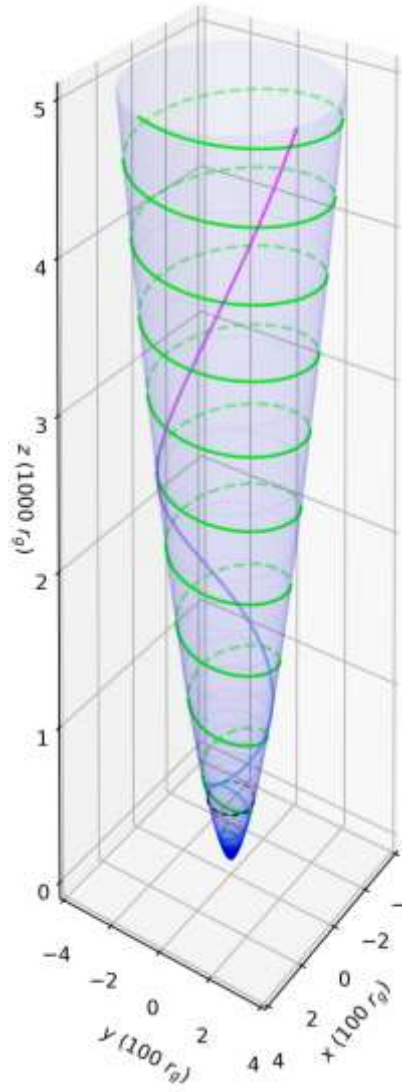

Magnetic driven-helical field

$$\Delta\chi = RM\lambda_{\mathrm{w}}^2$$
$$RM \propto \int n_{\mathrm{e}} B_{\parallel} dl$$

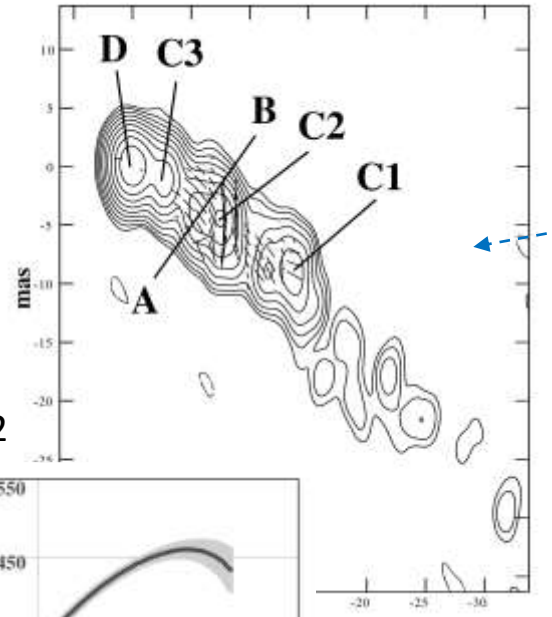

Asada et al. 2002

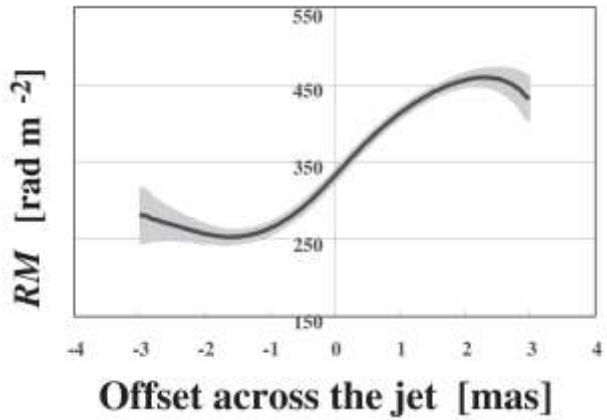

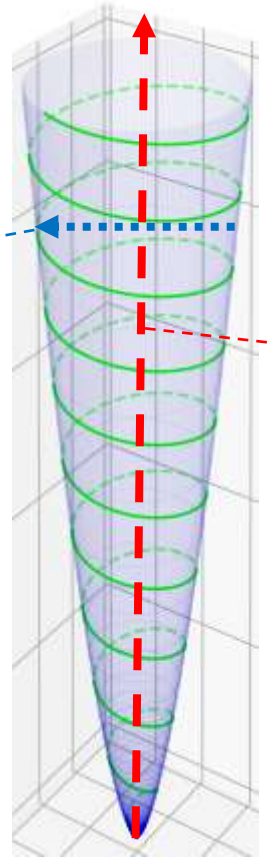

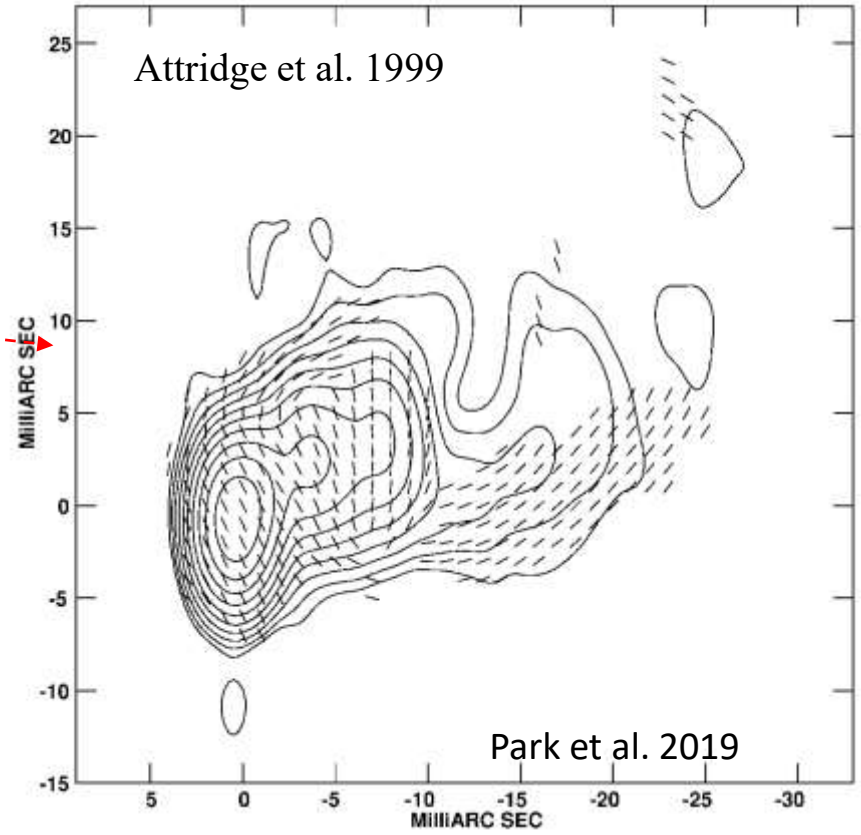

Park et al. 2019

Magnetic driven

- Ordered helical magnetic field

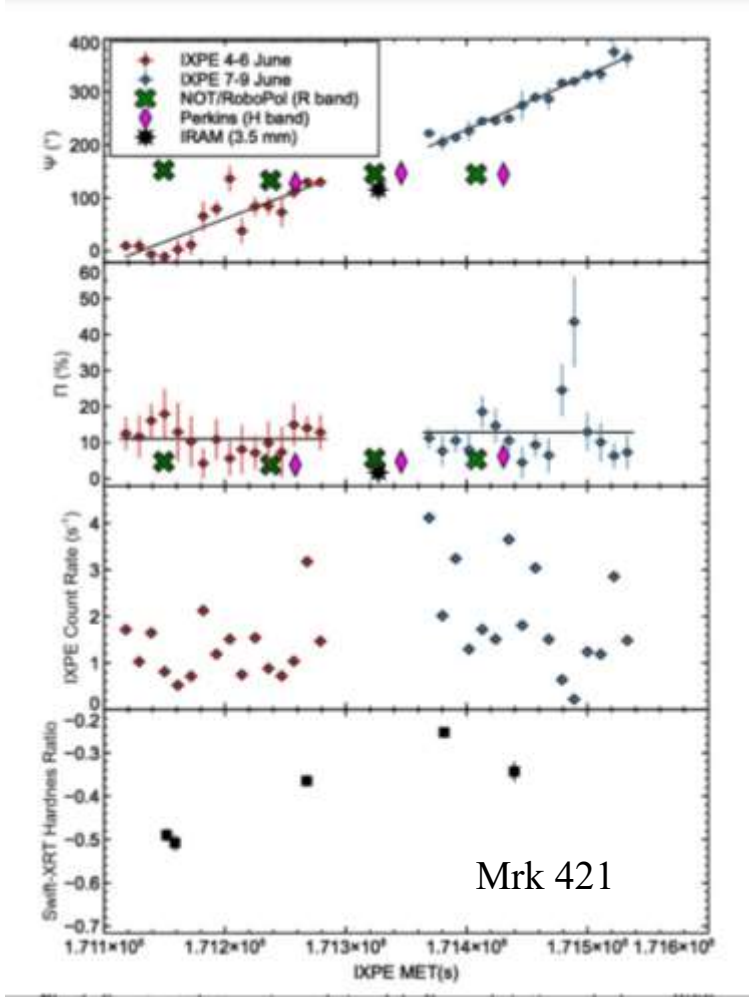

IXPE, Di Gesu et al. 2023

helical field
helical motion

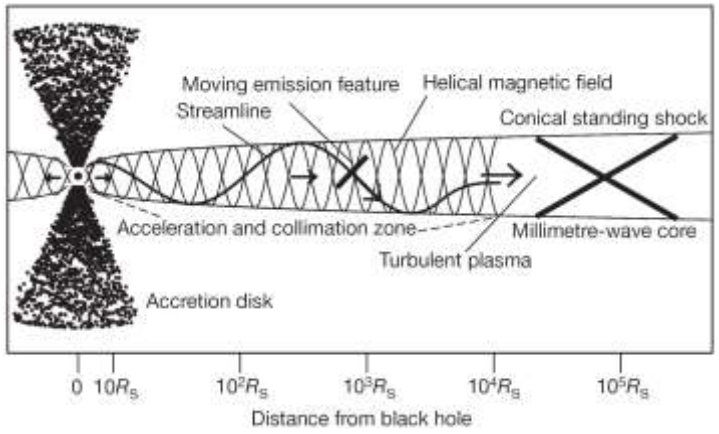

polarization angle
continuous changing

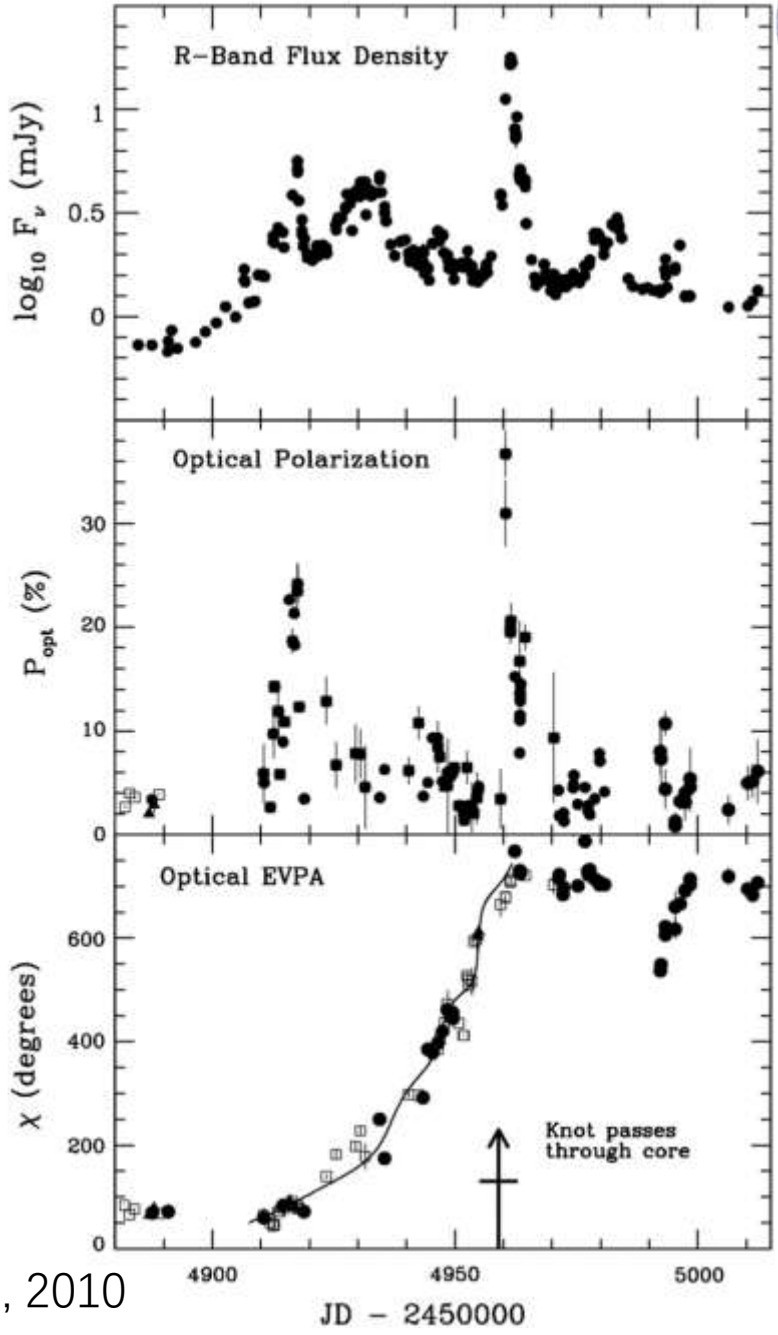

Marscher et al. 2008, 2010

Jet structure: helical motion

- Periodic variability

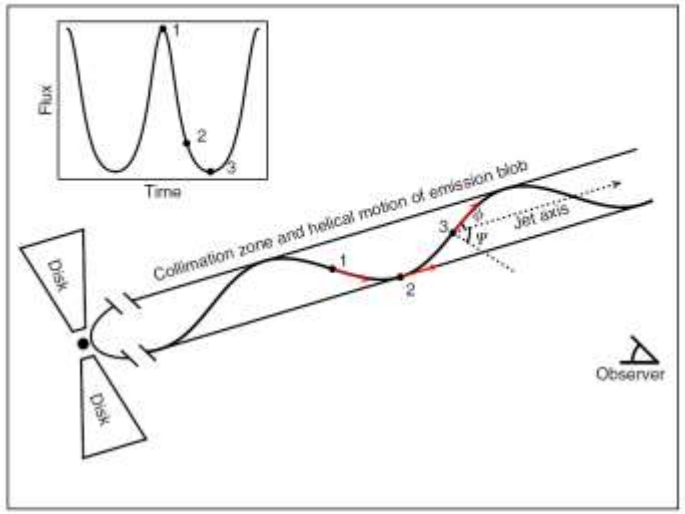

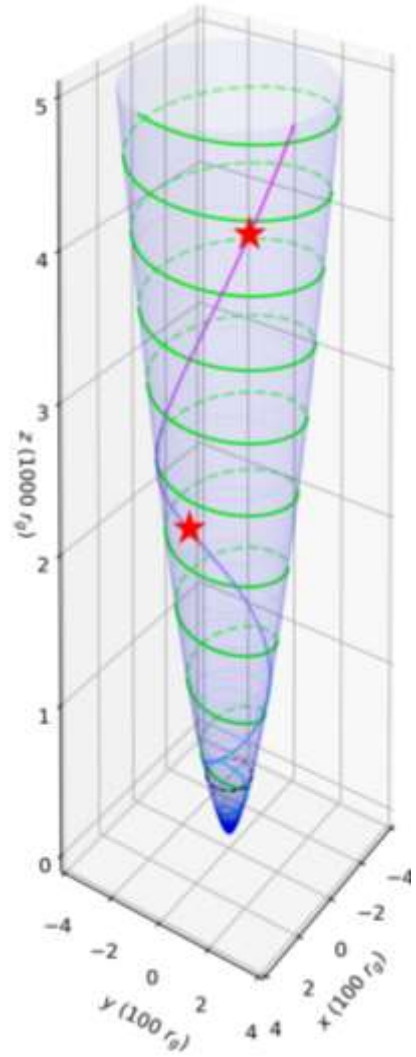

Jet structure: helical motion

- Periodic variability

  monthly

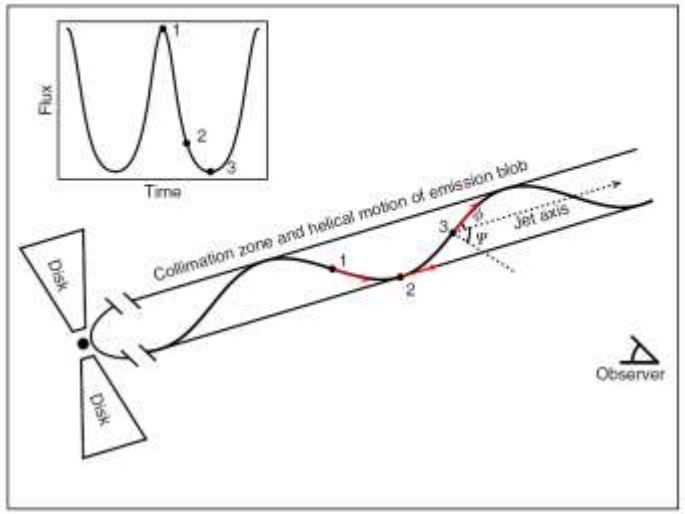

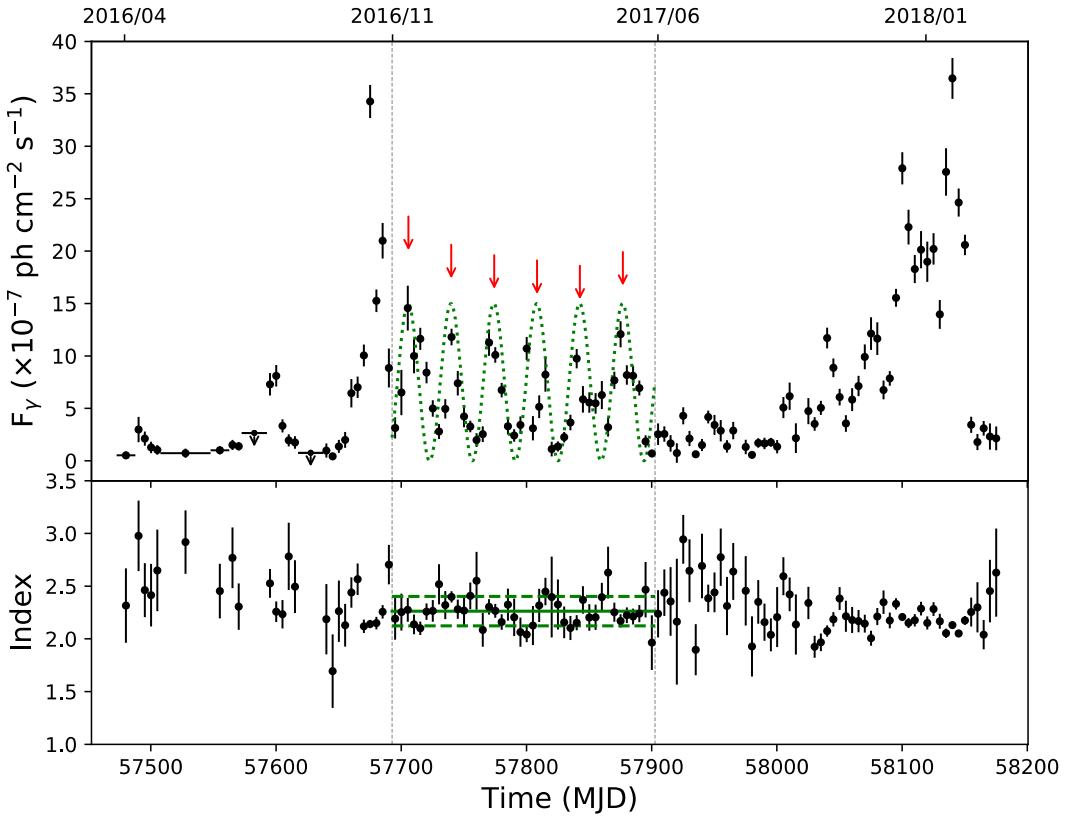

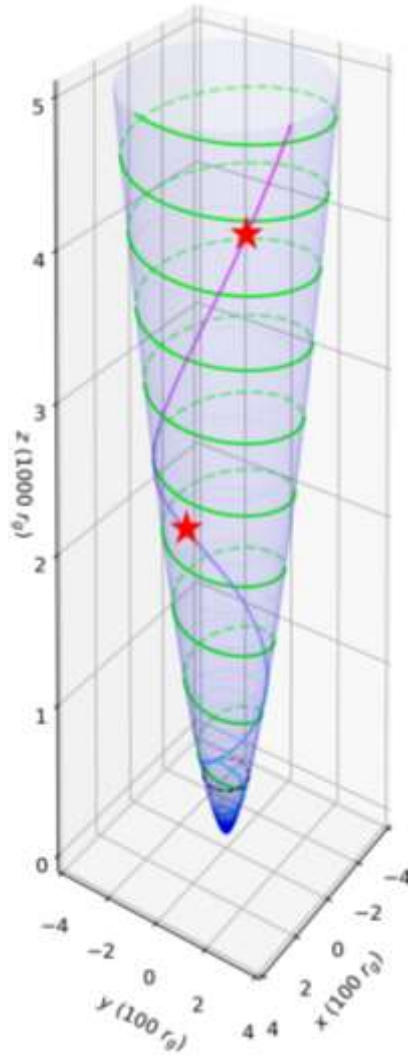

Zhou et al. 2018

Spine/layer

The velocity difference between spine and layer amplify the photon energy density → increase inverse Compton luminosity

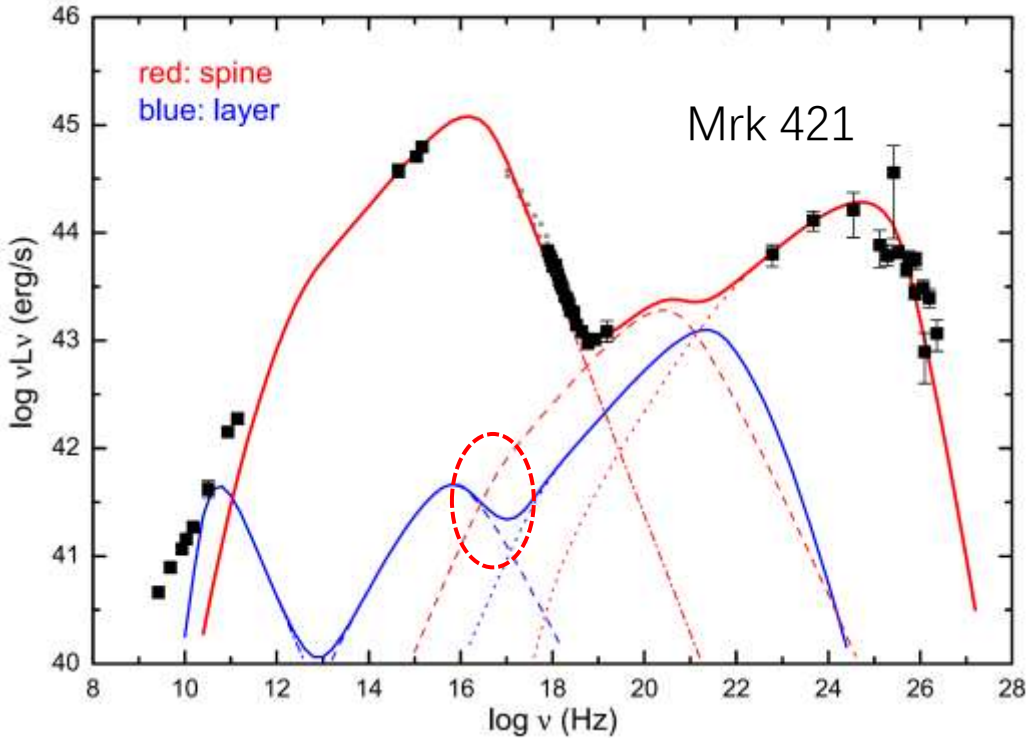

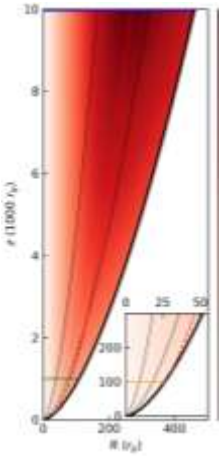

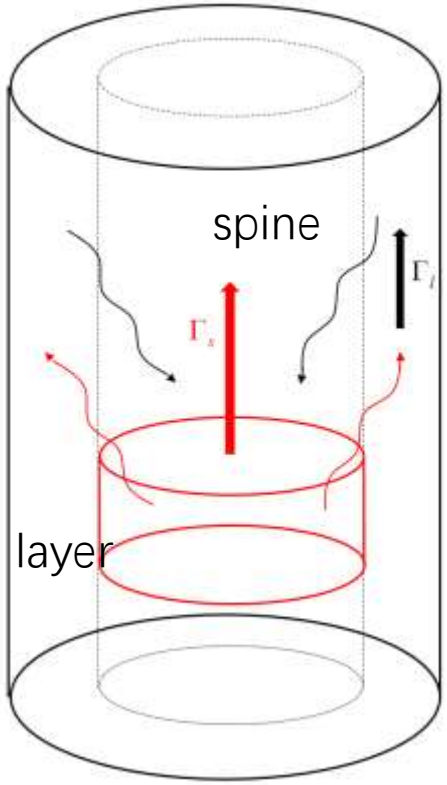

Ghisellinie et al. 2005
Chen 2017
Gaur, Chen, et al. 2017

Jet structure/spine layer

- Limb brighten （~ 10 jets)

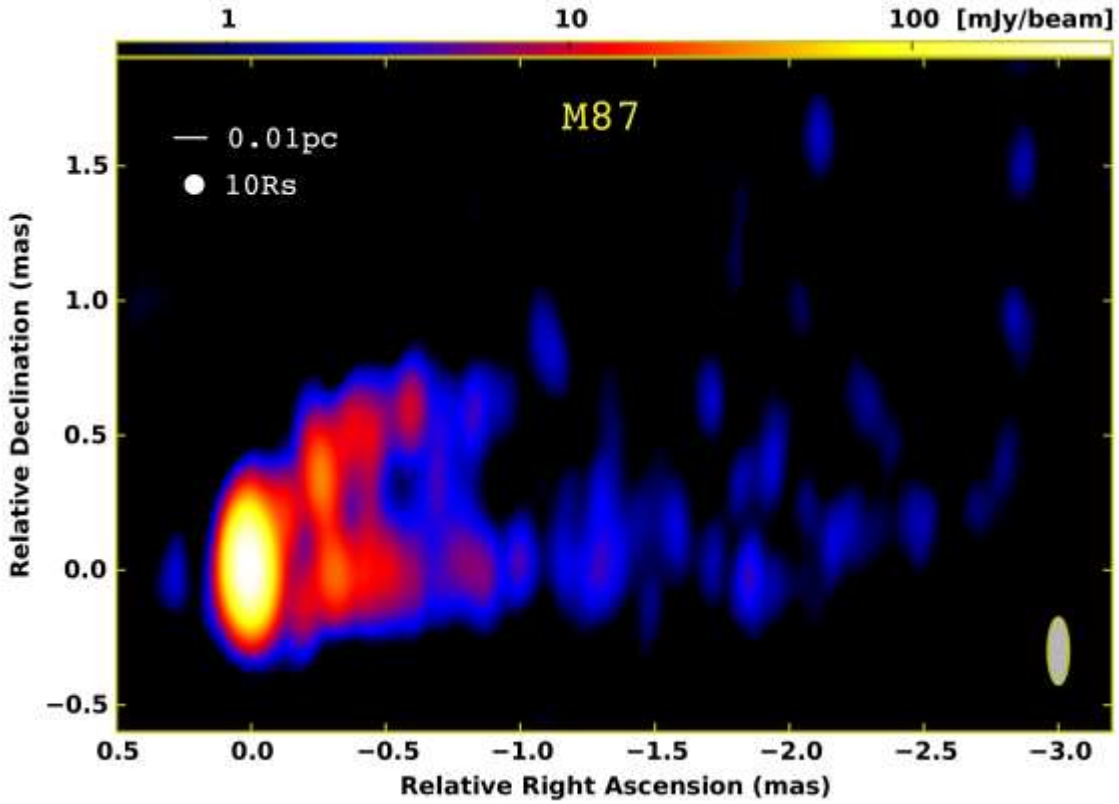

Hada et al. 2016

磁场驱动喷流？

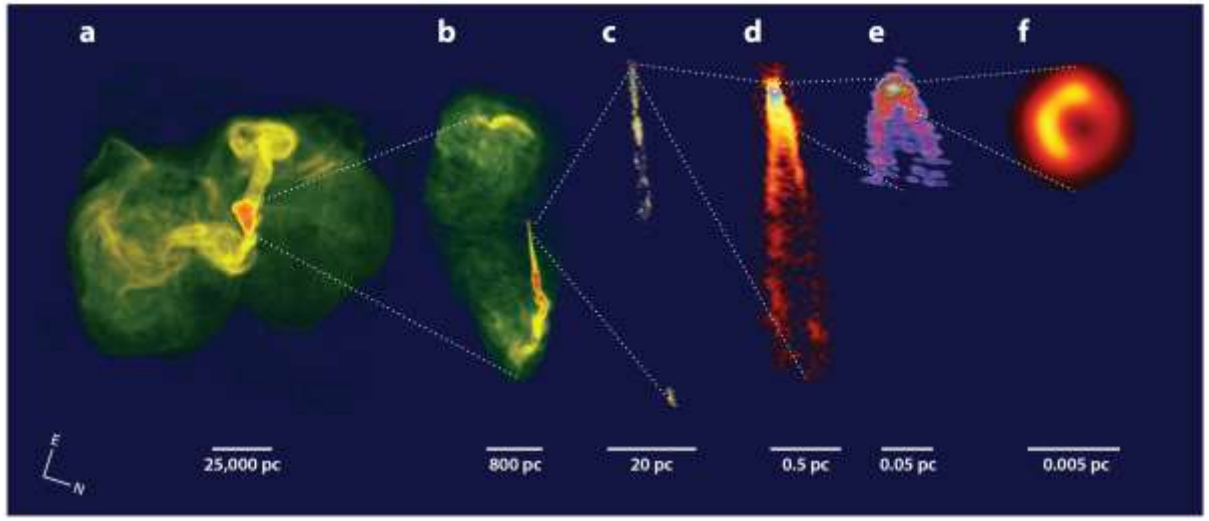

- 最内区
- 极向磁场
- 环向速度
- 磁主导

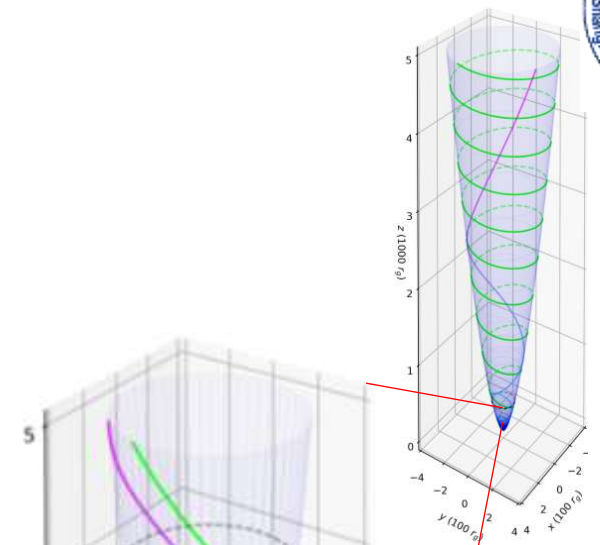

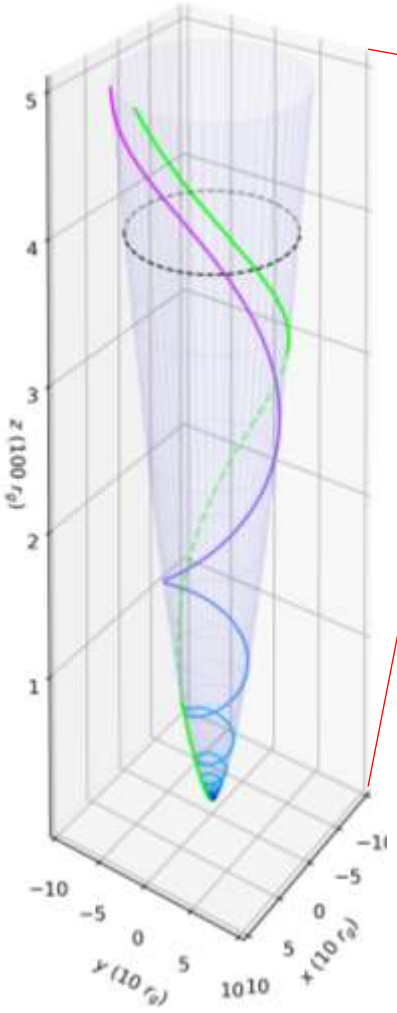

第一阶段	第二阶段	第三阶段
磁主导		
抛物线轮廓	抛物线轮廓	锥形轮廓
逐渐加速		
非相对论性速度	相对论性速度	(非)相对论性速度
环向速度主导		
极向磁场主导	环向磁场主导	环向磁场主导

什么算是“决定性”证据？’

AGN辐射

- 吸积盘
- 宽窄线区
- 尘埃环

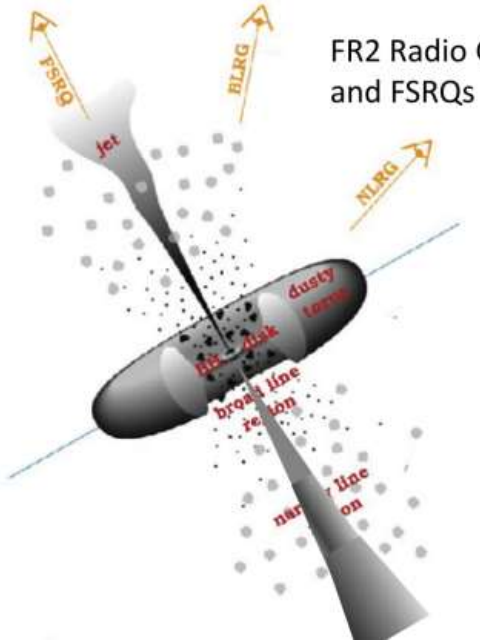

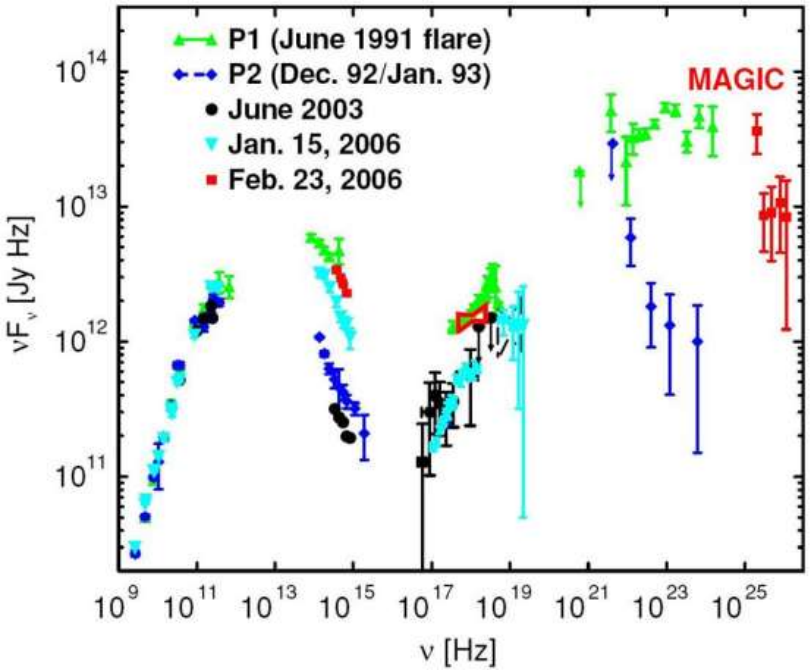

- 喷流：非热辐射

  射电、光学、X-ray、伽玛射线

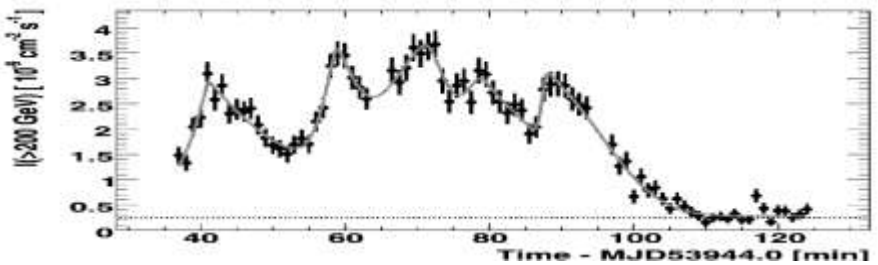

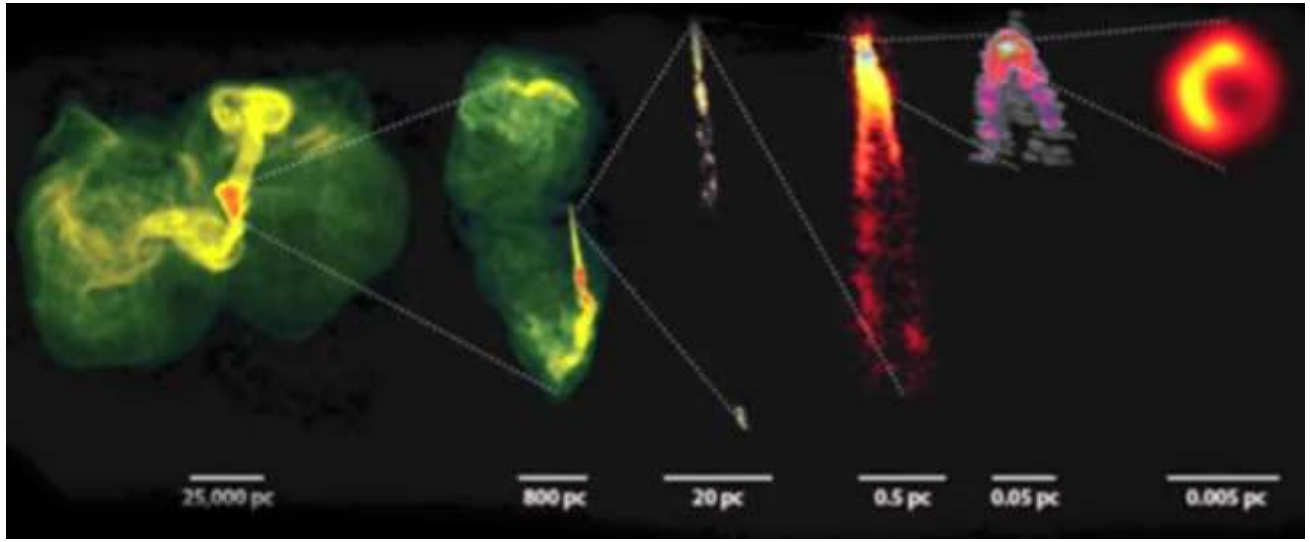

AGN喷流的辐射

Gamma-ray AGNs

- Ajello et al. 2022, The Fourth Catalog of Active Galactic Nuclei Detected by the Fermi Large Area Telescope: Data Release 3

GeV

Table 2
Census of 4LAC-DR3 Sources

AGN Type	High-latitude Sample	Clean Sample[a]	Low-latitude Sample
All	3407	2896	407
FSRQ	755	640	37
…LSP	672	581	35
…ISP	20	18	0
…HSP	4	4	0
…no SED classification	59	37	2
BL Lac Object	1379	1261	79
…LSP	353	332	20
…ISP	347	309	8
…HSP	425	394	29
…no SED classification	254	226	22
Blazar of Unknown Type	1208	945	285
…LSP	508	397	78
…ISP	135	115	12
…HSP	117	99	10
…no SED classification	448	334	185
Nonblazar AGN	65	50	6
…radio galaxies	42	32	4

TeV

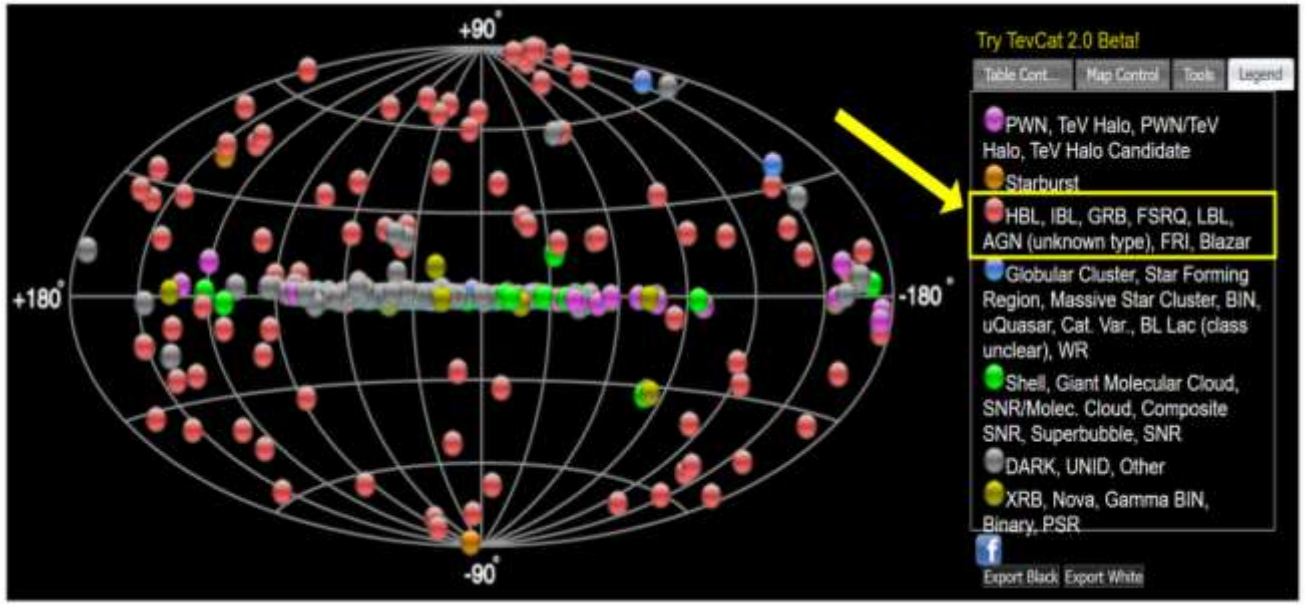

AGN wind vs jet

- 16 RL Seyfert I
- Wind inverse correlate with radio loudness
- Similar to microquasar GRS 1915+105

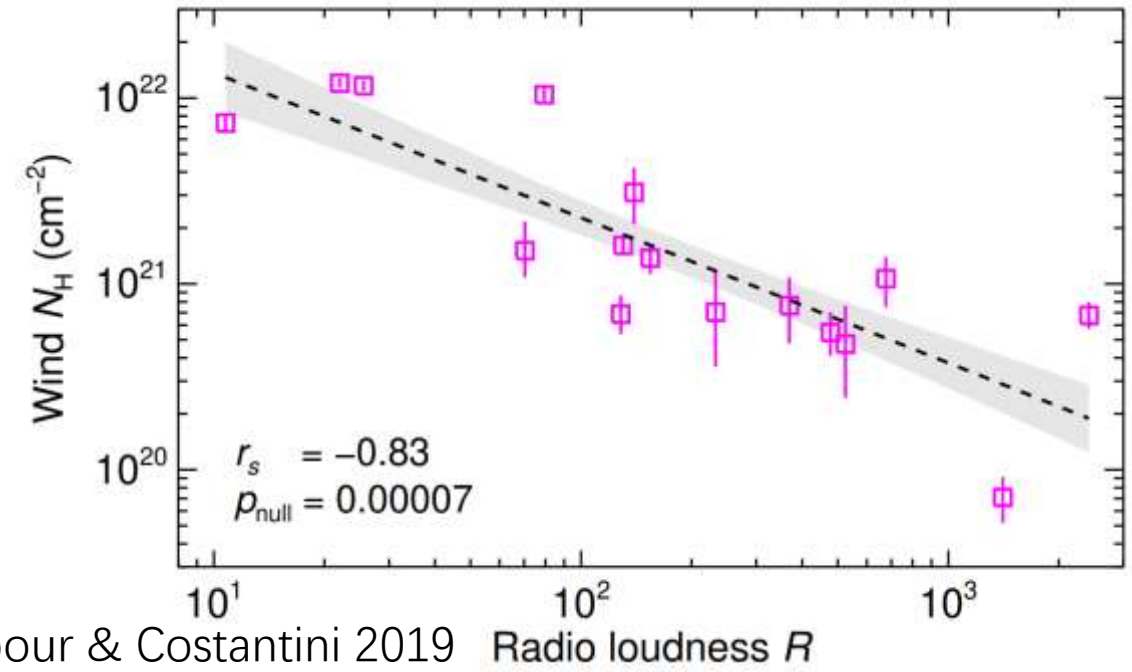

Mehdipour & Costantini 2019

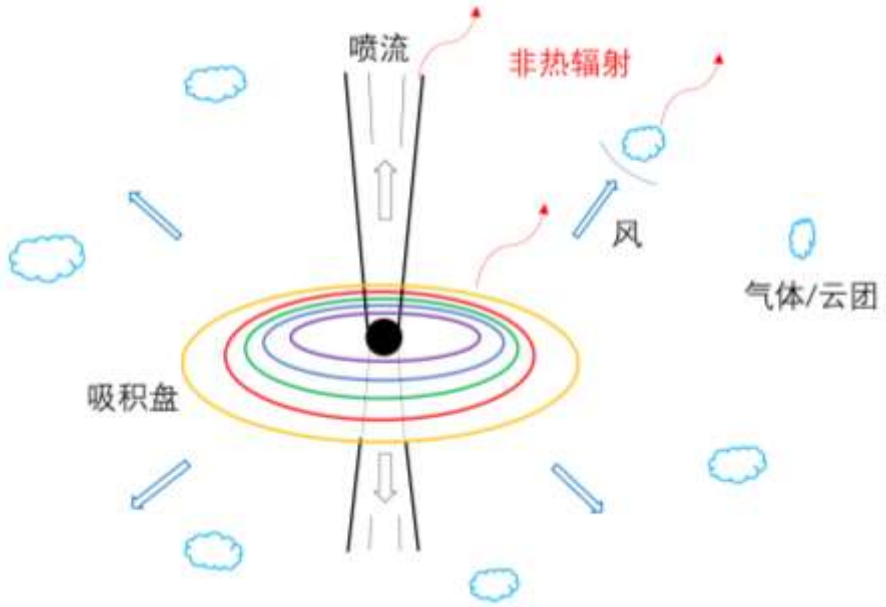

AGN with ultrafast outflow

- Radio quite AGN
- v=0.1 c
- Fermi/LAT
- ~ 5.1 sigma

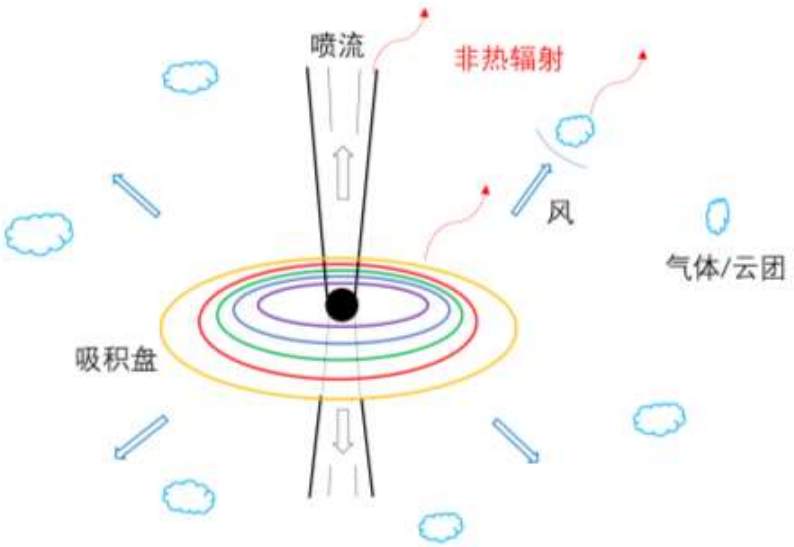

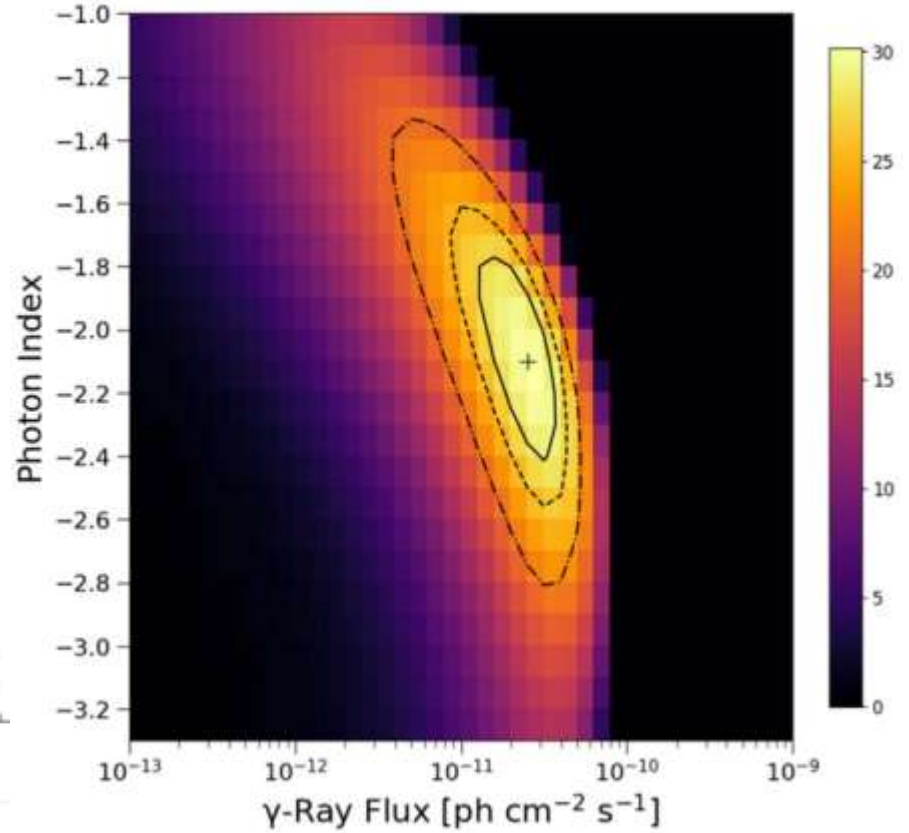

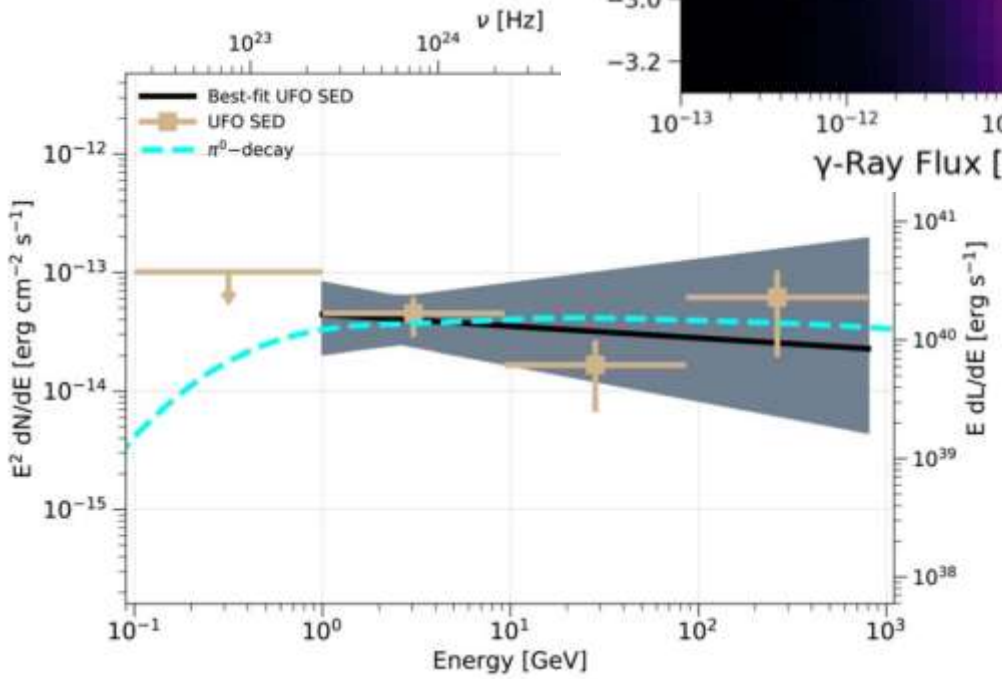

Ajello et al. 2021

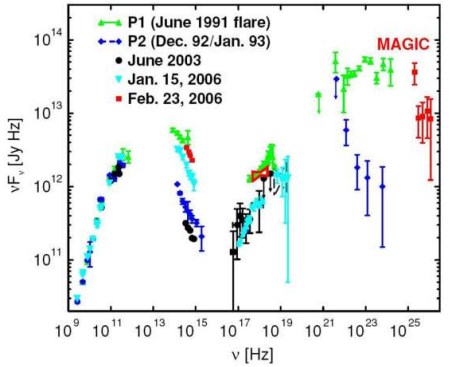

喷流能量耗散、粒子加速、辐射区位置？

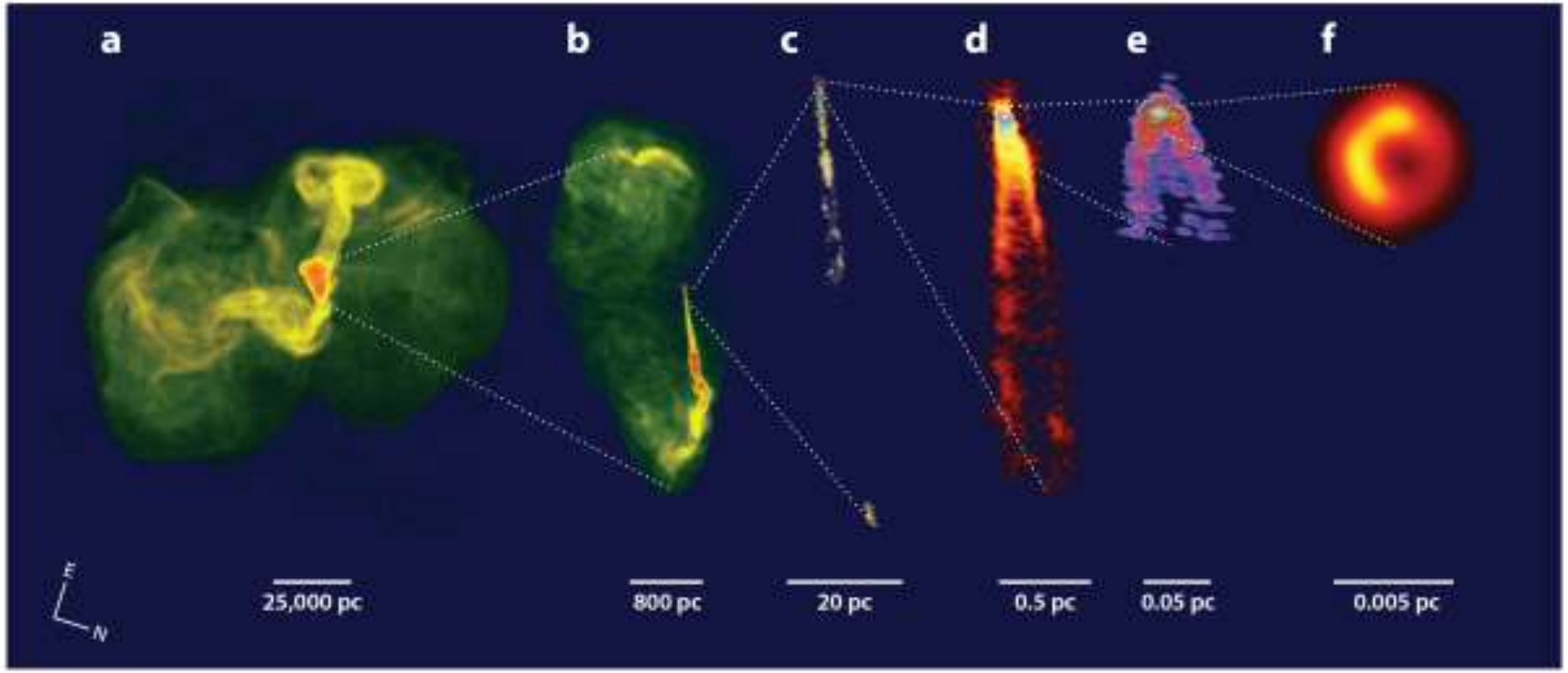

Cen A extended VHE emission

HESS

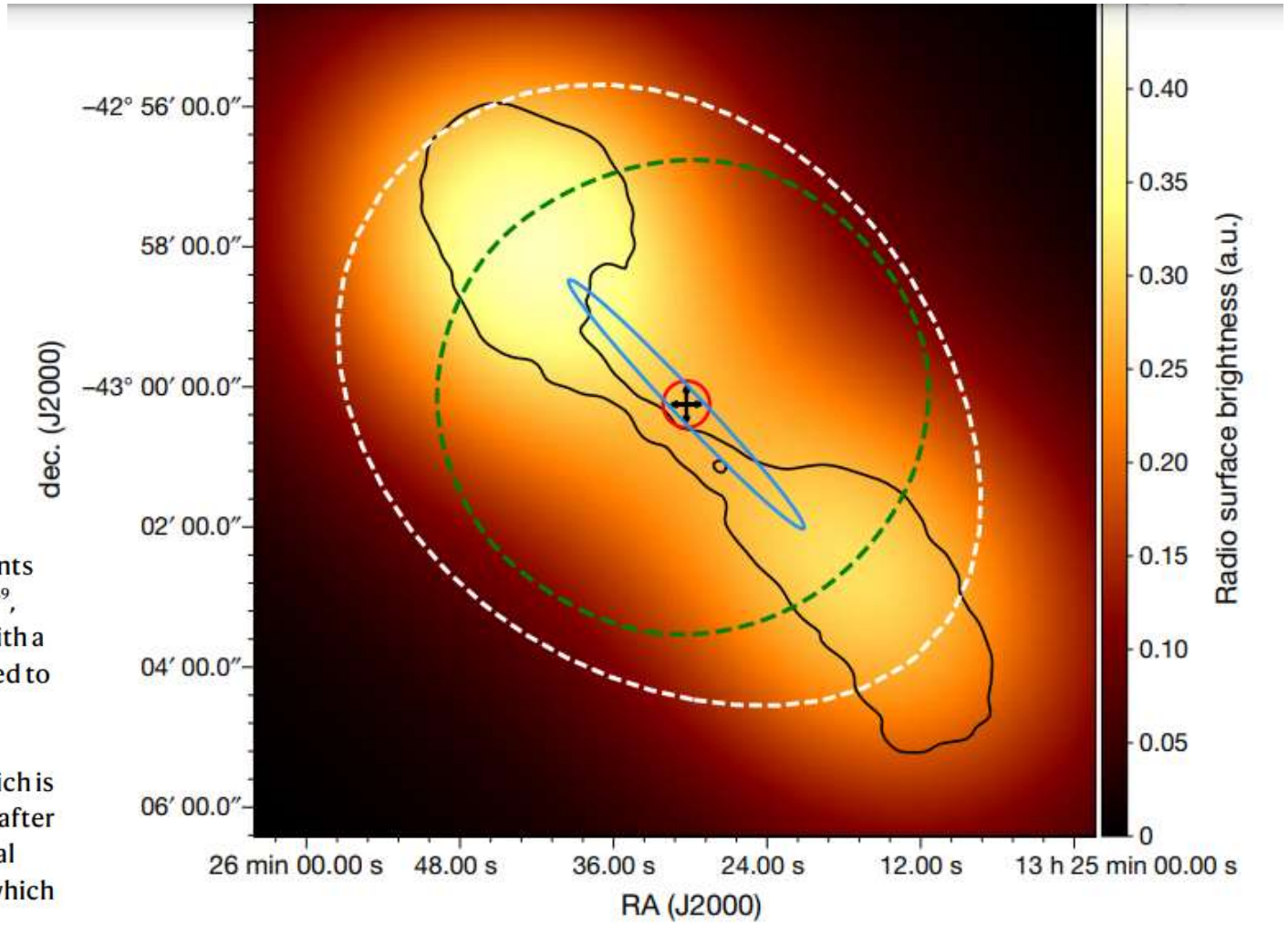

Fig. 1 | Multiwavelength image of Centaurus A. The colour map represents the radio surface brightness (21 cm wavelength) VLA map of Centaurus A[39], after convolution with the H.E.S.S. PSF and an additional oversampling with a radius of 0.05°. Contours of the unconvolved VLA map, with levels adjusted to highlight the core (corresponding to 4 Jy per beam) as well as the kiloparsec-scale jet (0.5 Jy per beam), are drawn in black. The VHE γ-ray morphology of Centaurus A is represented by a white dashed contour which is derived from the 5σ excess significance level of the H.E.S.S. sky map, also after oversampling with a radius of 0.05°. The result of the best fit of an elliptical Gaussian to the H.E.S.S. measurement is shown in blue by its 1σ contour, which corresponds to a model containment fraction of 39%. The 1σ statistical uncertainties of the fitted position are drawn as black arrows, and the estimated pointing uncertainties with a red circle. The dashed green line denotes the 68% containment contour of the H.E.S.S. PSF.

M87 VHE emission

- 2005outburst @HST-1 ~ 100 pc
- 2008outburst @<1.2mas ~ 150 Rs

Aharonian et al. 2006; VERITAS Collaboration 2009

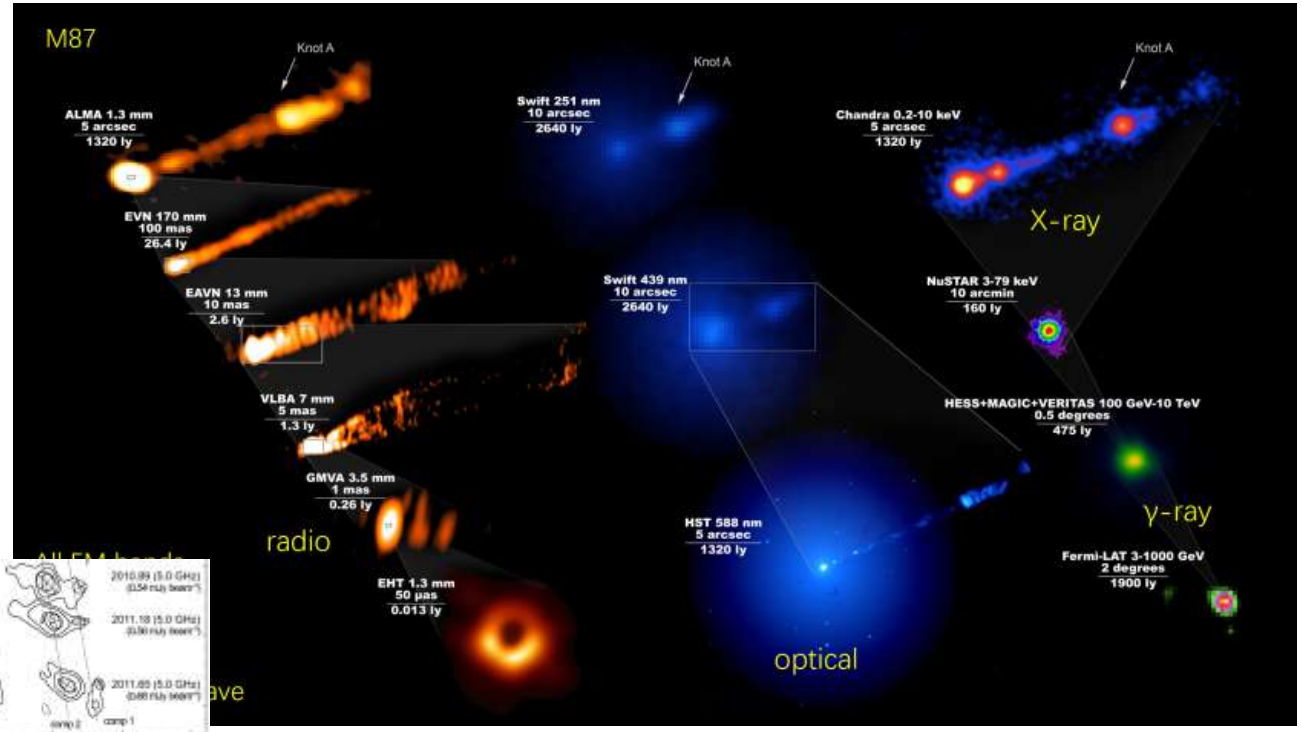

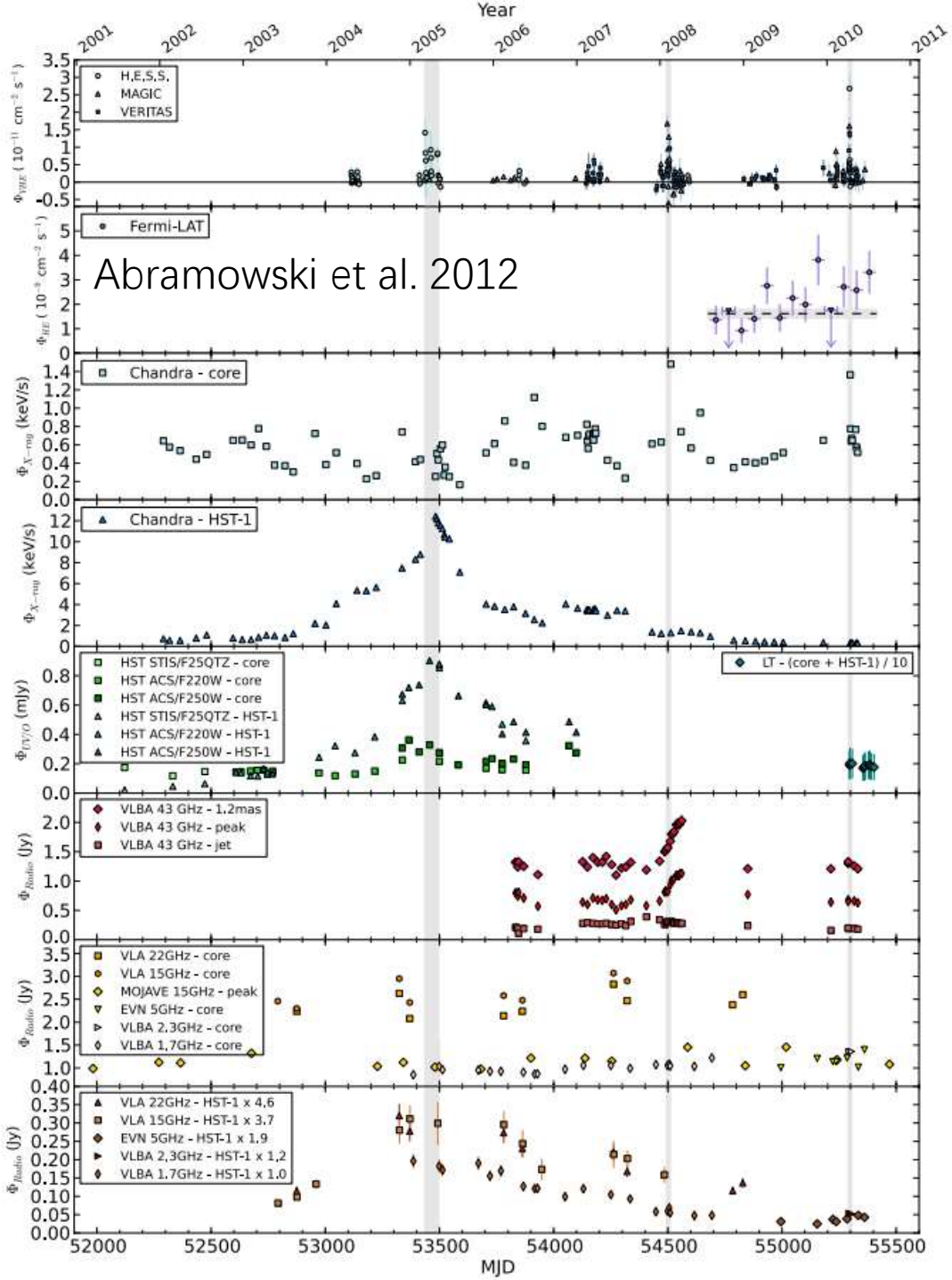

喷流团块碰撞

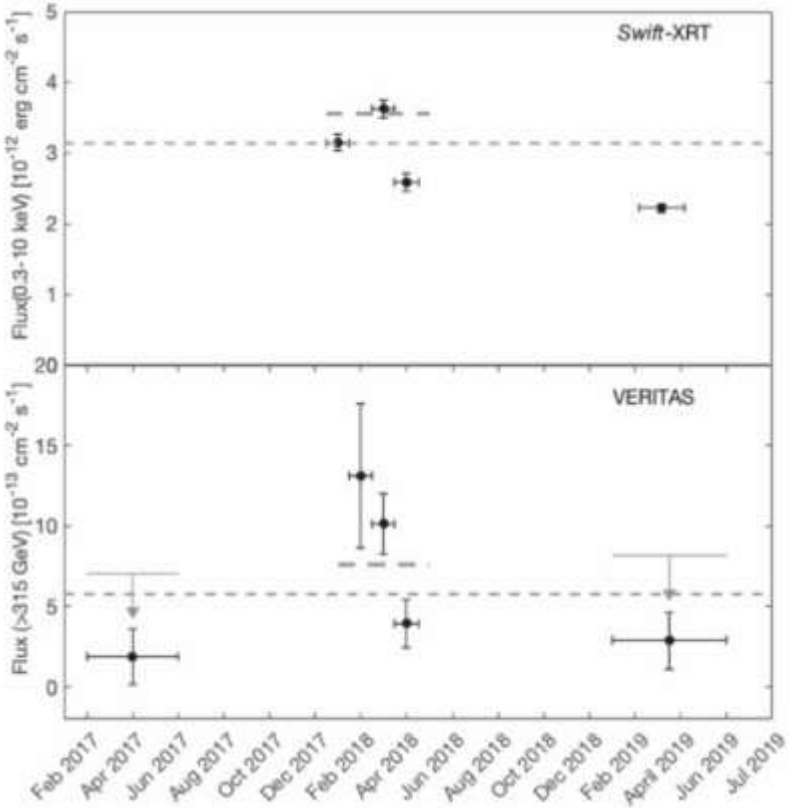

Archer et al. 2020

3C 264, radio

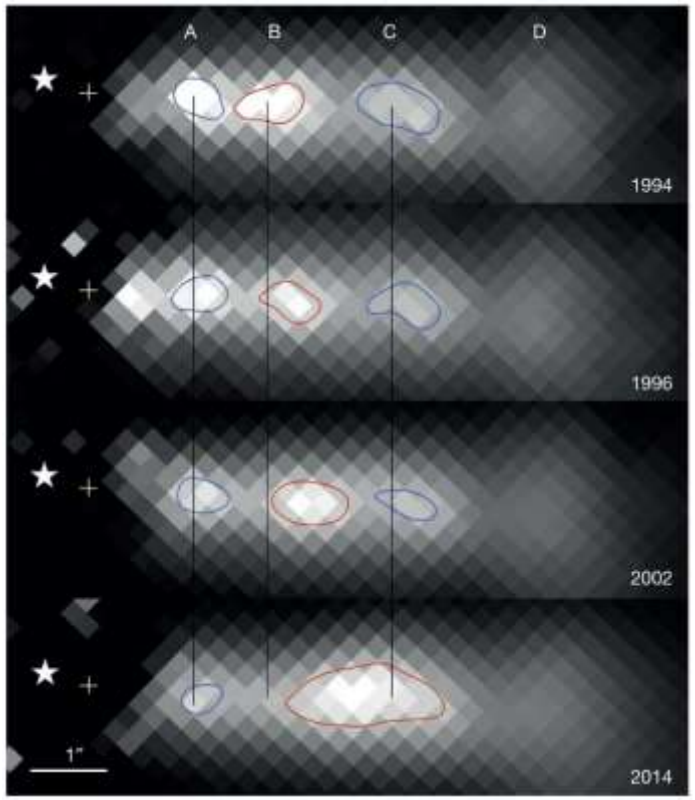

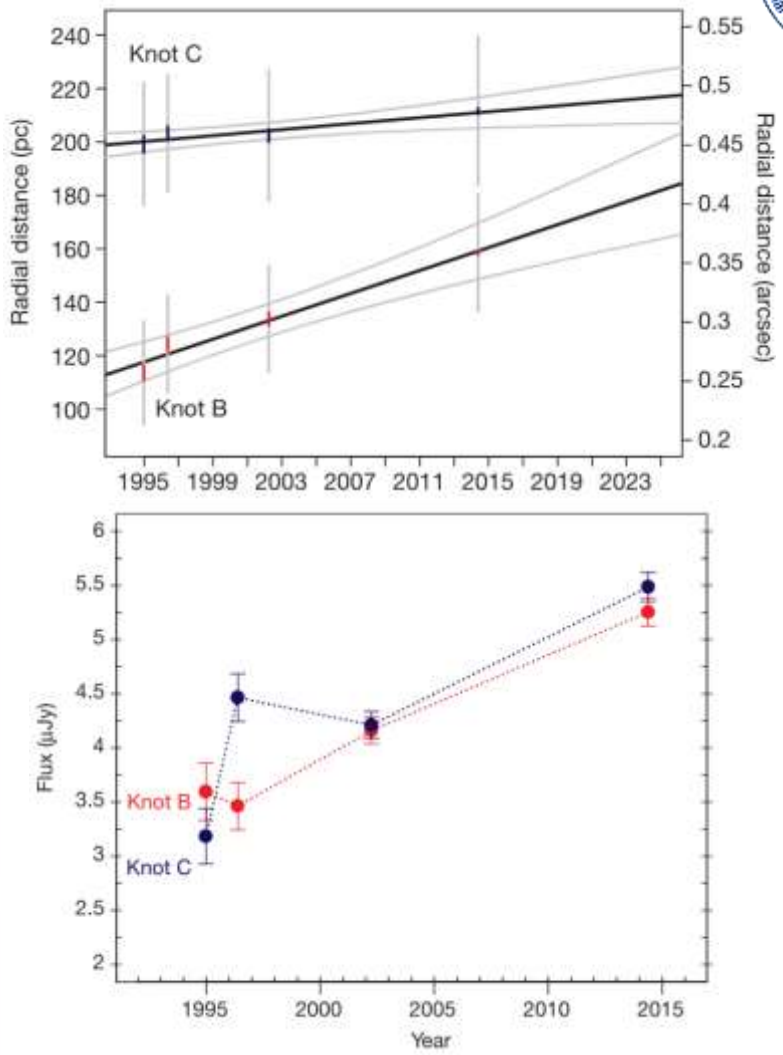

Meyer et al. 2015

极速光变

- 分钟

Name	GeV	TeV	X-ray	optical	Type
BL Lacertae	~1 min	~13 min		~1.7 hour	LBL/IBL
3C 279	~5 min				FSRQ
PKS 1510-089	~20 min				FSRQ
PKS 2155-304	~1.2pm0.2 hour	~3 min			HBL
Mrk 501		~2 min	~1 min		HBL
IC 310		~4.8-1 min			RG/BL
Mrk 421		~15 min			HBL
PKS 1222+216	<1.6 hour	~8.6 min			FSRQ
S5 0716+714			~3 min	<0.2 day	IBL
PKS 2005-489			~0.5 min		HBL
3C 371				~10min	BL

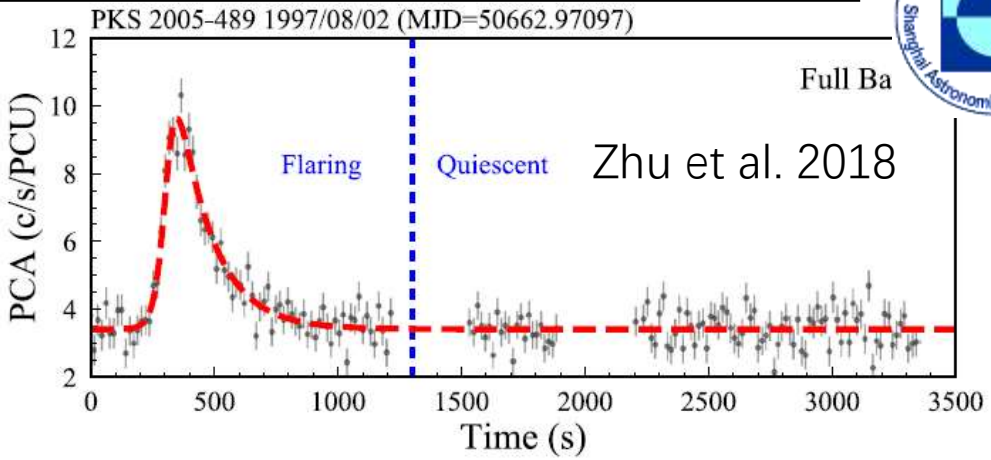

Zhu et al. 2018

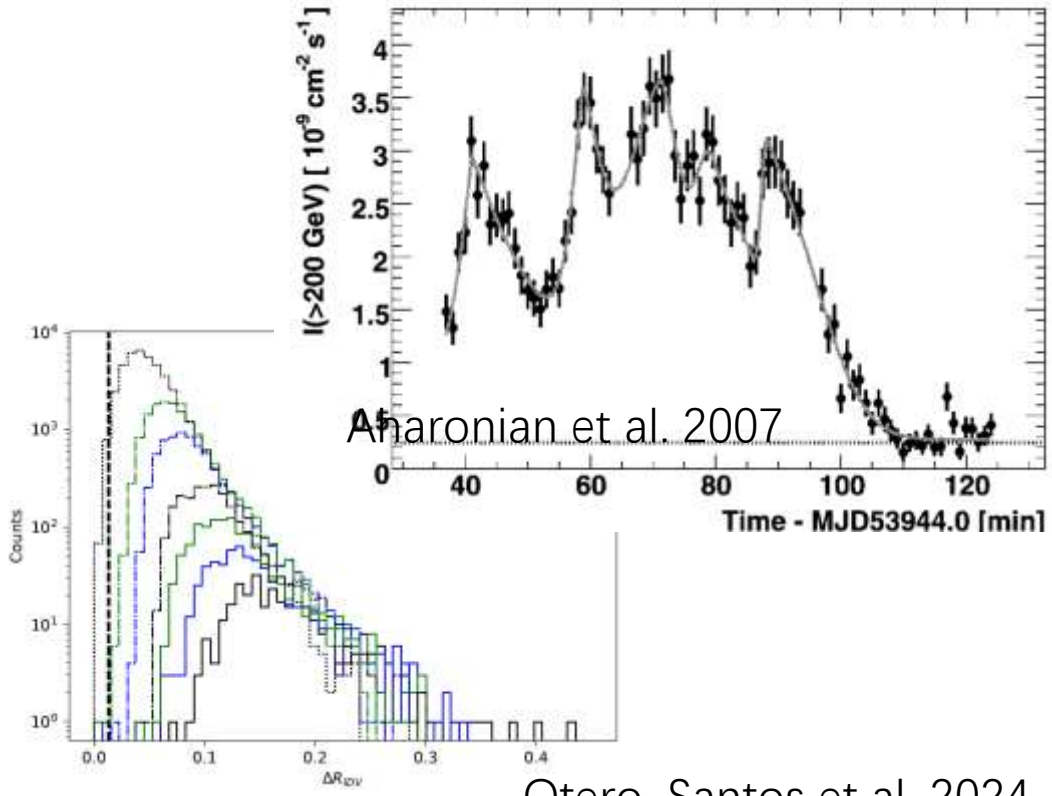

Aharonian et al. 2007

Otero-Santos et al. 2024

On the origin - 磁重联?

- Mini-jet
- Magnetosphere

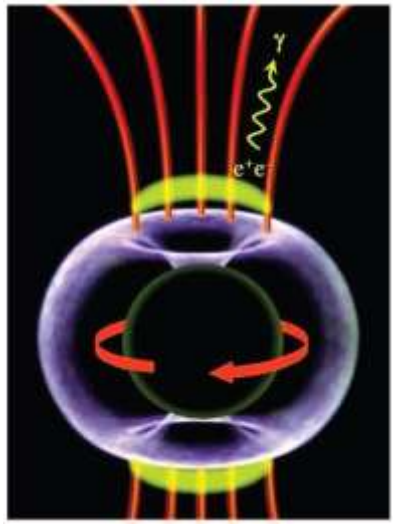

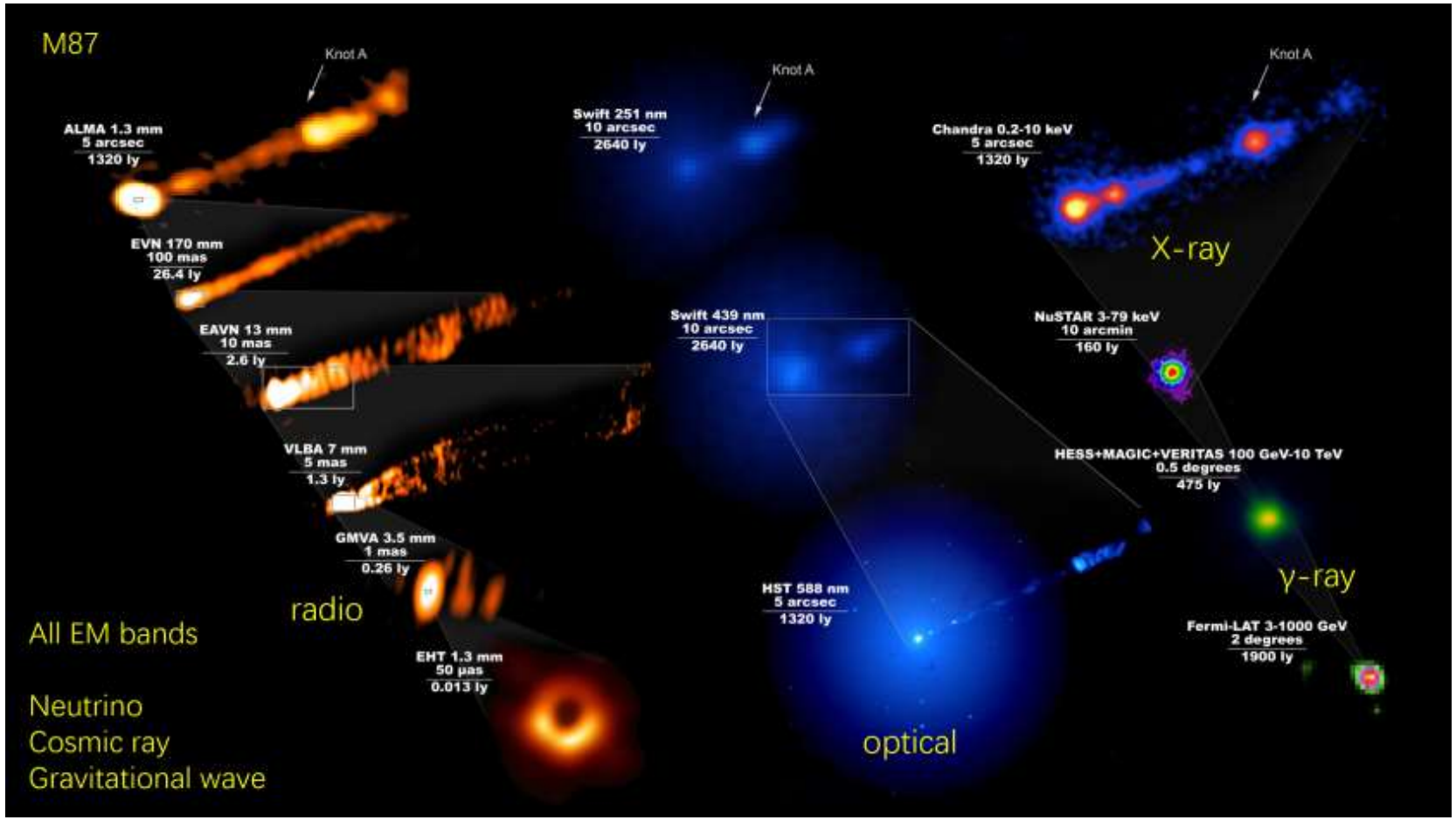

The EHT collaboration

通过能谱限制辐射区位置

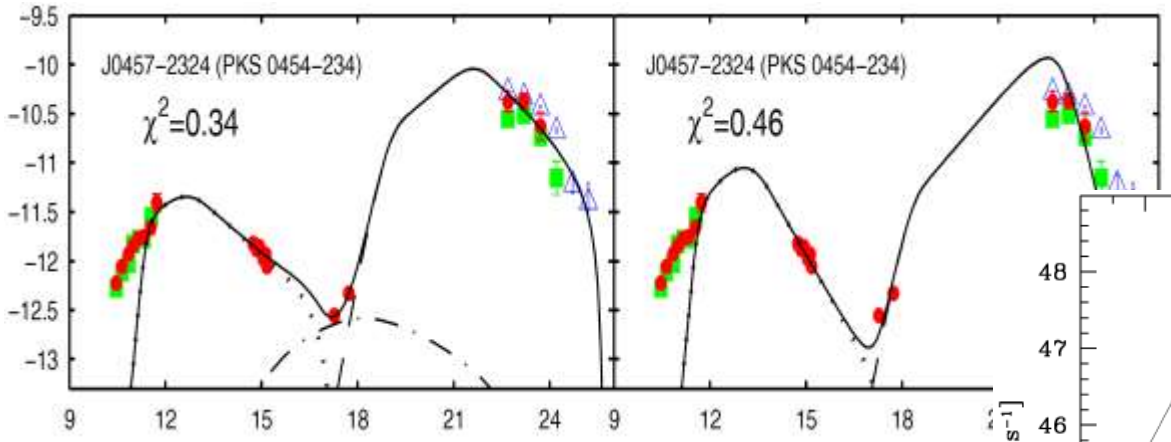

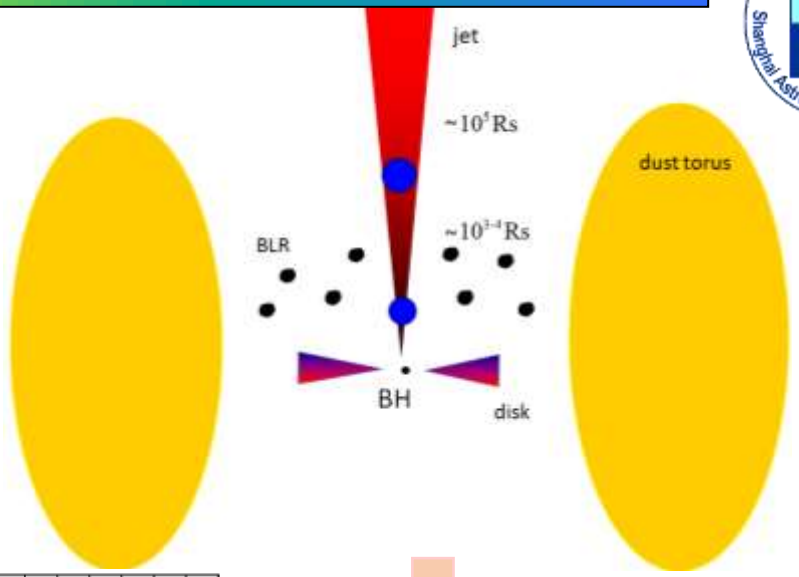

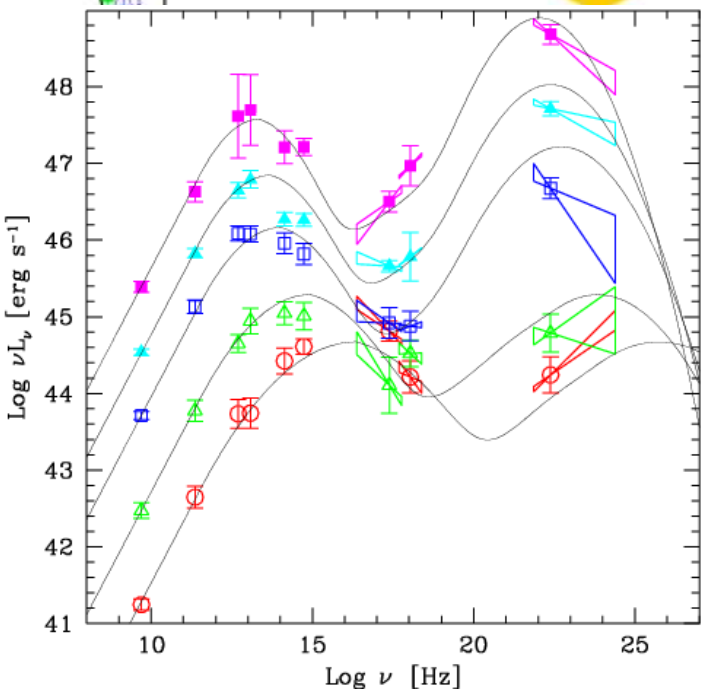

Chen & Bai 2011
Kang et al. 2015

Magnetic dominated?

- Emission region
- SED modeling
- Variability

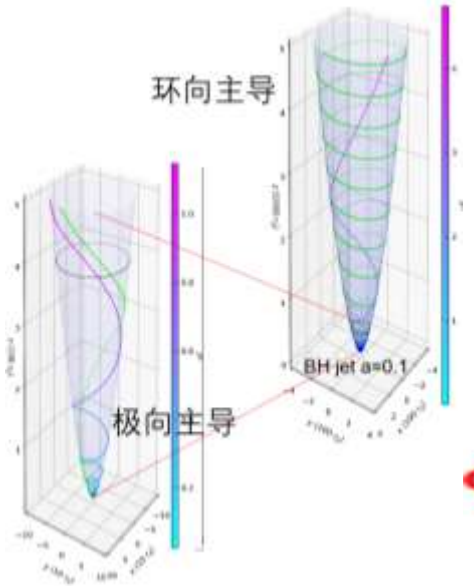

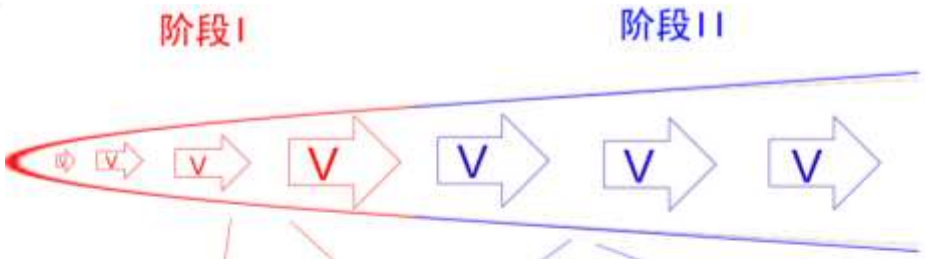

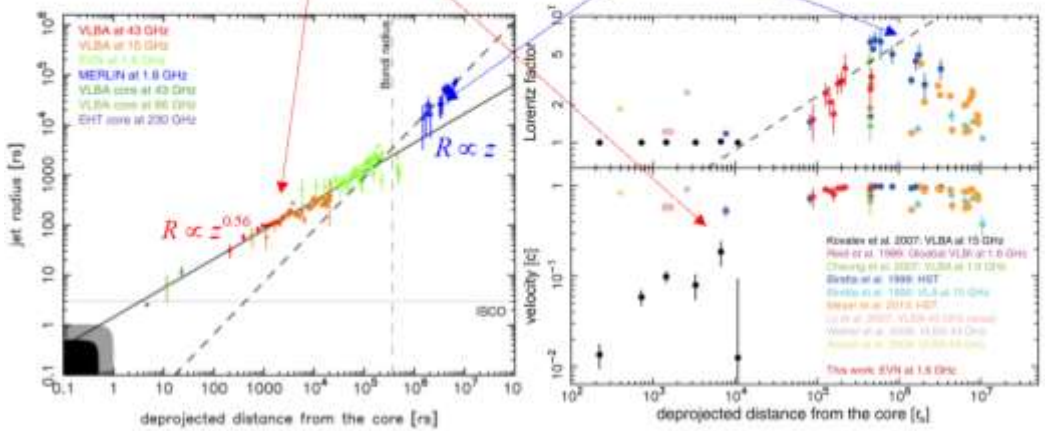

Asada & Nakamura 2012
Nakamura & Asada 2013

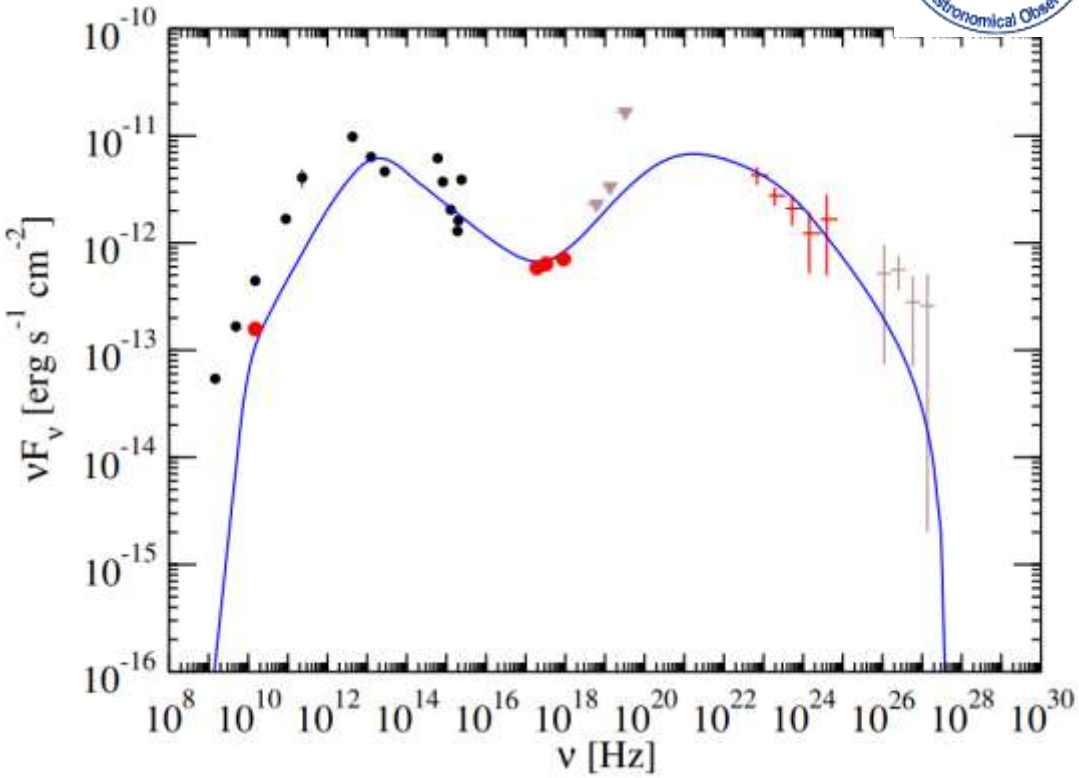

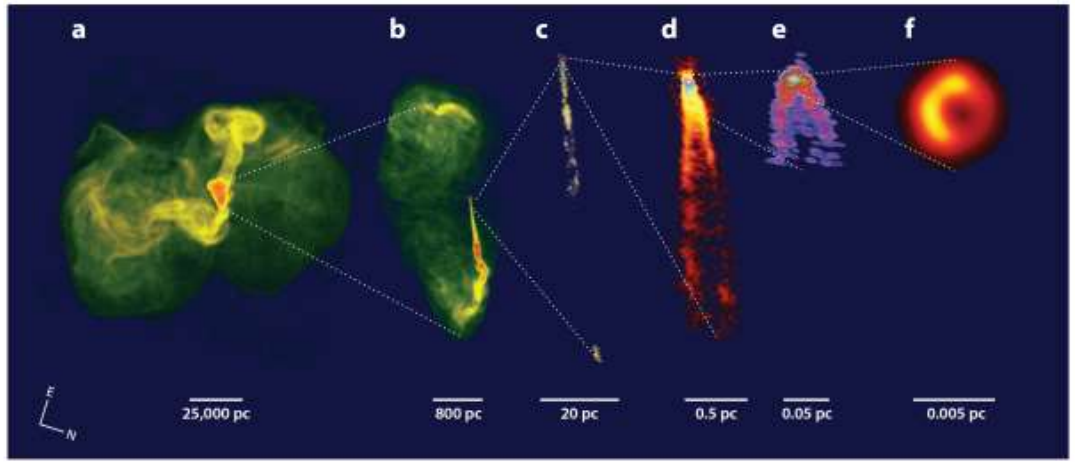

SED

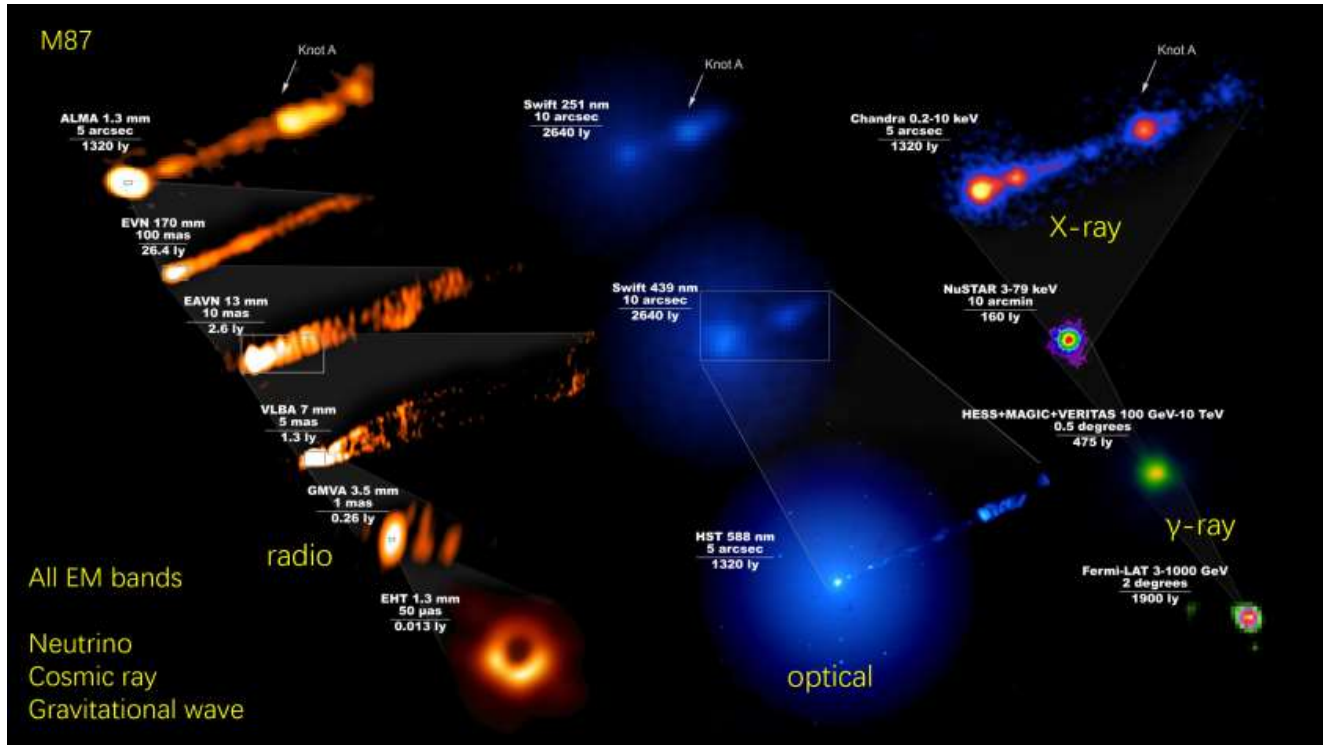
M87
Knot A
Knot A
Knot A
ALMA 1.3 mm
5 arcsec
1320 ly
EVN 170 mm
100 mas
26.4 ly
EAVN 13 mm
10 mas
2.6 ly
VLBA 7 mm
5 mas
1.3 ly
GMVA 3.5 mm
1 mas
0.26 ly
EHT 1.3 mm
50 μas
0.013 ly
Swift 251 nm
10 arcsec
2640 ly
Swift 439 nm
10 arcsec
2640 ly
HST 588 nm
5 arcsec
1320 ly
Chandra 0.2-10 keV
5 arcsec
1320 ly
X-ray
NuSTAR 3-79 keV
10 arcmin
160 ly
HESS+MAGIC+VERITAS 100 GeV-10 TeV
0.5 degrees
475 ly
γ-ray
Fermi-LAT 3-1000 GeV
2 degrees
1900 ly
radio
optical
All EM bands
Neutrino
Cosmic ray
Gravitational wave

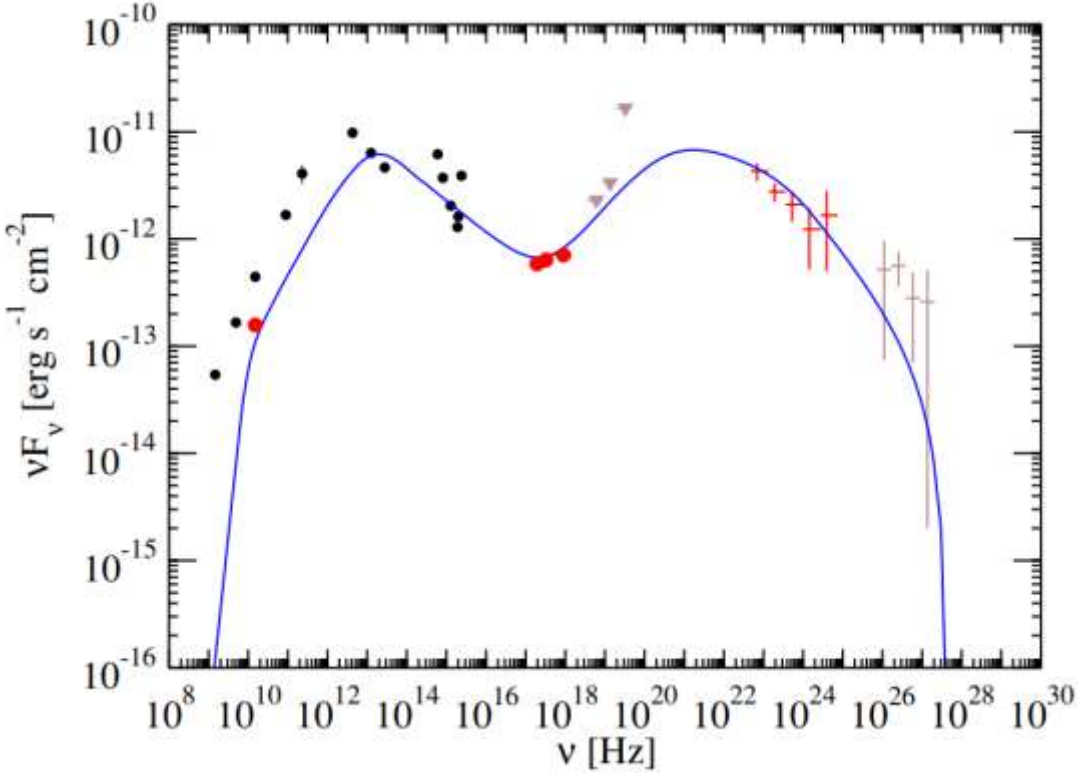
10^{-10}
10^{-11}
10^{-12}
10^{-13}
10^{-14}
10^{-15}
10^{-16}
νF_ν [erg s^{-1} cm^{-2}]
10^{8} 10^{10} 10^{12} 10^{14} 10^{16} 10^{18} 10^{20} 10^{22} 10^{24} 10^{26} 10^{28} 10^{30}
ν [Hz]

SED

- Two bumps
  synchrotron
  IC or hadronic?

- Blazar sequence
  LSP, ISP, HSP
  cooling?

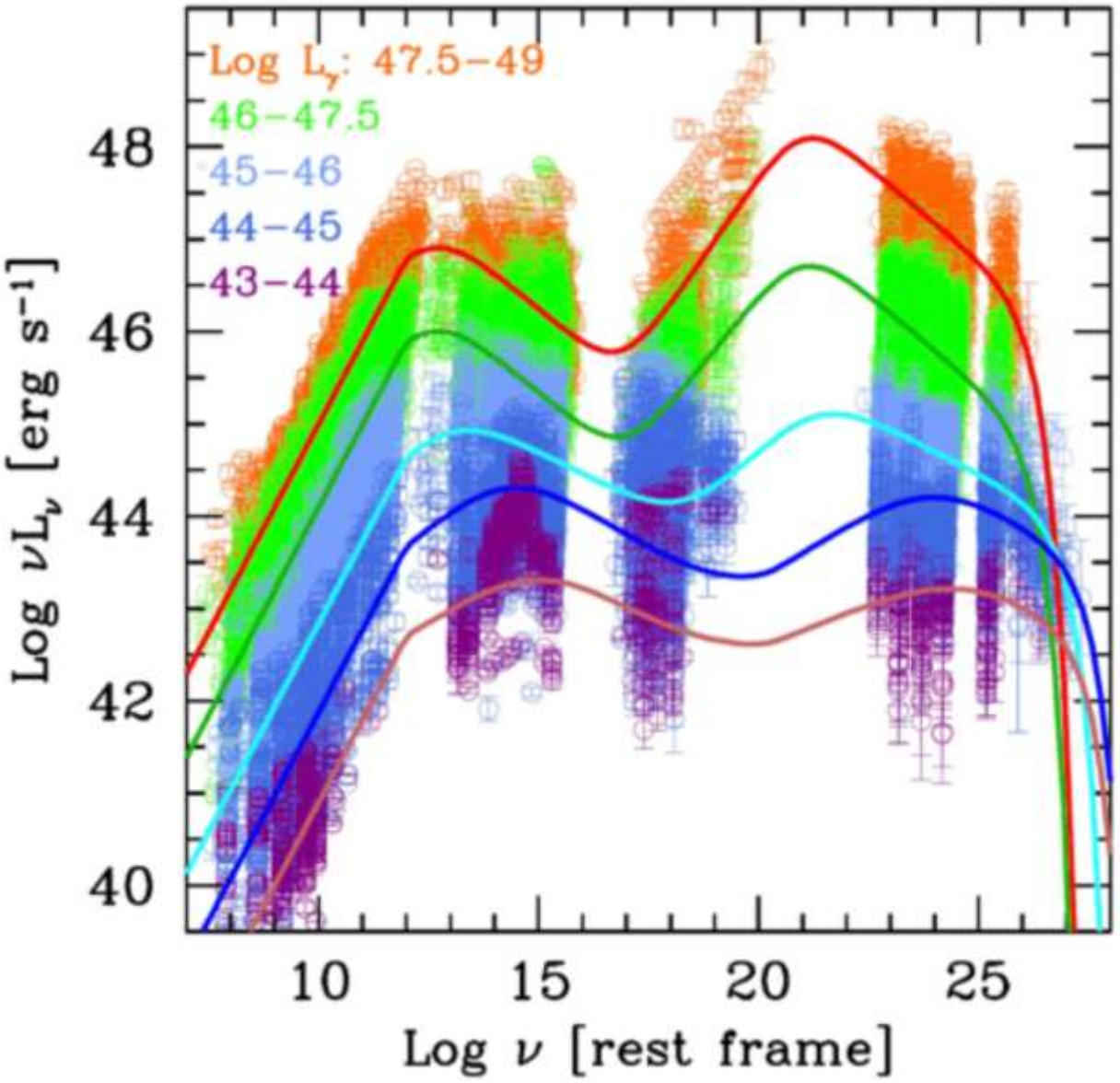

Gamma-ray spectra

- A possible extra (3rd) component?
- Simultaneous data, variability
- Origin?

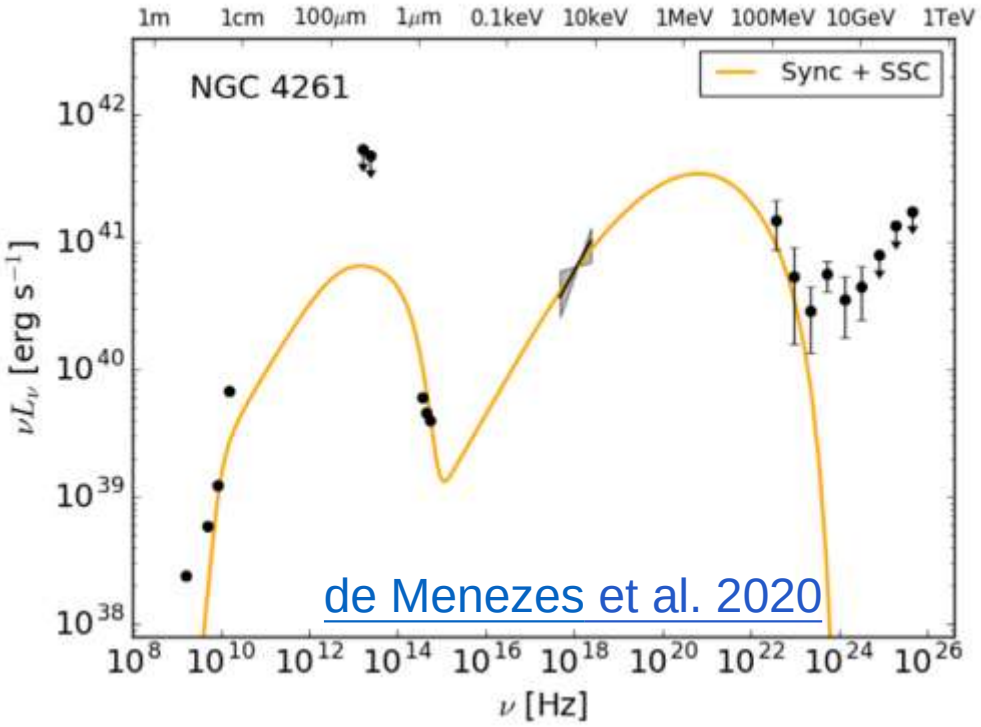

de Menezes et al. 2020

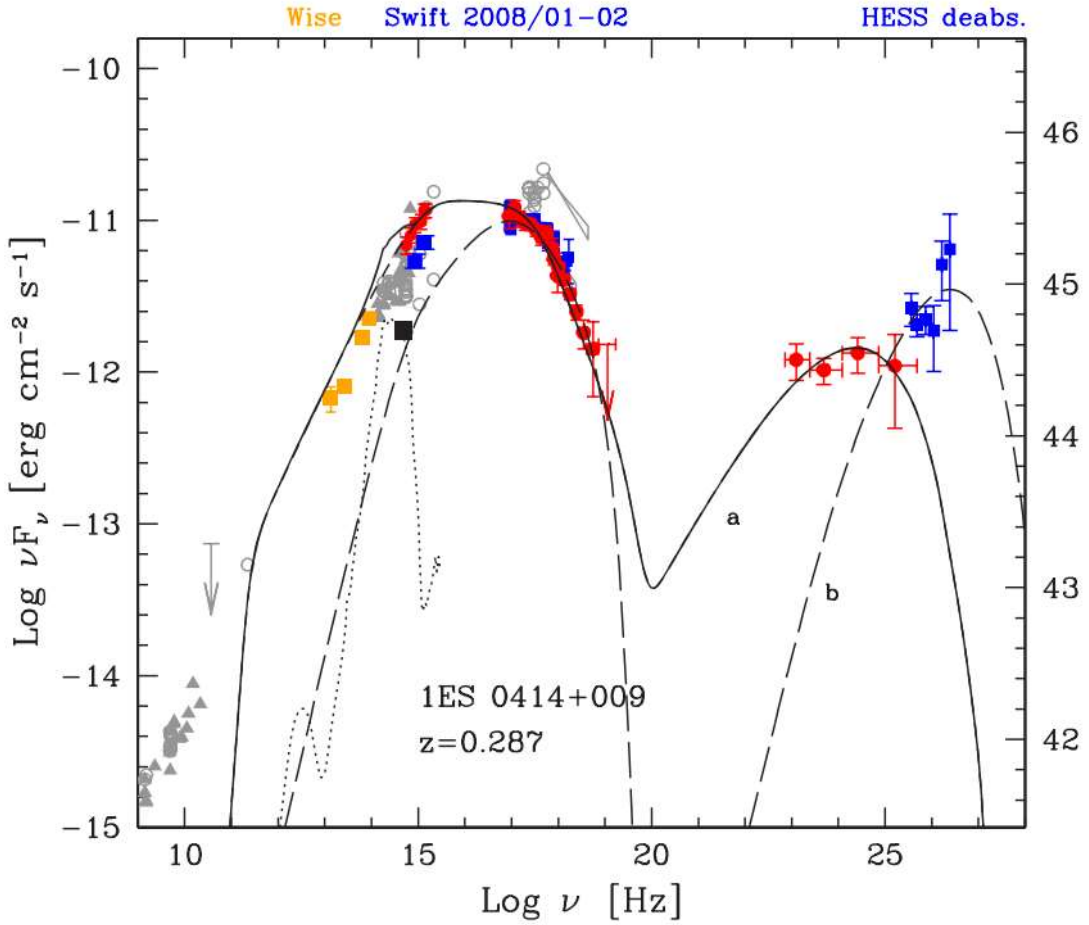

Costamante et al. 2018

SED

- State?
- Power-low
- Log-parabolic
- ……

The H. E. S. S. Collaboration 2024

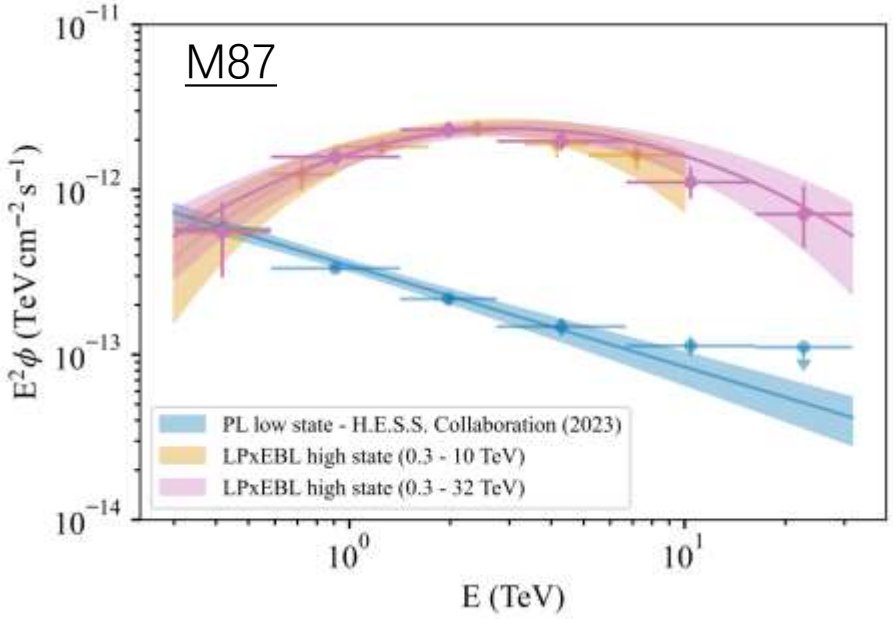

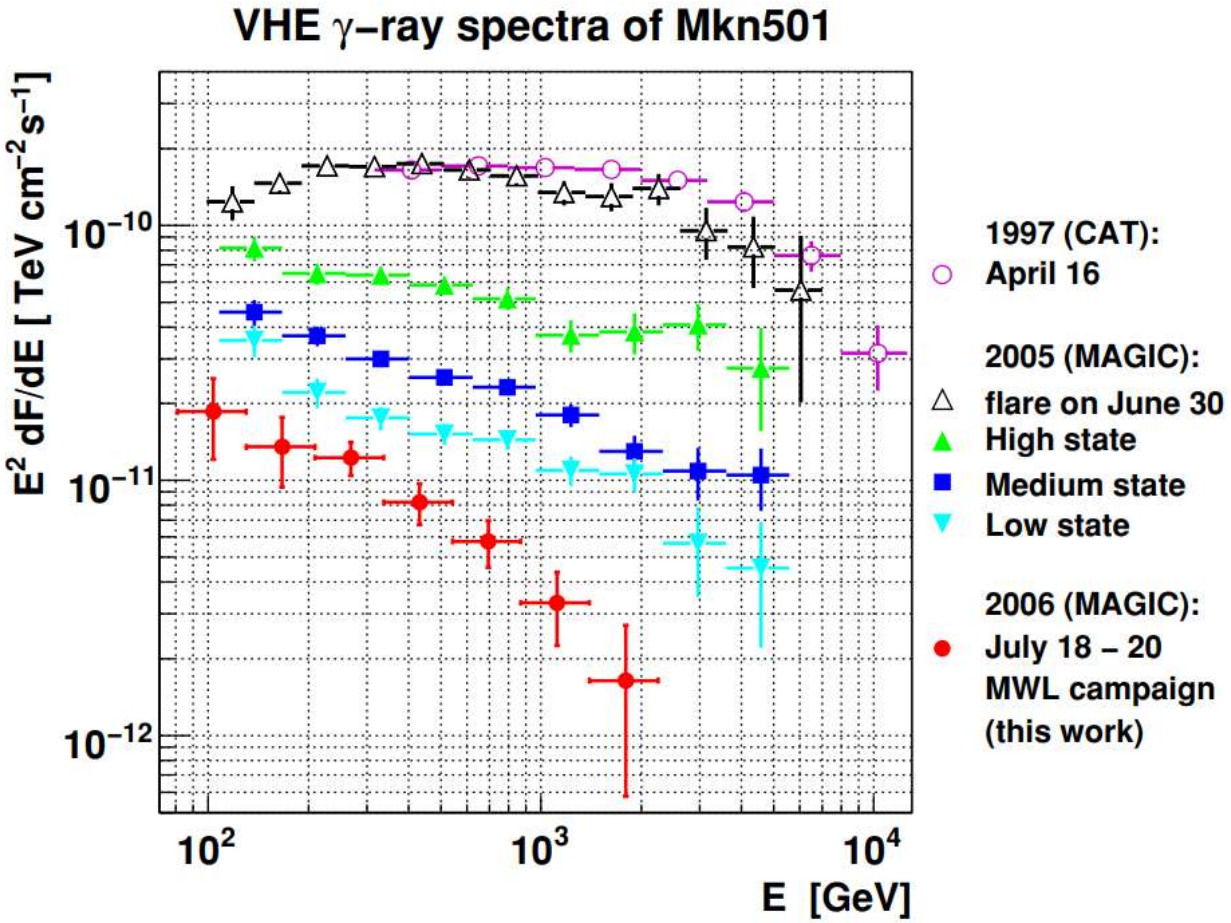

Anderhub et al. 2009

粒子加速：抛物线能谱

- 能谱曲率和峰值频率反相关

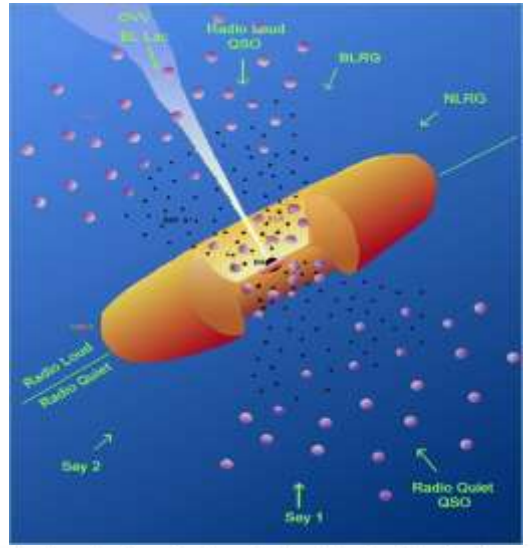

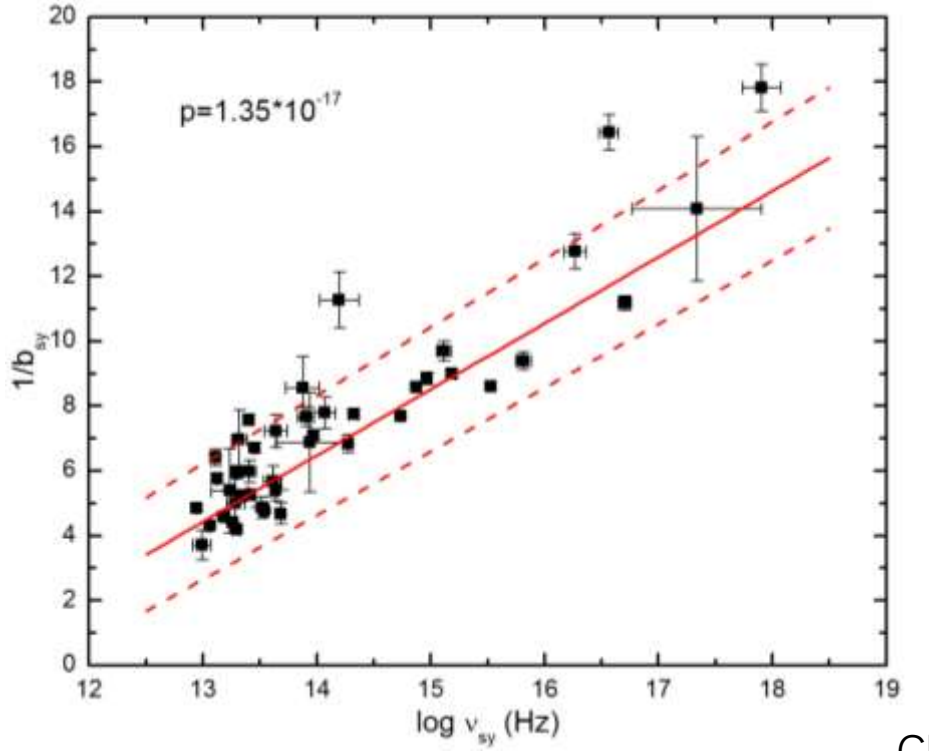

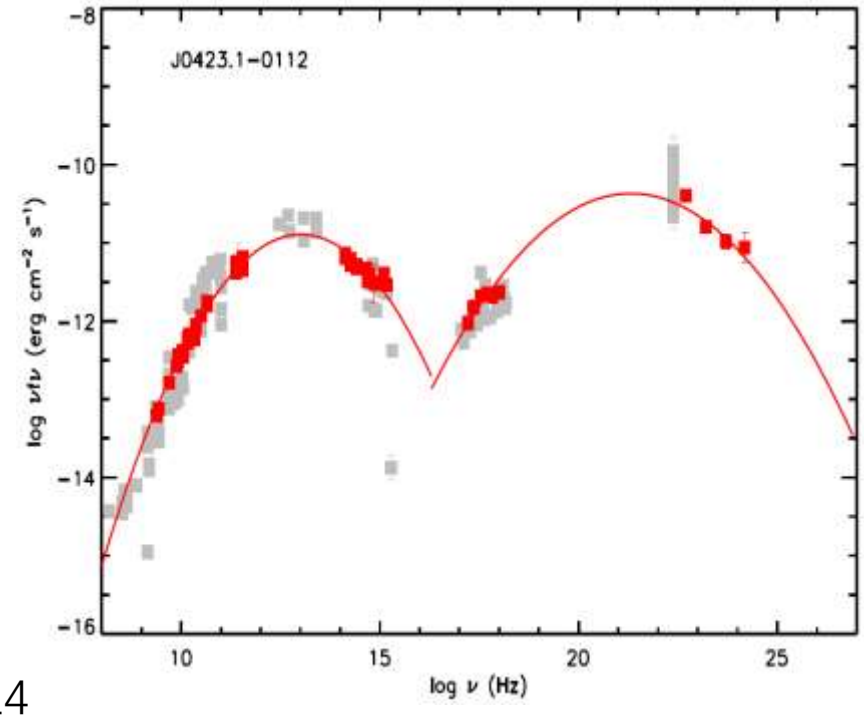

Chen 2014

粒子加速

- Fermi一阶

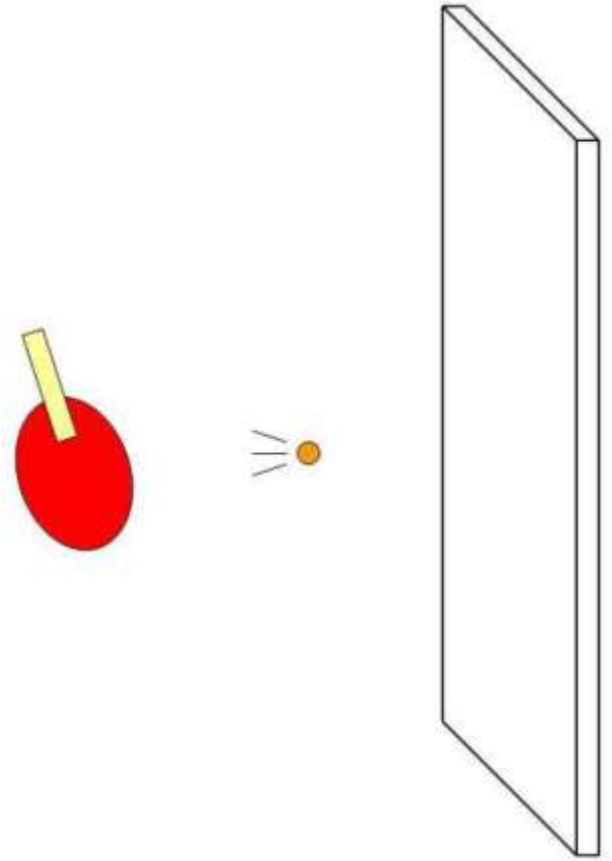

粒子加速

- Fermi一阶

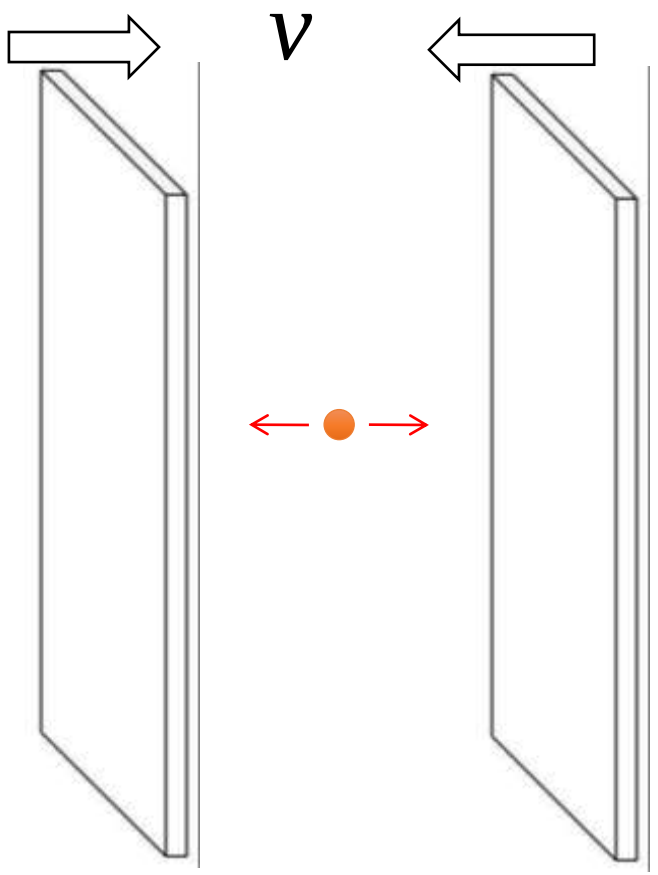

u1>u2

$$\frac{\Delta E}{E} \propto \frac{|u_1 - u_2|}{c}$$

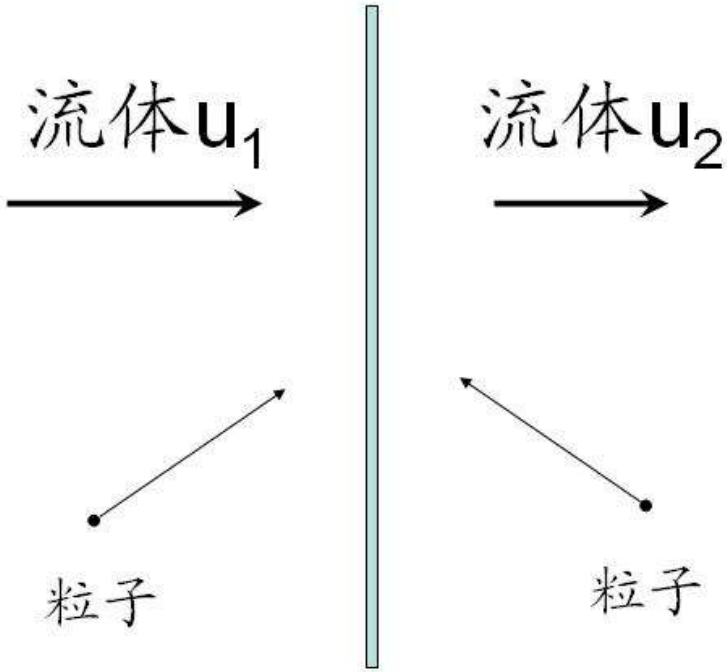

粒子加速

- Fermi一阶
- 加速概率 $p_a = g$
- 能量增加比值 $\varepsilon = cons.$
- 初始能量 γ_0
- 幂率谱 $N(\gamma) \propto \gamma^{\ln g / \ln \varepsilon}$

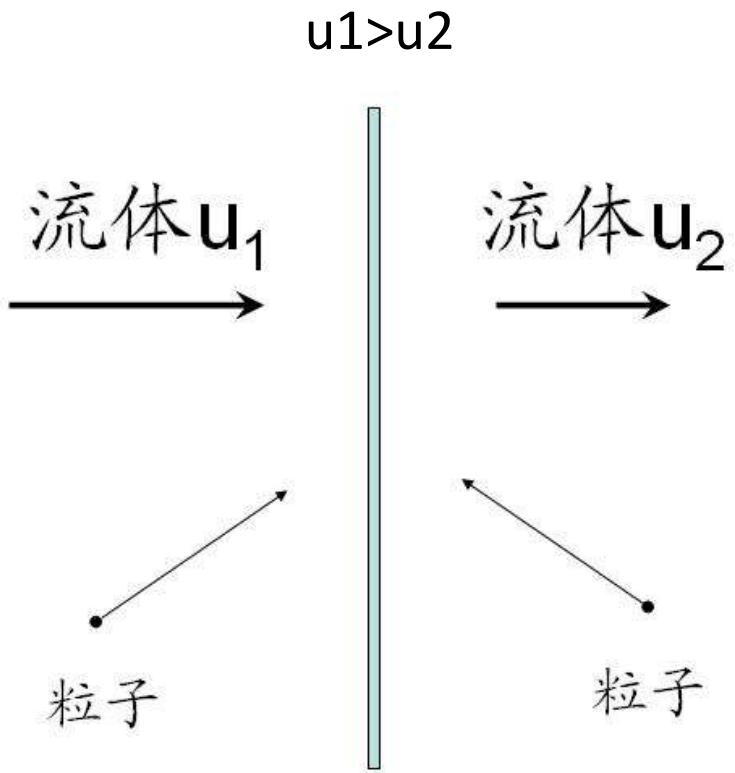

粒子加速

- Fermi一阶
- 加速概率 $p_a = g/\gamma^q$
- 能量增加比值 $\varepsilon = cons.$
- 初始能量 γ_0
- 抛物线谱 $N(\gamma) \approx cons. \left(\frac{\gamma}{\gamma_0}\right)^{-s-r\log(\gamma/\gamma_0)}$

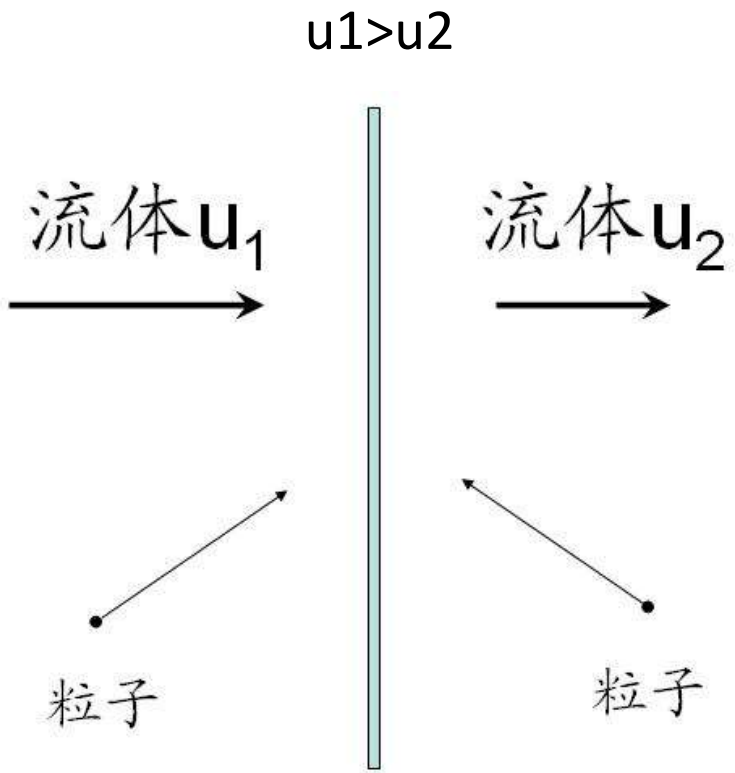

粒子加速

- Fermi一阶
- 加速概率 $p_a = 1$
- 能量增加比值 $\varepsilon = \overline{\varepsilon} + \chi$

  χ probability density: zero mean and variance σ_ε^2
- 初始能量 γ_0
- 抛物线谱 $N(\gamma) = \dfrac{N_0}{\gamma\sigma_\gamma\sqrt{2\pi}} \exp\left[-\dfrac{(\ln\gamma - \mu)^2}{2\sigma_\gamma^2}\right]$

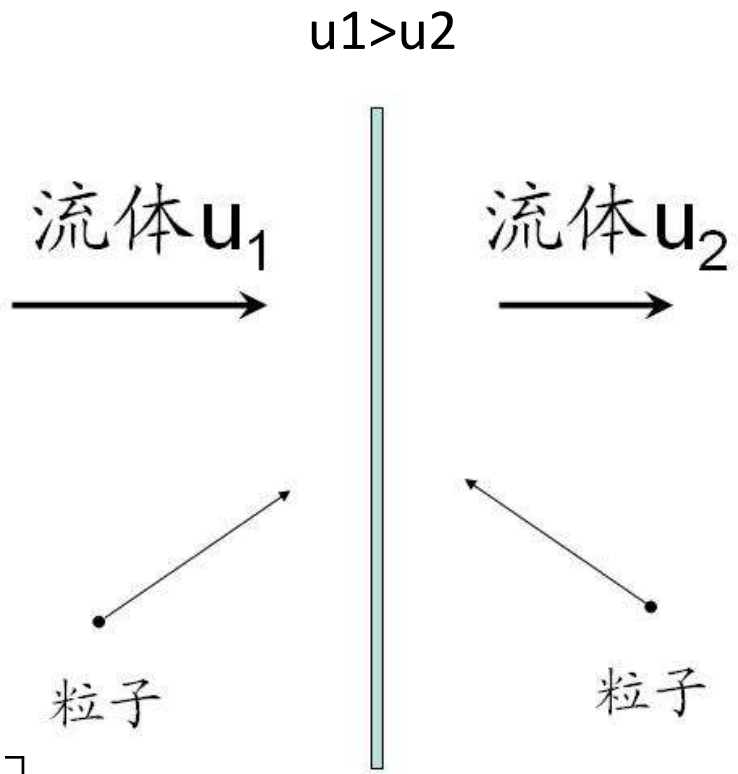

光变

Blazar variability

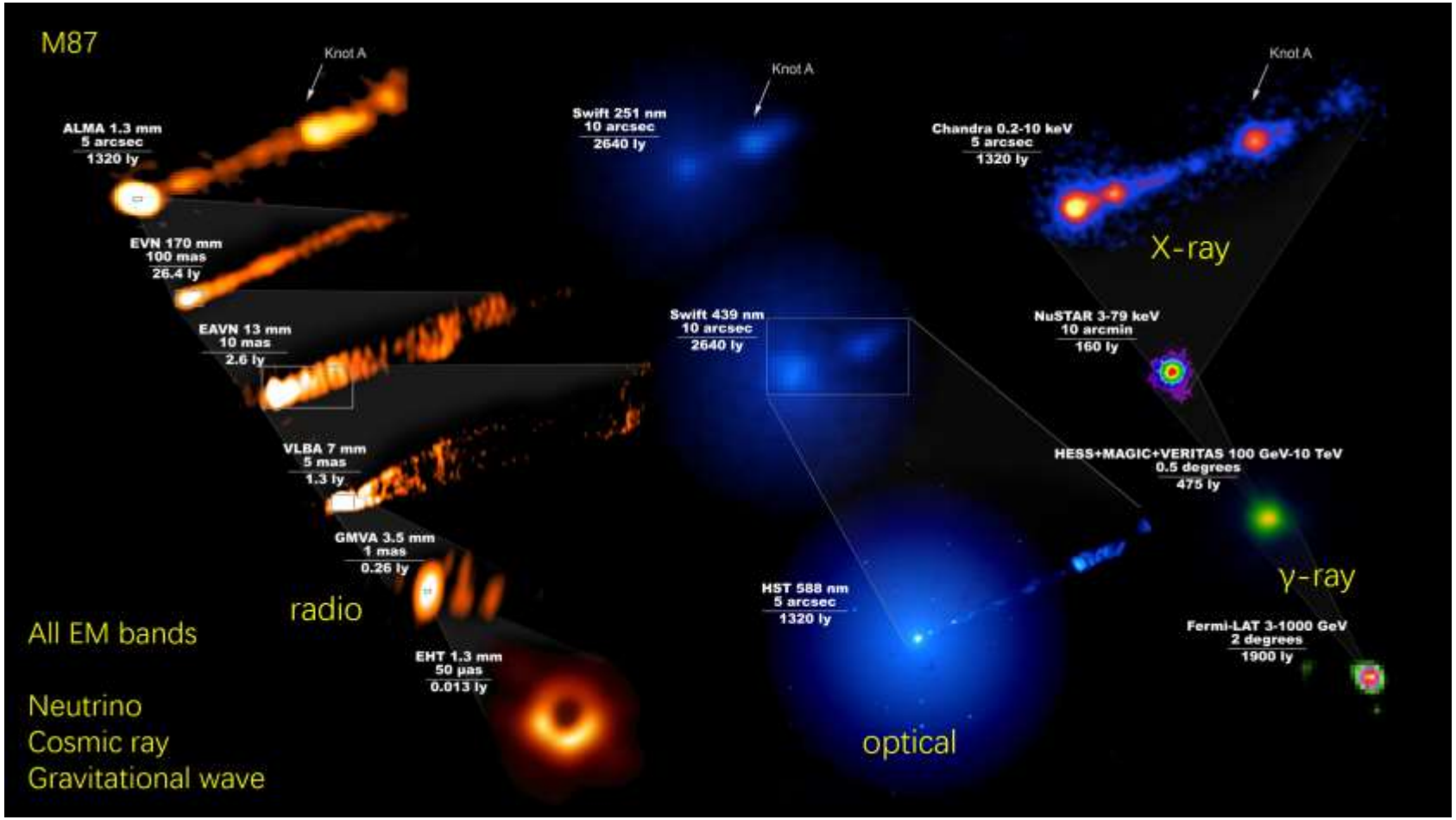

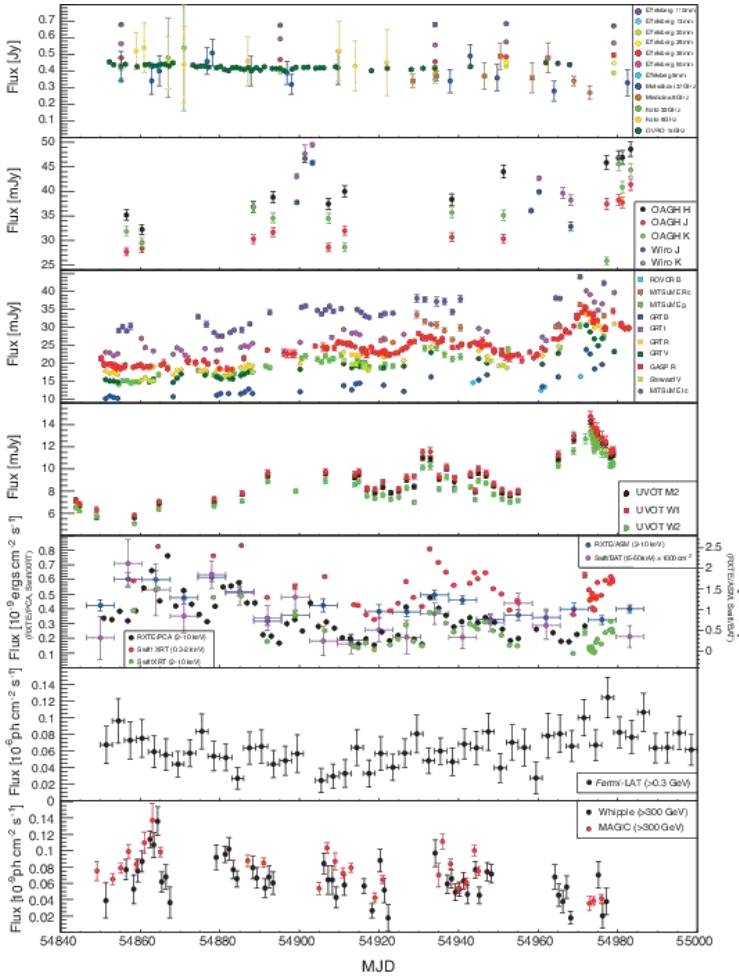

光变特征

- 规则性光变，QPO，时标，起源
- 高频领先低频
- 短时标光变

光深问题，相对论聚束效应

$$\tau_{\gamma\gamma} \simeq \frac{f_{\rm r} d^2 \sigma_{\rm T} \delta_{\rm j}^{-6} E}{8 m_{\rm e}^2 c^6 \Delta t} \simeq 0.065 f_{-10} \Delta t_{\rm day}^{-1} \delta_{10}^{-6} H_{60}^{-2} E_{\rm TeV}$$

$$h\nu \simeq 100 \delta_{10}^2 E_{\rm TeV}^{-1} \, {\rm eV}$$

PG 1553+113, Ackermann et al. 2015

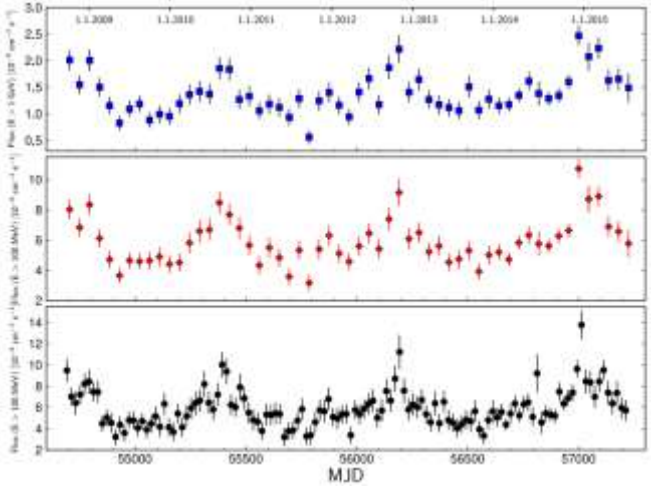

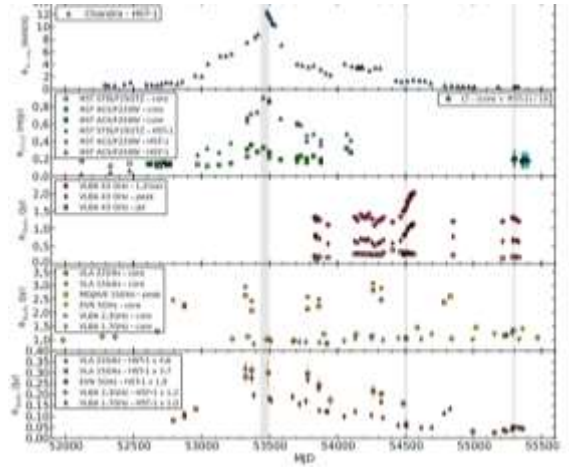

Name	GeV	TeV	X-ray	optical	Type
BL Lacertae	~1 min	~13 min		~1.7 hour	LBL/IBL
3C 279	~5 min				FSRQ
PKS 1510-089	~20 min				FSRQ
PKS 2155-304	~1.2pm0.2 hour	~3 min			HBL
Mrk 501		~2 min	~1 min		HBL
IC 310		~4.8-1 min			RG/BL
Mrk 421		~15 min			HBL
PKS 1222+216	<1.8 hour	~8.6 min			FSRQ
S5 0716+714			~3 min	<0.2 day	IBL
PKS 2005-489			~0.5 min		HBL
3C 371				~10min	BL

Fractional variability

$$F_{var} = \sqrt{\frac{S^2 - \langle \sigma_{err}^2 \rangle}{\langle f \rangle^2}}$$

$$\Delta F_{var} = \sqrt{F_{var}^2 - err(\sigma_{NXS}^2)} - F_{var}$$

$$\langle \sigma_{err}^2 \rangle = \frac{1}{N} \sum_{i=1}^{N} \sigma_{err,i}^2$$

$$err(\sigma_{NXS}^2) = \sqrt{\left(\sqrt{\frac{2}{N}} \frac{\langle \sigma_{err}^2 \rangle}{\langle f \rangle^2} \right)^2 + \left(\sqrt{\frac{\langle \sigma_{err}^2 \rangle}{N}} \frac{2F_{var}}{\langle f \rangle^2} \right)^2}$$

$$S^2 = \frac{1}{N-1} \sum_{i=1}^{N} (f_i - \langle f \rangle)^2$$

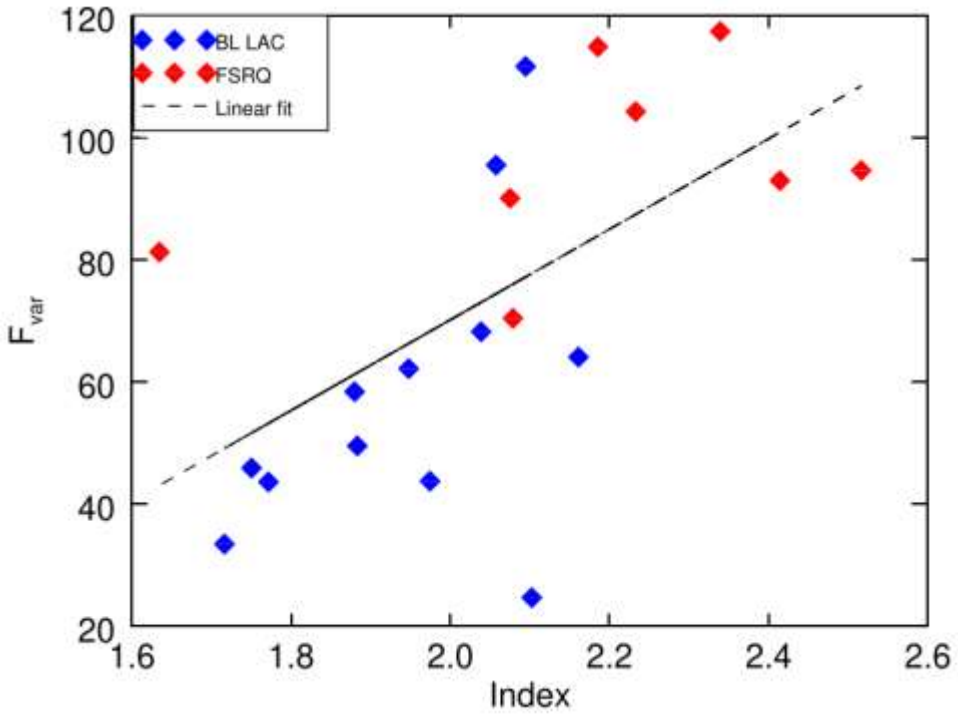

Fermi/LAT, Bhatta and Dhital 2020

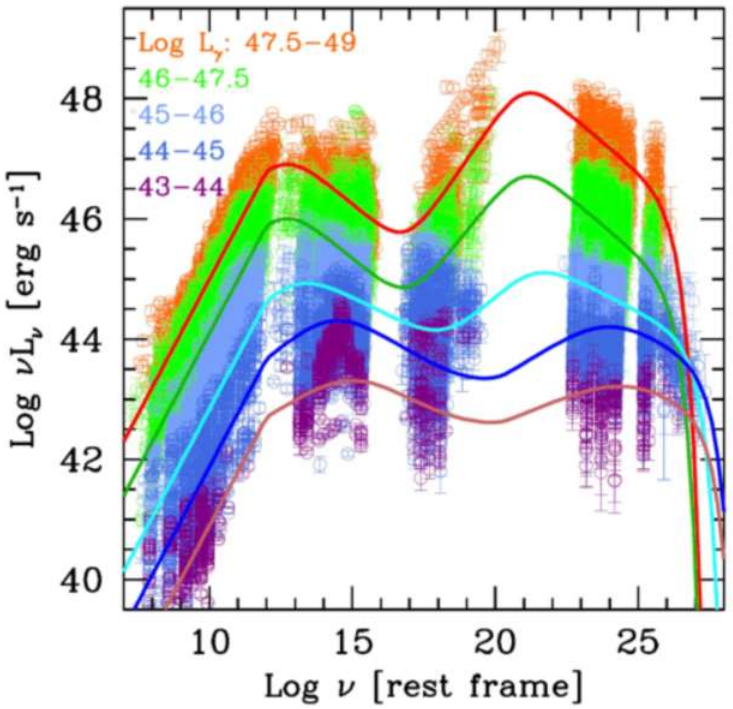

Fractional variability

- 起源
- 幅度
- 时间

$$F_{var} = \sqrt{\frac{S^2 - \langle \sigma_{err}^2 \rangle}{\langle f \rangle^2}}$$

$$\Delta F_{var} = \sqrt{F_{var}^2 - err(\sigma_{NXS}^2)} - F_{var}$$

$$\langle \sigma_{err}^2 \rangle = \frac{1}{N} \sum_{i=1}^{N} \sigma_{err,i}^2$$

$$err(\sigma_{NXS}^2) = \sqrt{\left(\sqrt{\frac{2}{N}} \frac{\langle \sigma_{err}^2 \rangle}{\langle f \rangle^2} \right)^2 + \left(\sqrt{\frac{\langle \sigma_{err}^2 \rangle}{N}} \frac{2F_{var}}{\langle f \rangle^2} \right)^2}$$

$$S^2 = \frac{1}{N-1} \sum_{i=1}^{N} (f_i - \langle f \rangle)^2$$

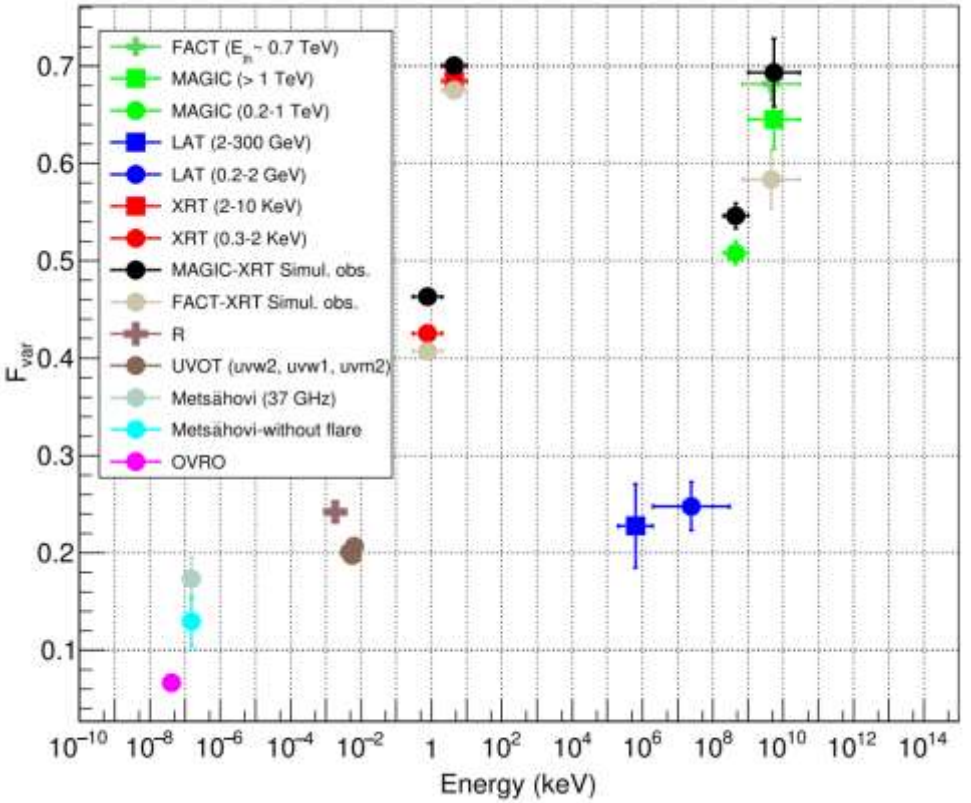

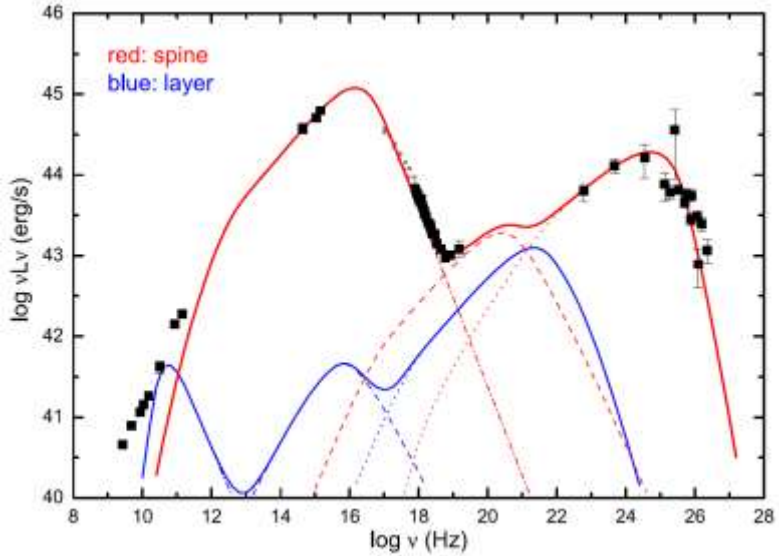

Log-normal distribution

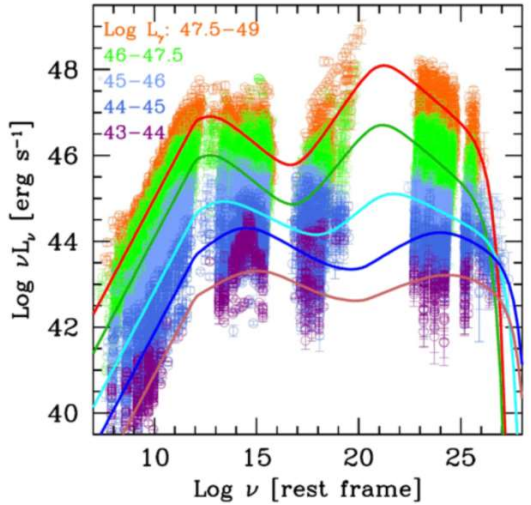

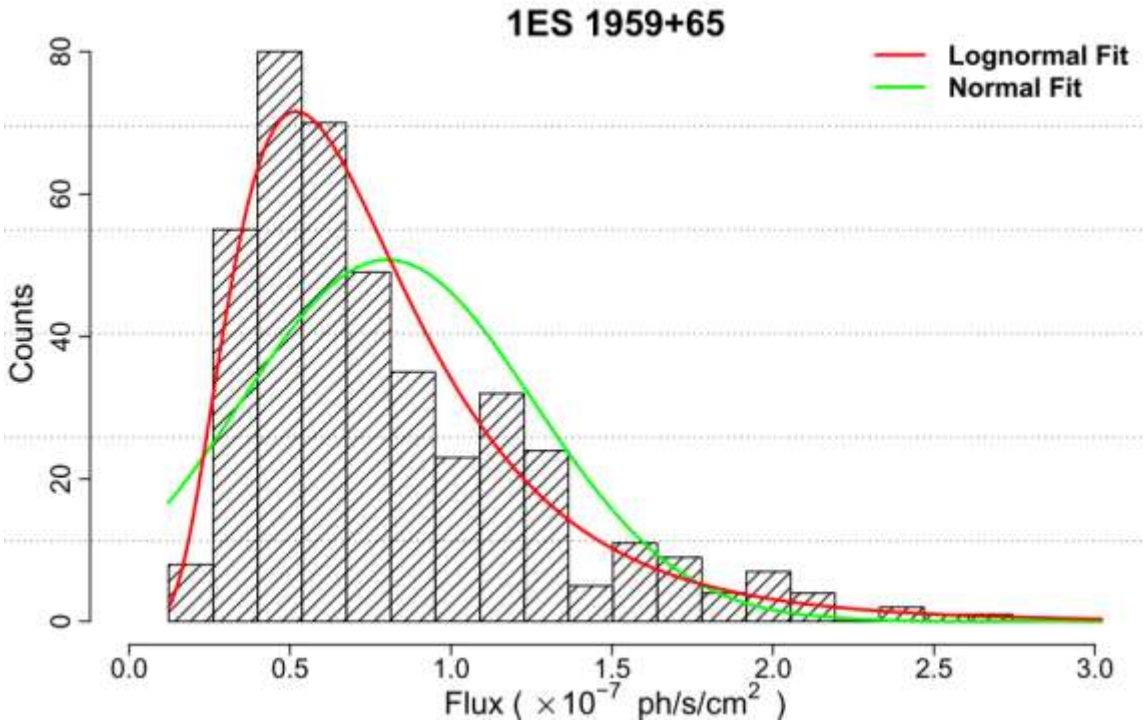

Bhatta and Dhital 2020

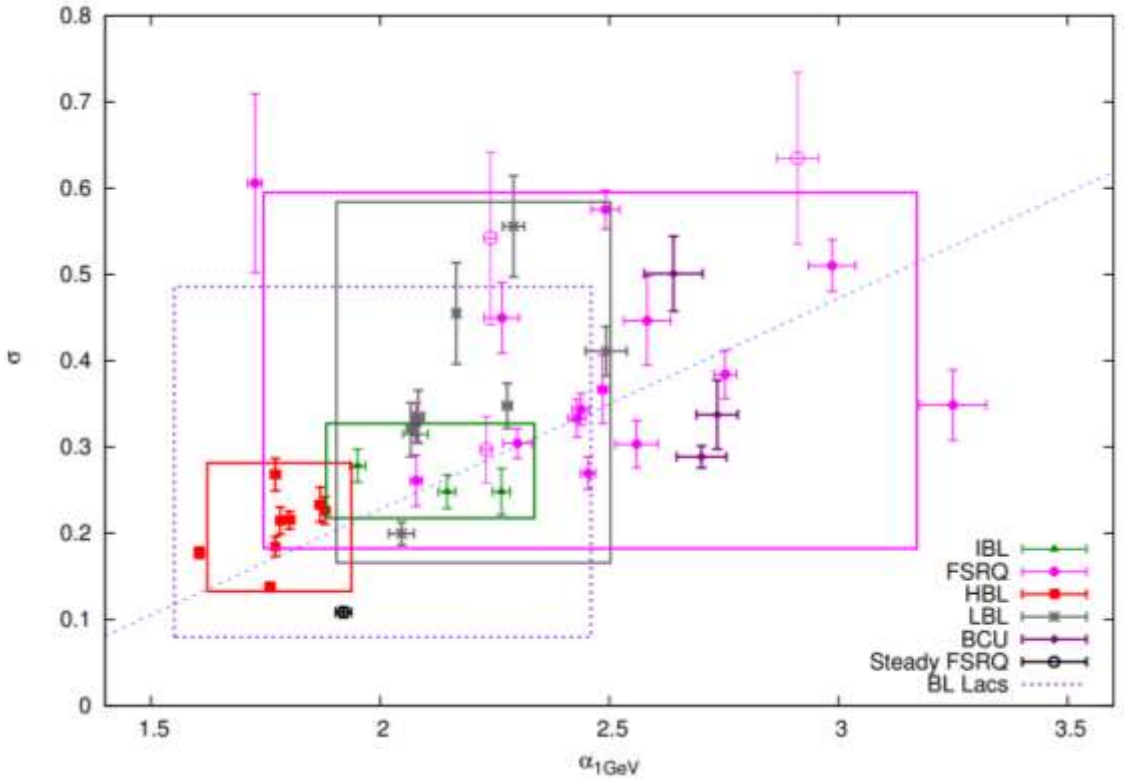

Shah et al. 2018

Power spectral density (PSD)

- 3C 279: radio – gamma-ray
- Slop: frequency dependent?
- PSD: break? timescale?

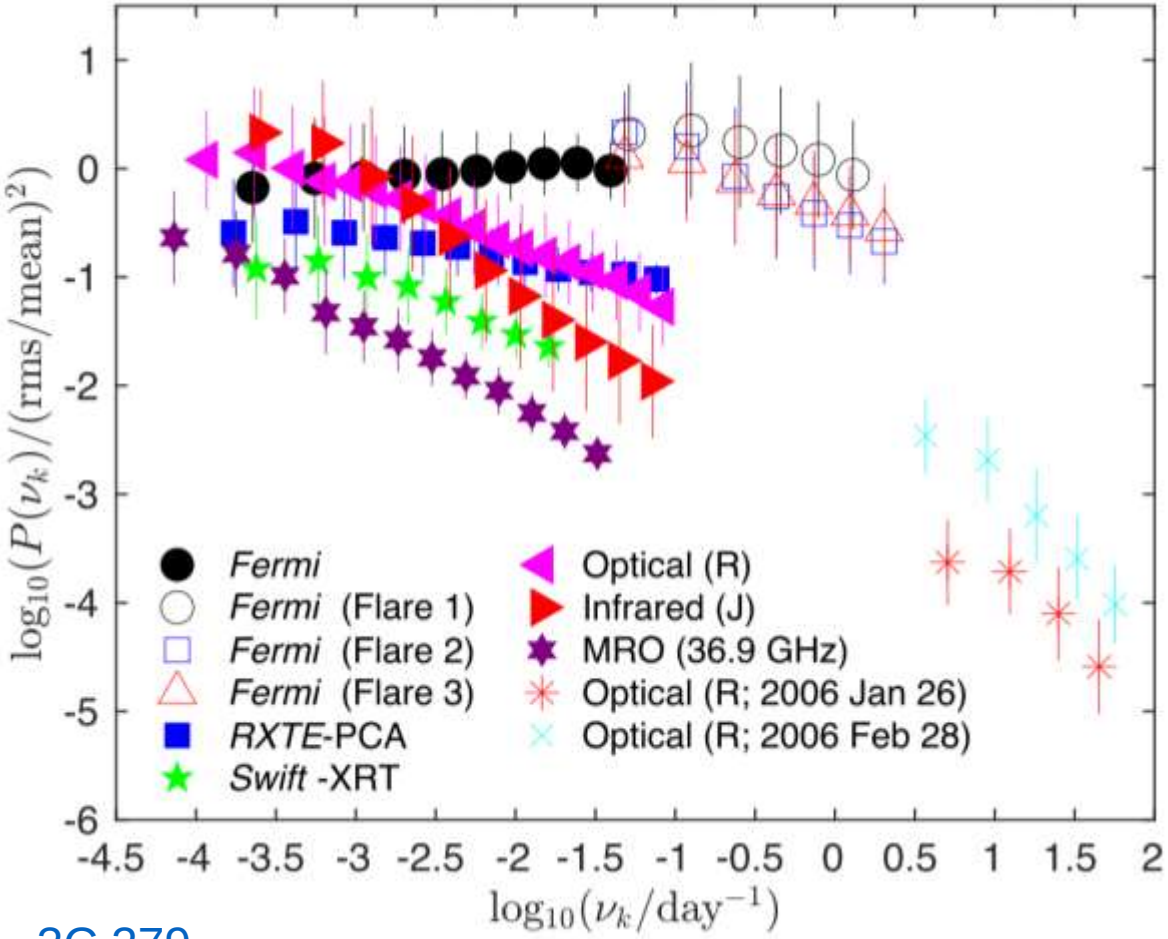

3C 279
Goyal et al. 2022

PSD: PKS 2155-304

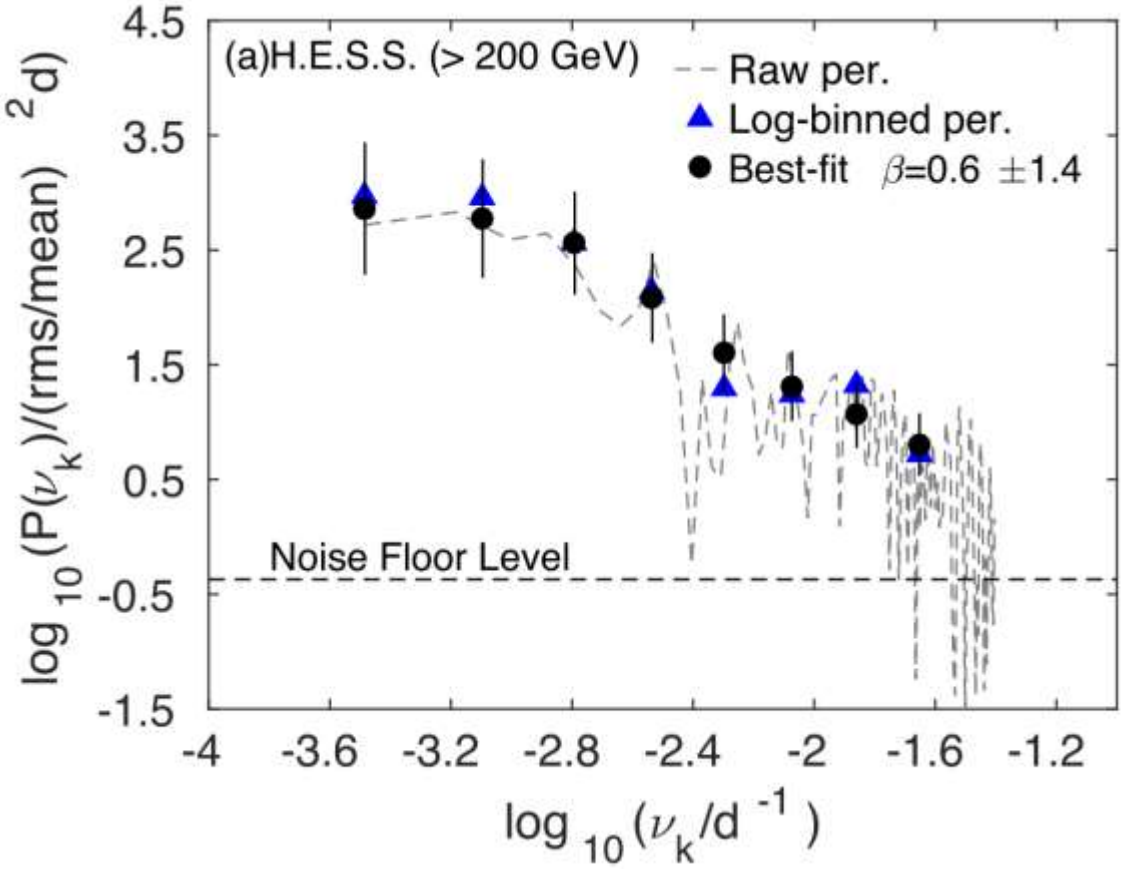

Goyal 2020

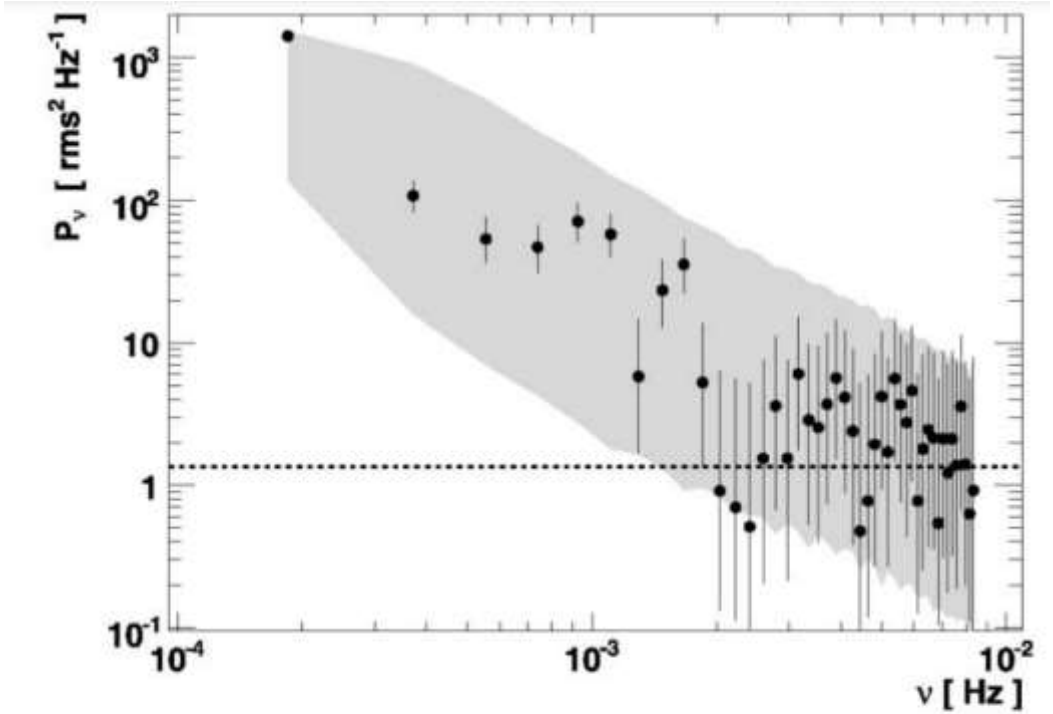

FIG. 2.—Fourier power spectrum of the light curve and associated measurement error. The gray shaded area corresponds to the 90% confidence interval for a light curve with a power-law Fourier spectrum $P_\nu \propto \nu^{-2}$. The horizontal line is the average noise level (see text).

Aharonian et al. 2007

EBL与河外高能光子

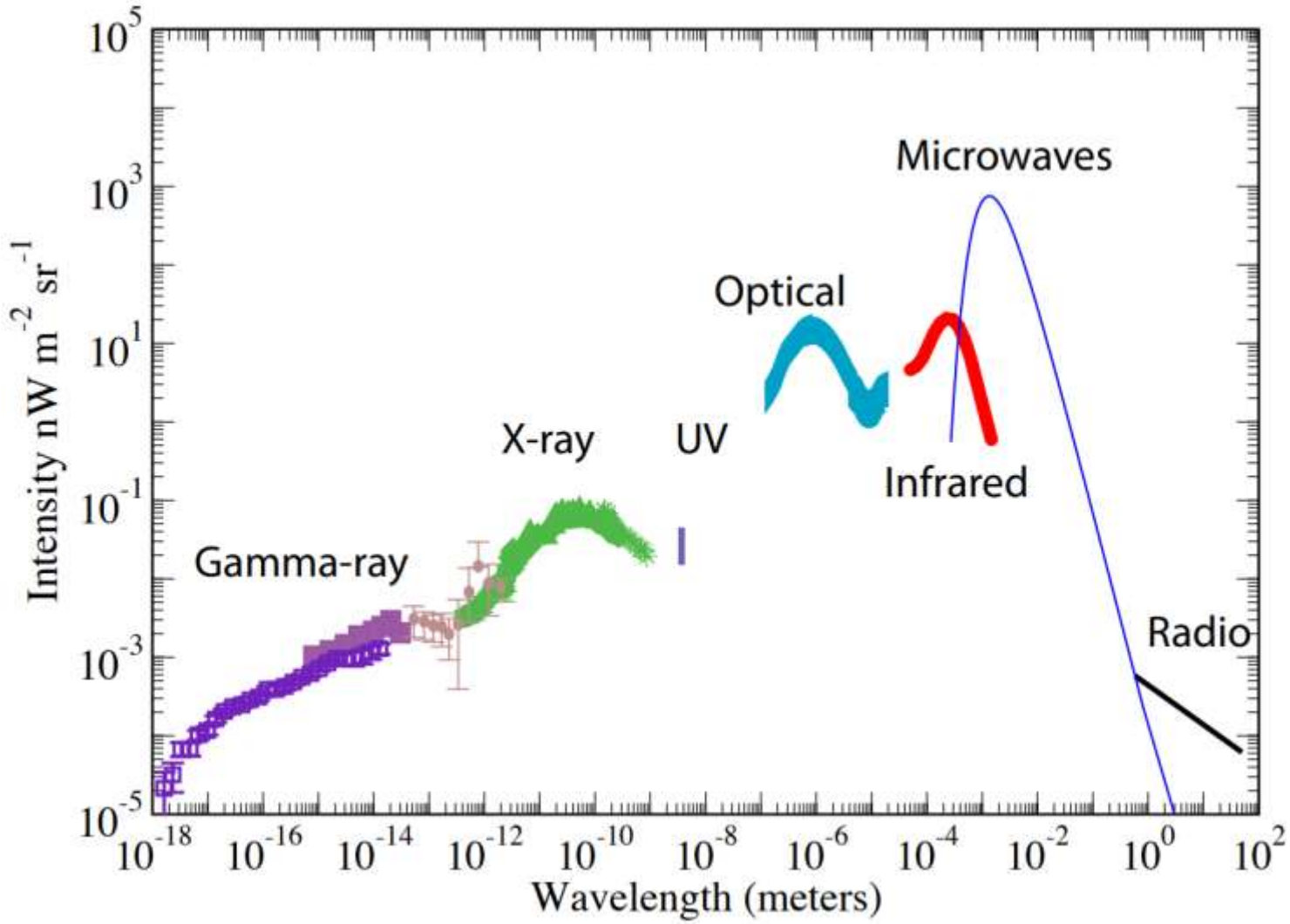

Cooray 2016

- 光学红外EBL
- 吸收VHE光子

EBL and IGMF: TeV and GeV

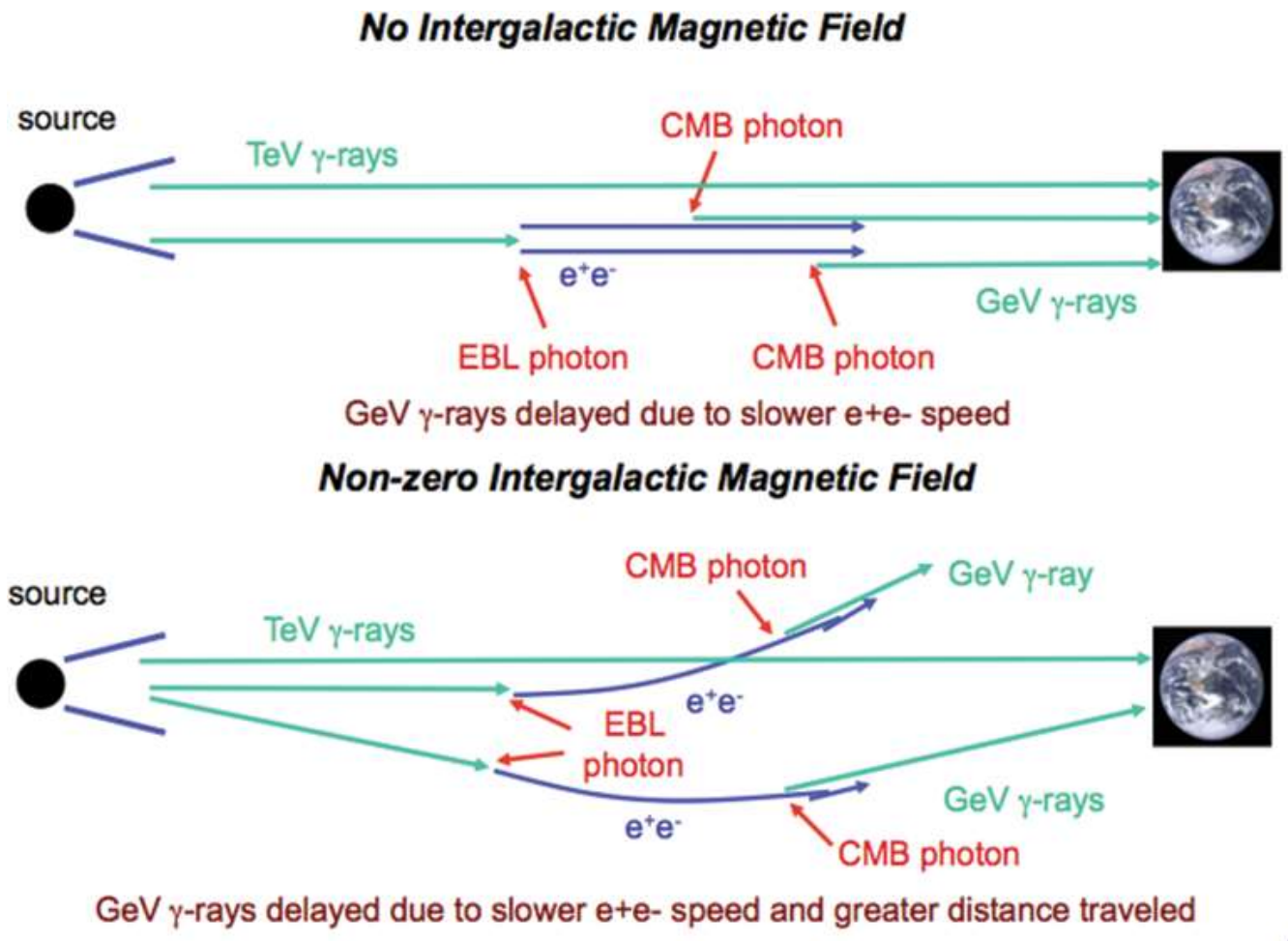

The maximum energy of extra-galactic photons

- @outburst
- Mrk 501:　~20 TeV
- M87: ~20 TeV

The H. E. S. S. Collaboration 2024

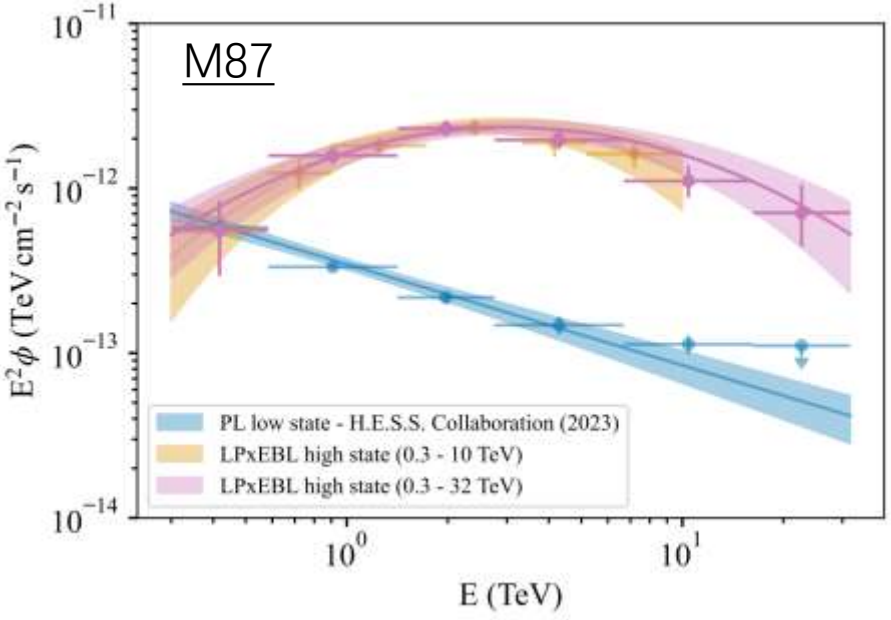

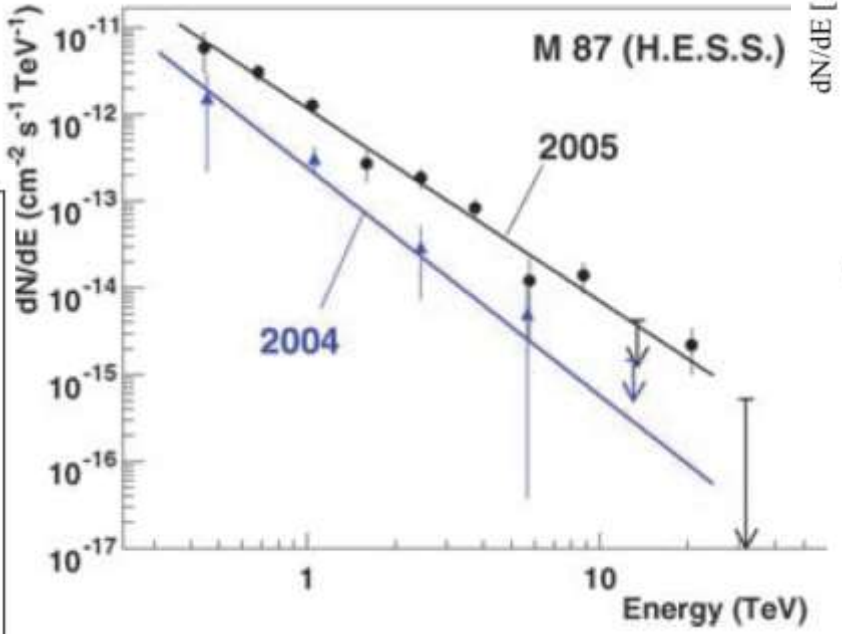

Aharonian et al. 2006

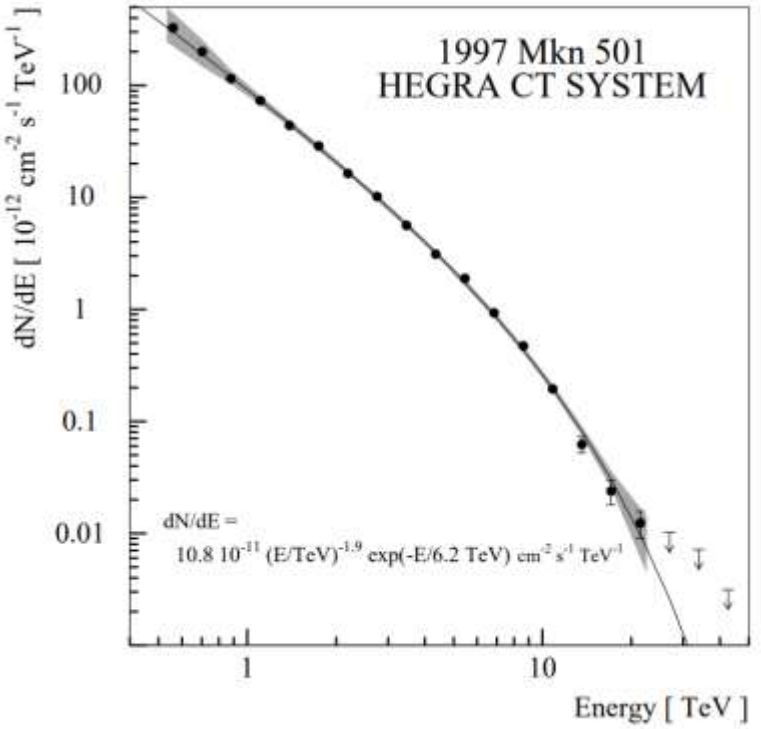

Aharonian et al. 1999

EBL constrain

- VERITAS
- PKS 1441+25
- z= 0.939
- ~200 GeV

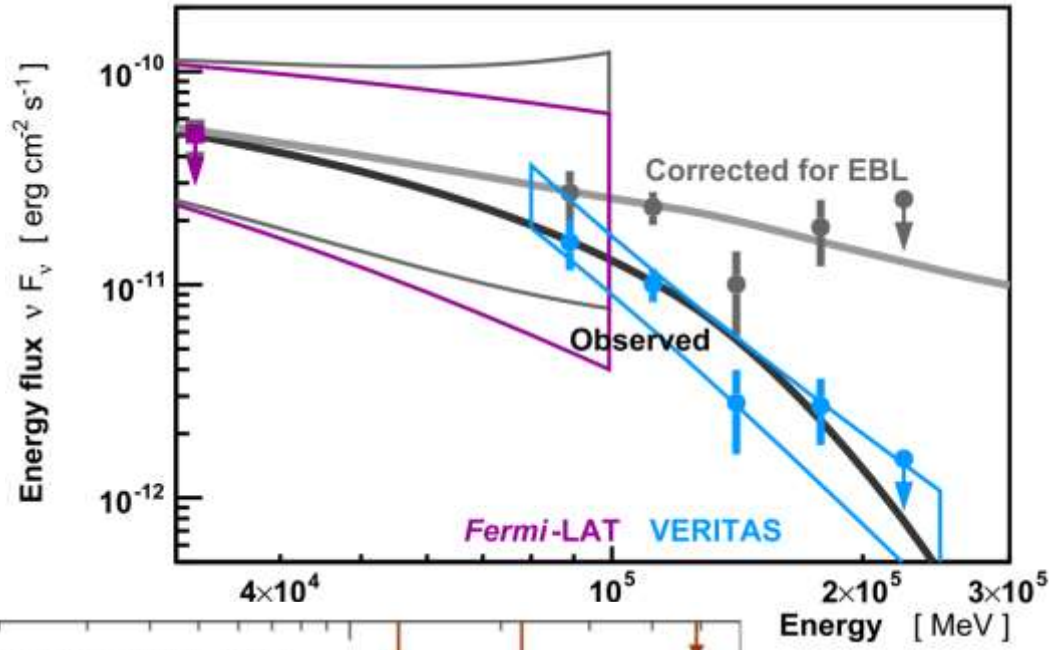

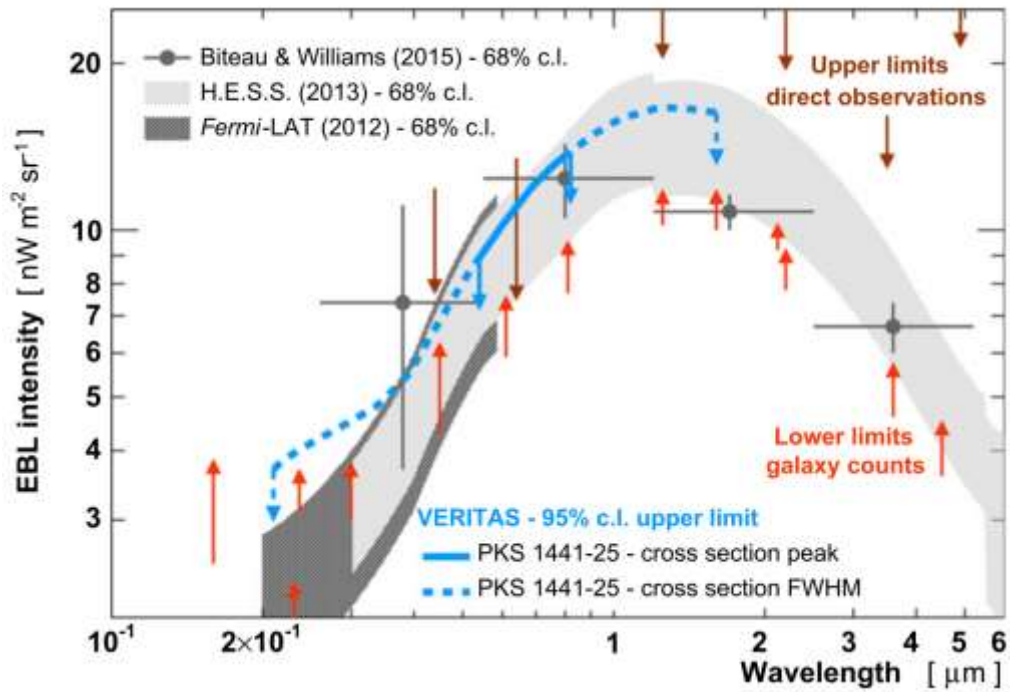

- EBL: near galaxy counts limit

Abeysekara et al. 2015

EBL constrain

- H.E.S.S. & VERITAS
- blazar samples

- EBL: near galaxy counts limit

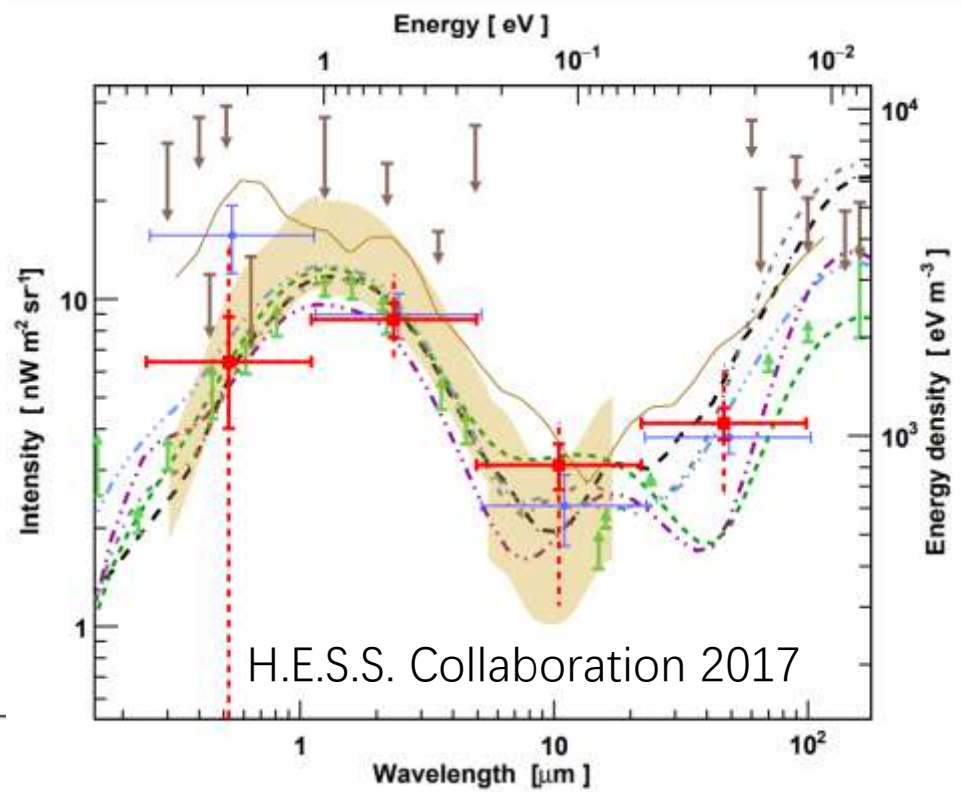

H.E.S.S. Collaboration 2017

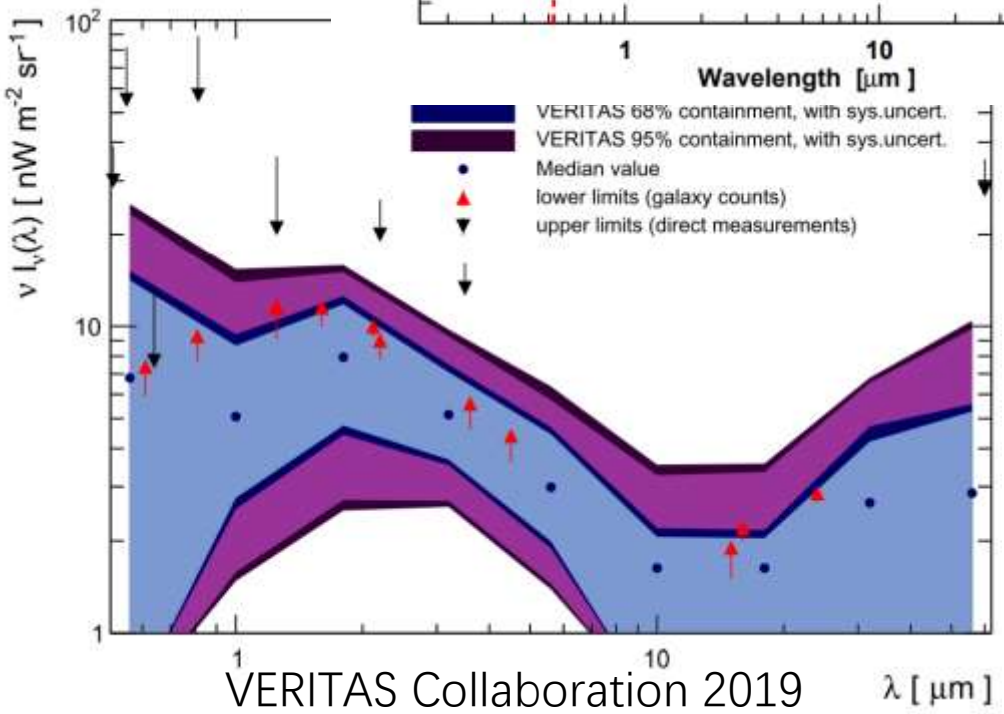

VERITAS Collaboration 2019

Gamma-ray halo and IGMF

- stack 24 HBLs
- $z < 0.5$
- Extended emission (halo):

  $p \sim 0.01$

- $B_{IGMF} \sim 10^{-17}$ - 10^{-15} Gs

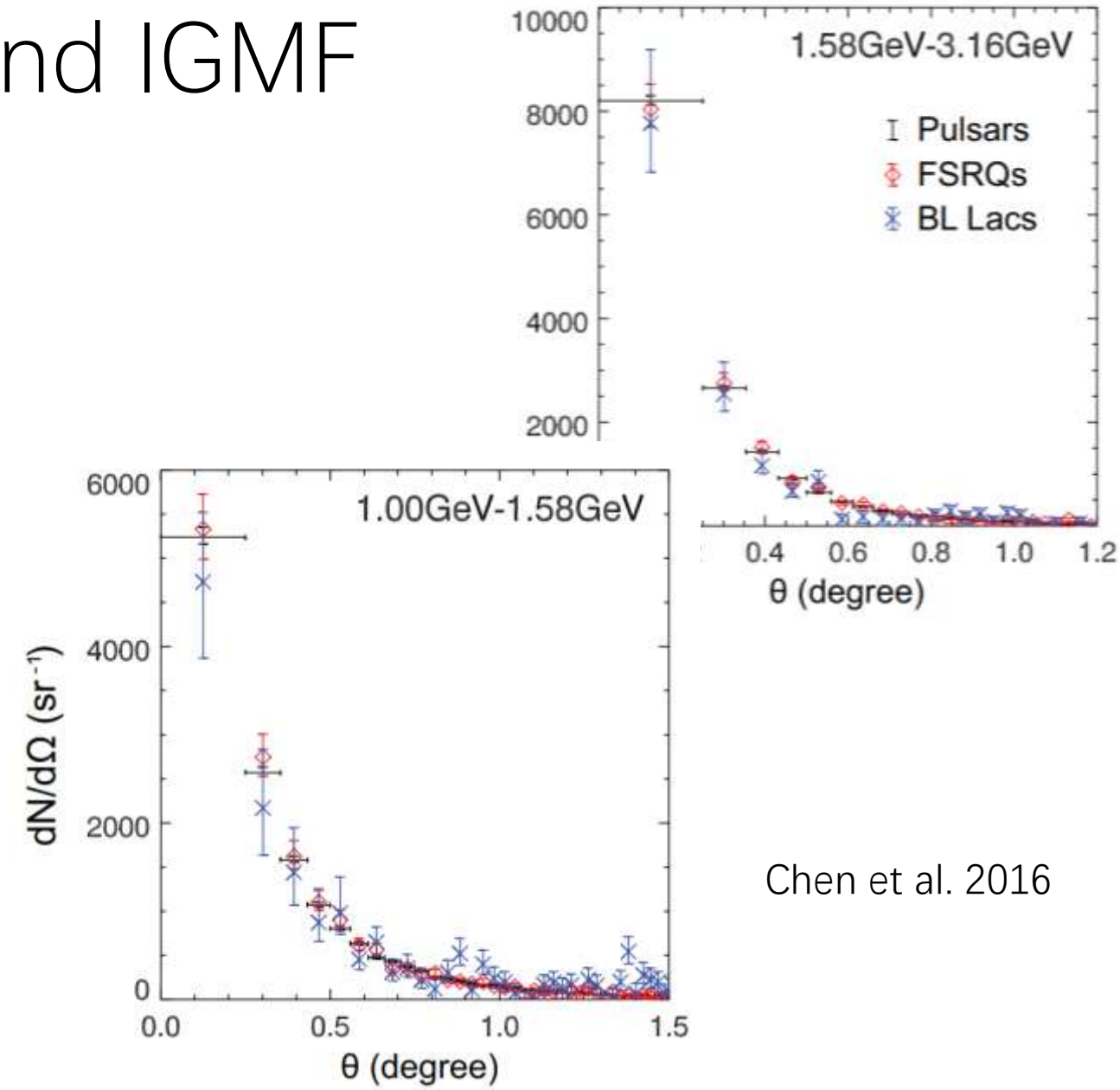

Chen et al. 2016

弯曲时空电动力学

电动力学　　广义相对论

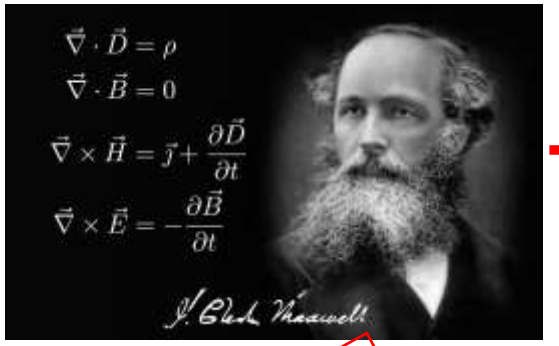

$R_{\mu\nu}-\frac{1}{2}Rg_{\mu\nu}+\Lambda g_{\mu\nu}=\frac{8\pi G}{c^4}T_{\mu\nu}$

- 弯曲时空电动力学的建立

  洛伦兹不变形式，闵可夫斯基度归替换为弯曲时空度归，偏微分替换为协变微分

- 其正确有效性是当代(天体)物理学应该回答的问题!

- 黑洞：磁层结构

  电磁辐射：伽玛射线和射电辐射

平直时空

$$\partial_\alpha F^{\alpha\beta}=-4\pi j^\beta$$
$$\partial_\alpha \tilde{F}^{\alpha\beta}=0$$
$$\partial_\mu T^{\mu\nu}=0$$

$\eta_{\mu\nu} \rightarrow g_{\mu\nu}$

偏微分 → 协变微分

弯曲时空

$$F^{\alpha\beta}_{;\alpha}=-4\pi j^\beta$$
$$\tilde{F}^{\alpha\beta}_{;\alpha}=0$$
$$T^{\mu\nu}_{;\mu}=0$$

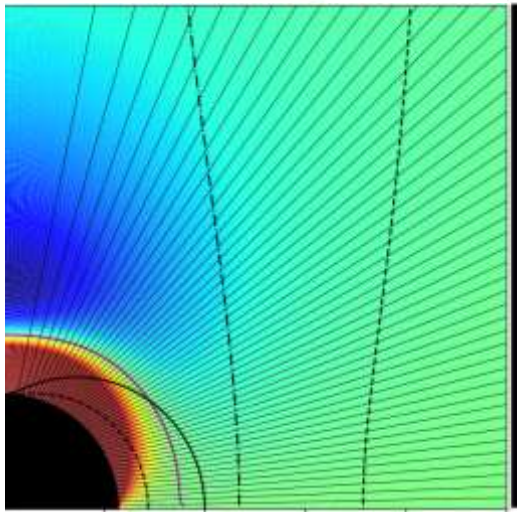

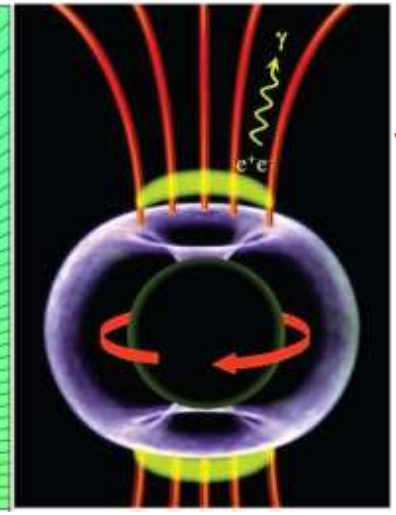

谢谢!

问题：

- 喷流是磁场驱动的吗？
- 喷流是黑洞还是吸积盘驱动的？
- 喷流准直和加速区域统一吗？
- 喷流磁场起源：有序和无序磁场？
- 喷流能量如何输运和耗散？
- 喷流是高能宇宙线起源地？
- ……

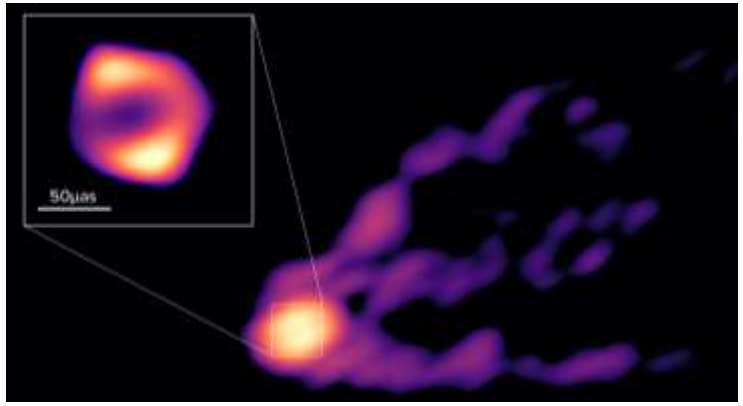

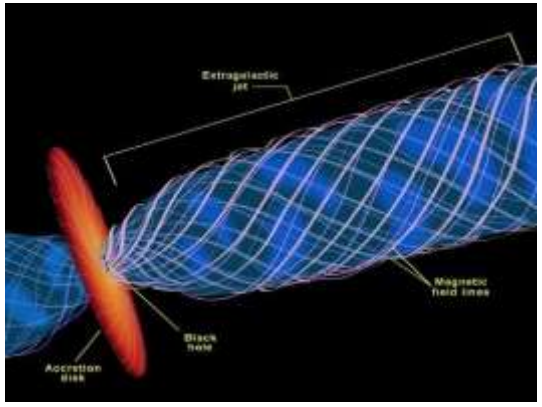

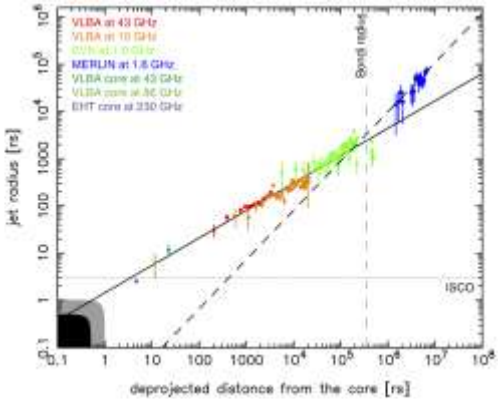

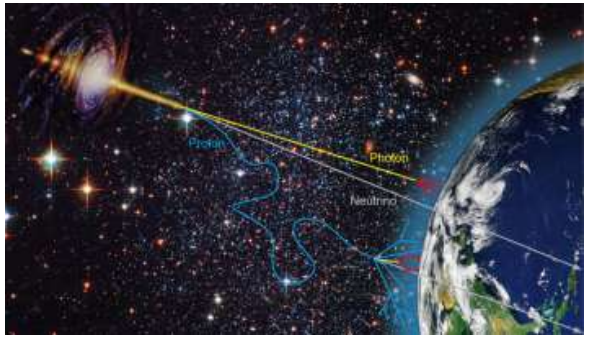

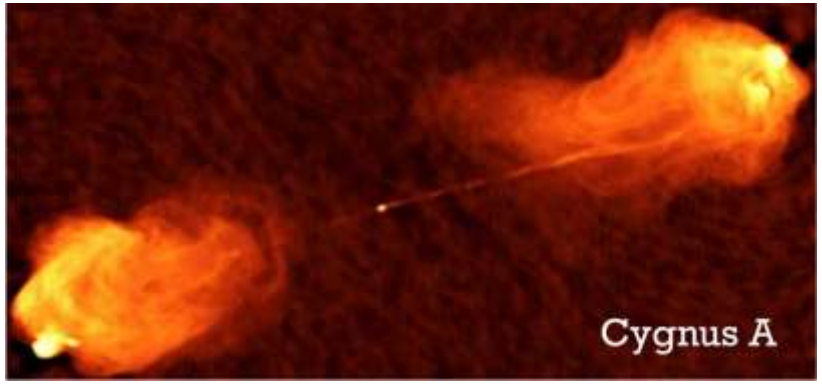

Radio loudness

- RL increase at low luminosity/Eddington ratio
- LLAGN

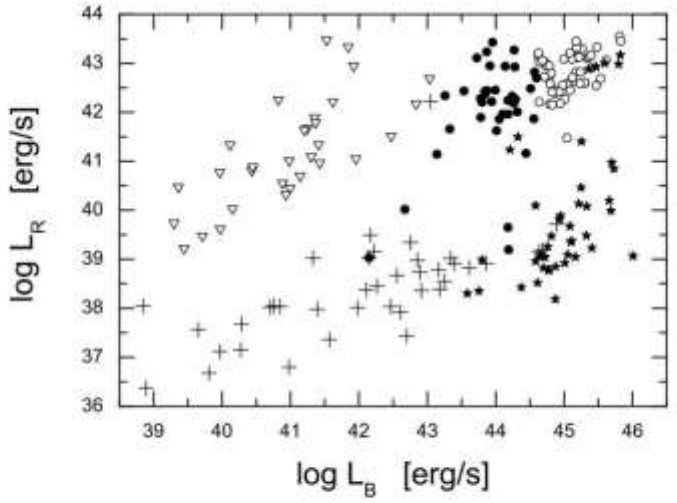

Fig. 1.— Total 5 GHz luminosity vs. B-band nuclear luminosity. BLRGs are marked by filled circles, radio-loud quasars by open circles, Seyfert galaxies and LINERs by crosses, FR I radio

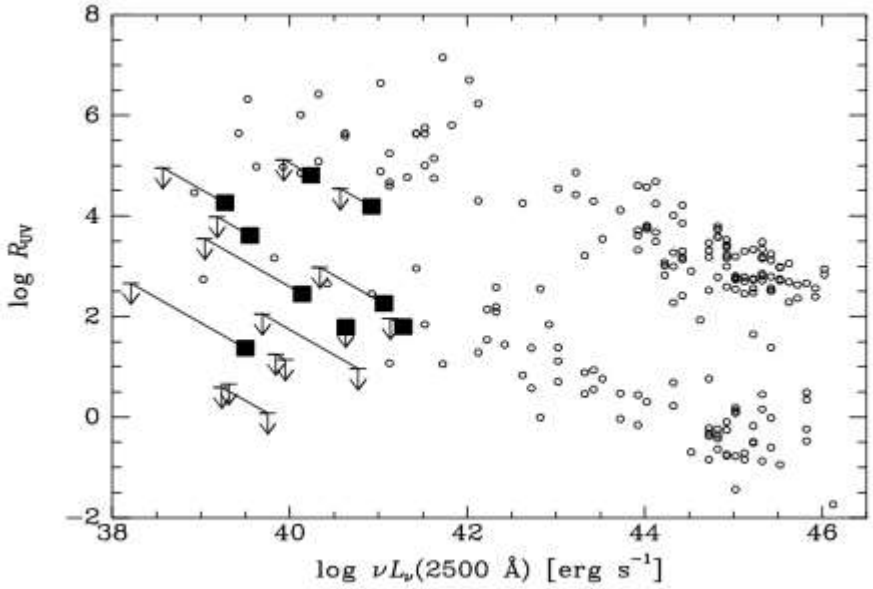

Maoz 2007

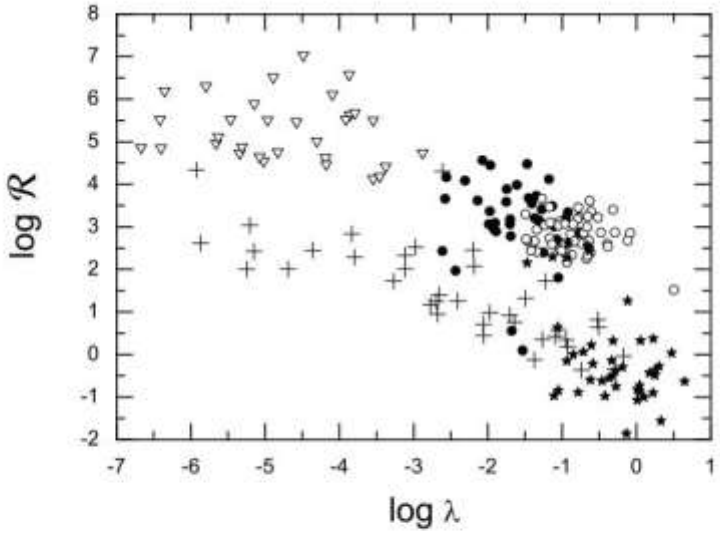

Sikora et al. 2007

Fig. 3.— Radio-loudness $\mathcal{R}$ vs. Eddington ratio λ. BLRGs are marked by the filled circles, radio-loud quasars by the open circles, Seyfert galaxies and LINERs by the crosses, FR I radio alaxies by the open triangles, and PG Quasars by the filled stars.

多波段辐射

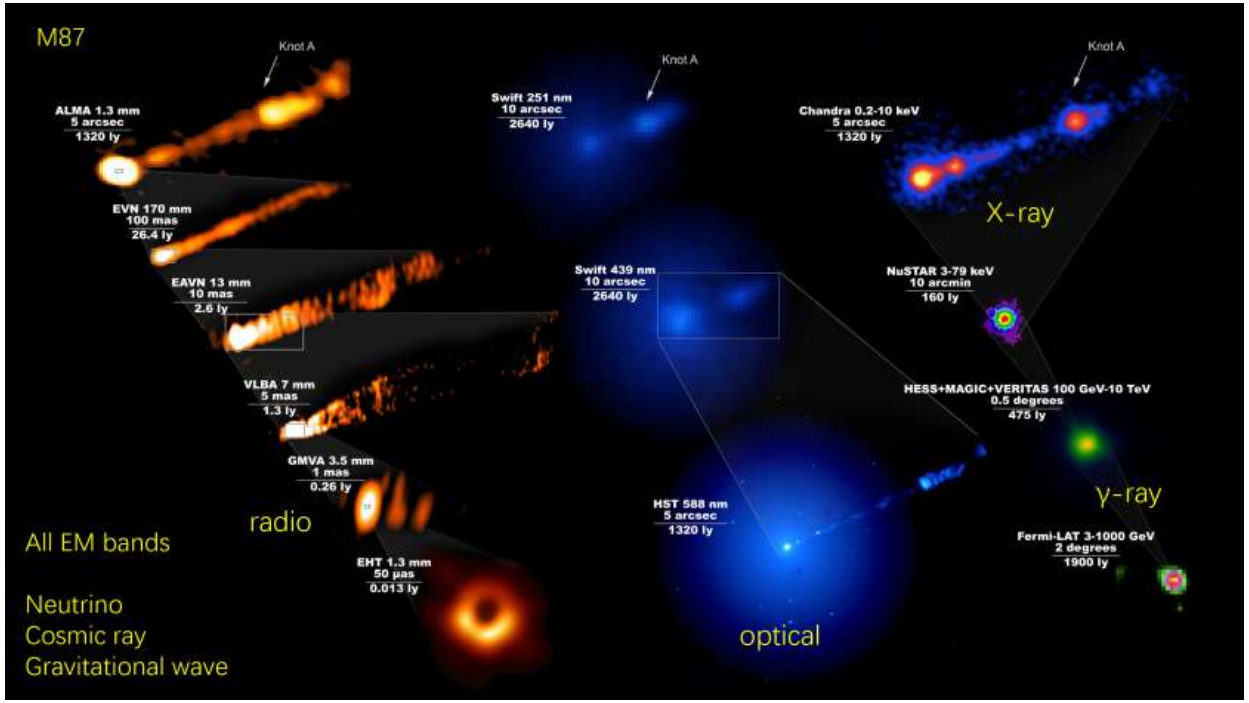

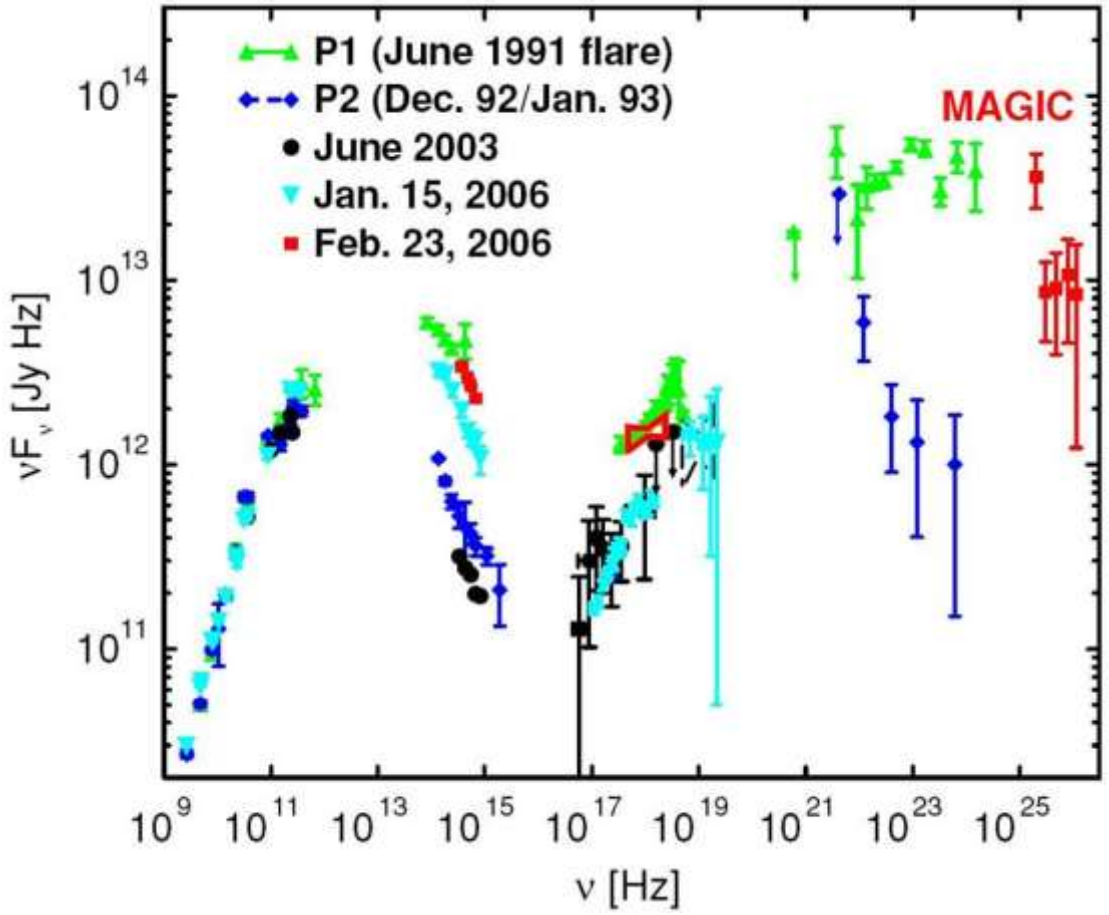

3C 279, Böttcher et al. 2009